TRANSPORT AND RELAXATION PHENOMENA IN POROUS MEDIA

R. HILFER

Institute of Physics, University of Oslo, 0316 Oslo, Norway

Institut für Physik, Universität Mainz, 55099 Mainz, Germany

CONTENTS

Advances in Chemical Physics, Volume XCII, Edited by I. Prigogine and Stuart A. Rice.
ISBN 0-471-14320-0 © 1996 John Wiley & Sons, Inc.

I. INTRODUCTION

A. The Problem

Almost all studies of transport and relaxation in porous media are motivated by one central question. How are the effective macroscopic transport parameters influenced by the microscopic geometric structure of the medium?

My presentation will divide this central question into three subproblems. The first subproblem is to give a quantitative geometric characterization of the complex porous microstructure. It will be discussed in Sections II and III. The second subproblem, treated in Sections IV and V, is to calculate effective macroscopic transport properties from the geometric characterization and the equations of motion for the phenomenon of interest. The third subproblem, known as the problem of "upscaling," runs as a common thread through all sections, and consists in defining and controlling the macroscopic limit. The macroscopic limit is a limit in which the ratio of a typical macroscopic length scale (e.g., the sample size) to a typical microscopic length scale (e.g., grain or pore size) diverges.

Distinguishing between the first and the second problem is conceptually convenient and important. Geometric properties of porous media are determined exclusively by the complex system of internal boundaries that defines the microstructure. Geometric properties can be calculated from a complete specification of the microstructure alone. Physical transport and relaxation properties on the other hand also require exact or approximate equations of motion describing the physical phenomenon of interest. Often, this involves the relaxation of small perturbations or the steady-state transport of physical quantities such as mass, energy, charge, or momentum. The distinction between geometric and physical properties of porous media has become blurred in the literature [1, 2], and physical transport properties such as fluid flow permeability or formation factors are sometimes referred to as geometric characteristics. This can be understood because practically employed experimental methods for observing the pore space geometry often involve observations of relaxation and transport phenomena from which the geometry is inferred by inversion techniques.

Geometric properties of porous media are observed in practice either directly using light microscopy, electron microscopy, scanning tunneling microscopes (STM), or indirectly from interpreting experimental measurements of transport and relaxation processes such as fluid flow,

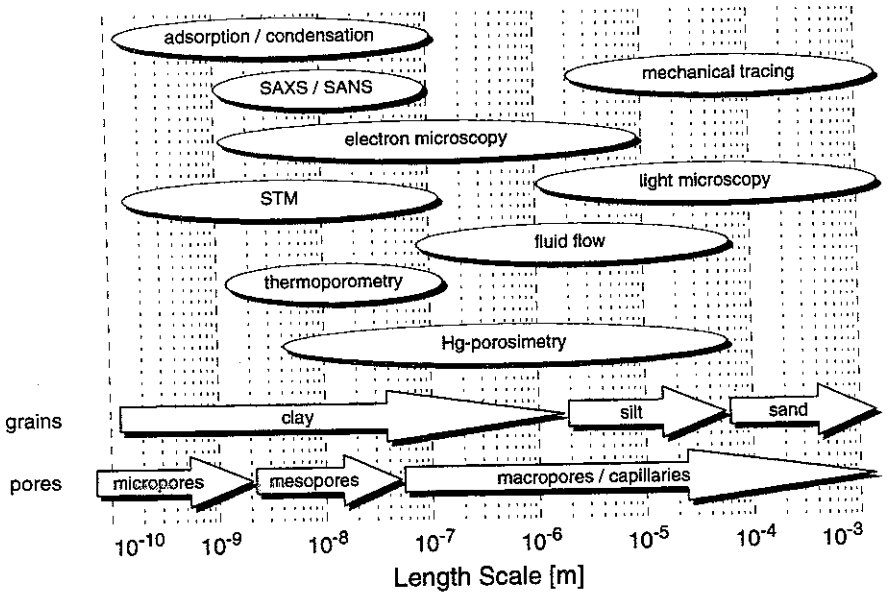

Figure 1. Overview of measurement techniques for observing porous microstructures and their range of sensitivity. The two lines of arrows at the bottom represent the DIN definition of grain sizes and the IUPAC definition of pore sizes.

electrical conduction, mercury intrusion, or small angle X-ray/small angle neutron scattering (SAXS/SANS). An overview over commonly used methods is given in Fig. 1. The different methods are represented on a length scale grid to indicate their ranges of applicability. The arrows in the lower part of Fig. 1 represent the IUPAC recommendation for classifying porous media into microporous, mesoporous, or macroporous media, and the DIN classification of porous media into clay, silt, and sand according to the grain size rather than pore size. Granular media with grains larger than 1 mm are called gravels or boulders.

Loosely speaking, a porous medium may be characterized as a medium containing a complex system of internal surfaces and phase boundaries. These internal interfaces define pores with a finite pore volume [3] and frequently a large surface area. Such a rough characterization applies also to other *heterogeneous media* and *composites*. Therefore some authors restrict the definition of porous media by requiring permeability [2], connectedness [4, 5], or randomness [5] as defining properties for porous media. Others [6–8], however, generalize the definition by including

liquids into the purview. The precise definition of porous media adopted for the present review will be given in Section II.B.

B. Scope of Review

The study of transport and relaxation in porous media is scattered throughout many fields of science and technology ranging from mathematics [9, 10], through solid state physics [11–13] and materials science [14–16], to applications in geology [17–19], hydrology [20, 21], geophysics [22, 23], environmental technology [24–26], petroleum engineering [27–29], or separation technology [30]. In recent years a large number of books [2, 5, 31–38, 38a] and comprehensive reviews [8, 17, 22, 39–45] have discussed transport and relaxation in porous media. Therefore, this chapter will try to emphasize those aspects of the central questions that are complementary to the existing discussions.

As pointed out by Landauer [46] more emphasis is often placed on calculational schemes for effective transport properties than on finding general geometric characterizations of the medium that can be used as input for such calculations. Consequently, this chapter puts more emphasis on the first subproblem of geometric characterization than on the second subproblem of solving equations of motion for media with correlated disorder. Geometrical characterizations of porous media are treated in Section III, and they fall into two categories discussed in Sections III.A and III.B. The first category contains general theories which attempt to identify general and well-defined geometric quantities that can be used to distinguish between different classes of porous media. The second category consists of specific models which attempt to idealize one particular class of porous media by abstracting its most essential geometrical features and incorporating them into a detailed model. The main difference between the two categories is the degree to which they specify the geometric microstructure. In general theories the microstructure remains largely unspecified while it is specified completely in modeling approaches.

Dielectric relaxation and fluid transport are discussed in Section V as representative examples for more general physical processes in porous media. Transport and relaxation processes in porous media invariably involve the disordered Laplacian operator $\nabla^T \cdot (\mathbf{C}(\mathbf{r})\nabla)$, where ∇ is the Nabla operator, the superscript T denotes transposition, and the second rank tensor field $\mathbf{C}(\mathbf{r})$ gives the fluctuating local transport coefficients. Dielectric relaxation and single-phase fluid transport in porous media are problems of practical and scientific interest, which show unexpected experimental behavior, such as permeability–porosity correlations, Archie's law, or dielectric enhancement. The discussion in Section V will

specifically address these issues. Methodically, the discussion in Section V will emphasize homogenization and local porosity theory because they allow one to control the macroscopic limit.

The upscaling problem as the controlled transition from microscopic to macroscopic length scales will then become the focus of attention in Section VI, which discusses two-phase fluid transport. The upscaling problem for two-phase flow is largely unresolved. Recent work [47, 48] has revisited the fundamental dimensional analysis [49] dating back more than 50 years, and uncovered a tacit assumption in the analysis that could help to resolve the upscaling difficulties. Thus the upscaling problem is treated in Section VI merely by comparing the microscopic and macroscopic dimensional analysis, and not by calculating effective relative permeabilities. Despite its simplicity the revisited dimensional analysis allows quantitative estimates of fluid transport rates and gravitational relaxation times based on the balance of viscous, capillary, and gravitational forces in the macroscopic limit.

II. DEFINITION AND EXAMPLES OF POROUS MEDIA

A. Examples of Porous Media

Most materials are porous when viewed at an appropriate length scale. Examples range from porous silicon, which is porous on the subnanometer scale, to limestone caves and underground river systems on the kilometer scale. An anthology of examples illustrates the variability of length scales and microstructures found in porous media.

Highly porous electrochemically etched silicon has recently found much interest because of its visible luminescence, which is attributed to its porous microstructure [12, 13, 50–54]. Figure 2 shows a transmission electron micrograph of the microstructure of porous silicon [13]. Other examples for microporous solids are zeolites.

Figure 3 shows a scanning electron micrograph (SEM) of a critical point dried gel consisting of ultrahigh molecular weight polyethylene [55]. The gel was obtained from 2% solutions in decalin under agitated conditions prior to gelation, and the fibrillar structure of the polyethylene crystals reflects flow prior to gelation. Thermoreversible gels consist of a macroscopic mechanically coherent network of macromolecules that is formed and stabilized through interconnected crystals. These materials are of considerable importance in the processing of high-performance polymers with very high tensile strength [55].

Figure 4 displays the microstructure of silicon nitride ceramics consisting of elongated Si_3N_4 grains embedded in a matrix of finer grains and a

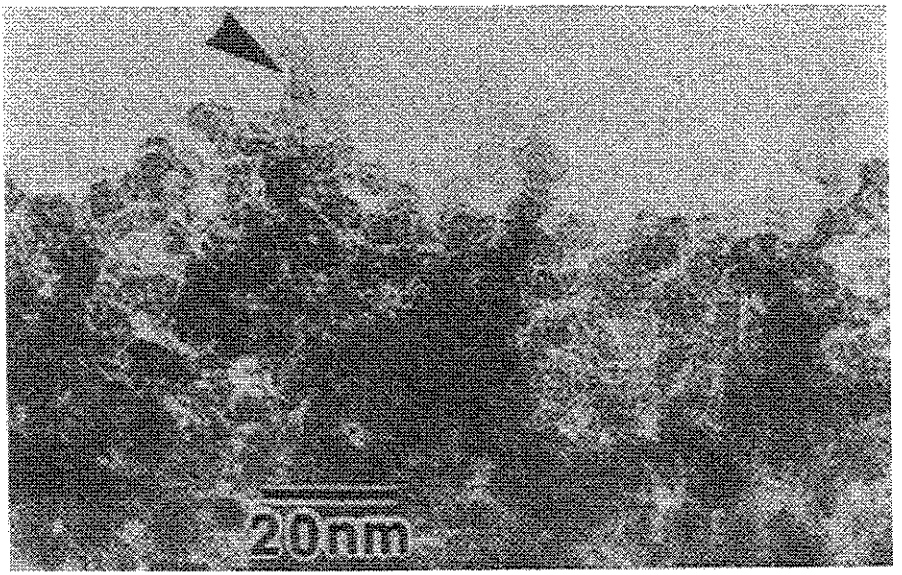

Figure 2. Transmission electron image of thin porous silicon layer showing irregular columnar microstructure of solid silicon. Some columns, such as the one indicated by the arrow, have cross-sectional diameter significantly less than 5 nm. [Reprinted with permission from *Nature*, A. Cullis and L. Canham, **353**, 335 (1991). Copyright © Macmillan Magazine Limited.]

grain boundary phase. Silicon nitride ceramics with high strength have a fine grained elongated microstructure, while materials with a high fracture toughness are more coarse grained [15].

Wood is a strongly anisotropic natural porous medium exhibiting cylindrical pores. Figure 5 shows an SEM of a partially cut and fractured surface from Malaysian Nemesu wood, which gives an impression of the irregularities within the material. The image shows tracheid cells of about 25 μm in diameter and vessel elements that are roughly an order of magnitude larger.

The large surface/volume ratio, which is characteristic for porous media (see Section III.A), is essential for the function of the lung consisting of some 300 million small air chambers. Figure 6 shows the foamlike structure formed by the respiratory air chambers in the lung. As emphasized by Weibel, biological porous media should *not be viewed as random* [56]. The general difficulty of modeling porous media as random or disordered media is further discussed in Section II.B.2.

Building and construction materials such as cements and concrete are porous media. Figure 7 shows an SEM of cement and lime mortar. Each

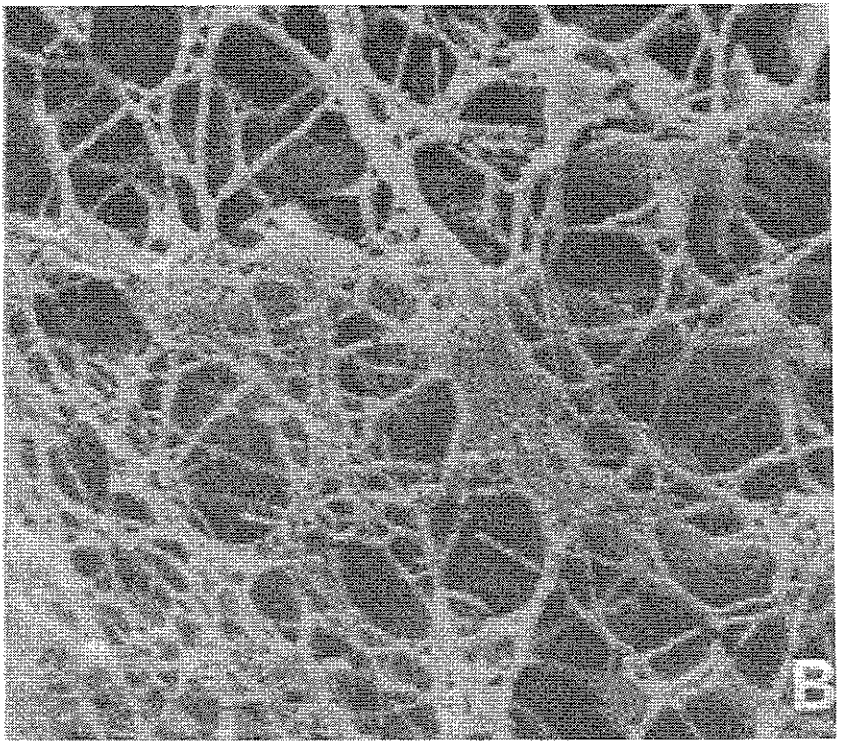

Figure 3. Scanning electron micrograph of critical point dried gel of ultrahigh molecular weight polyethylene. (Reproduced with permission from [55].)

dash in the dashed line visible in the image corresponds to 10 μm. The micrograph shows an extended network of fissures whose properties govern the moisture transfer and sorption properties of such materials [57].

An understanding of transport and relaxation in rocks, soils, and other geologically important heterogeneous media is of crucial importance in hydrology, exploration geology, petroleum engineering, and environmental research. Figure 8 shows a thin section of a clastic sandstone formed by fluvial deposits. Sandstones and other sedimentary rocks have attracted much research interest, and are among the best investigated examples of porous media.

The variety of two component porous media is enormous. Most of the following discussion will focus on irregular, random media. Regular and

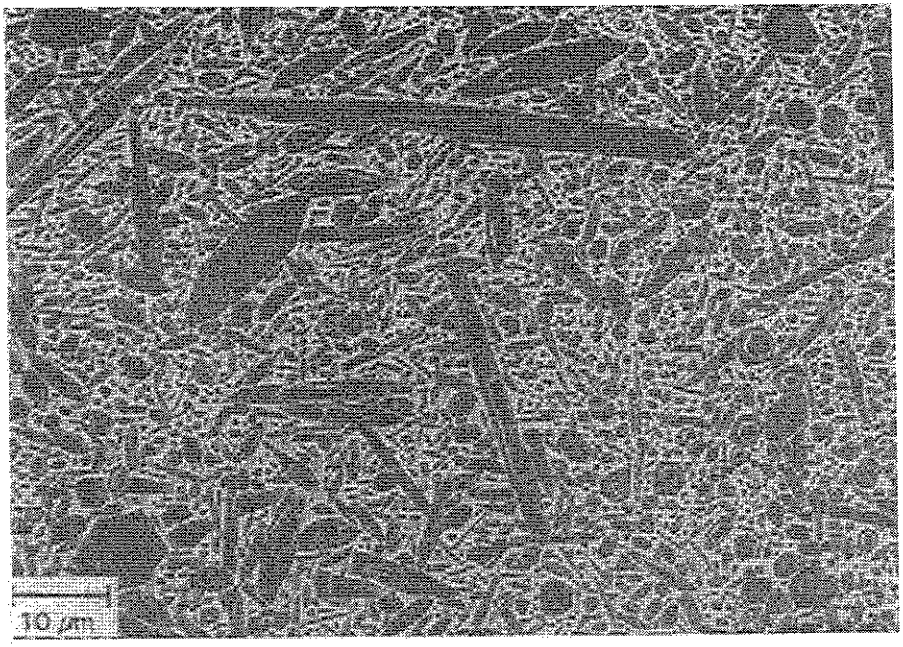

Figure 4. Scanning electron micrograph of a sintered silicon nitride (Si_3N_4) ceramic [15].

ordered microstructures (such as in zeolites) may be considered as a special case of irregular porous media.

B. Definition of Porous Media

1. *Deterministic Geometries*

An n-component *porous medium* in d dimensions is defined as a compact and singly connected subset $\mathbb{S}$ of $\mathbb{R}^d$, which contains n closed subsets $\mathbb{P}_i \subset \mathbb{S}$ such that

$$\mathbb{S} = \mathbb{P}_1 \cup \cdots \cup \mathbb{P}_n \tag{2.1}$$

$$0 = V_d(\partial \mathbb{P}_i) \tag{2.2}$$

for all $1 \leq i \leq n$. The set $\mathbb{S}$ is called the sample space and may represent, for example, a piece of porous rock. The subsets $\mathbb{P}_i$ $(i = 1, \ldots, n)$ represent n different phases or components, such as different minerals or

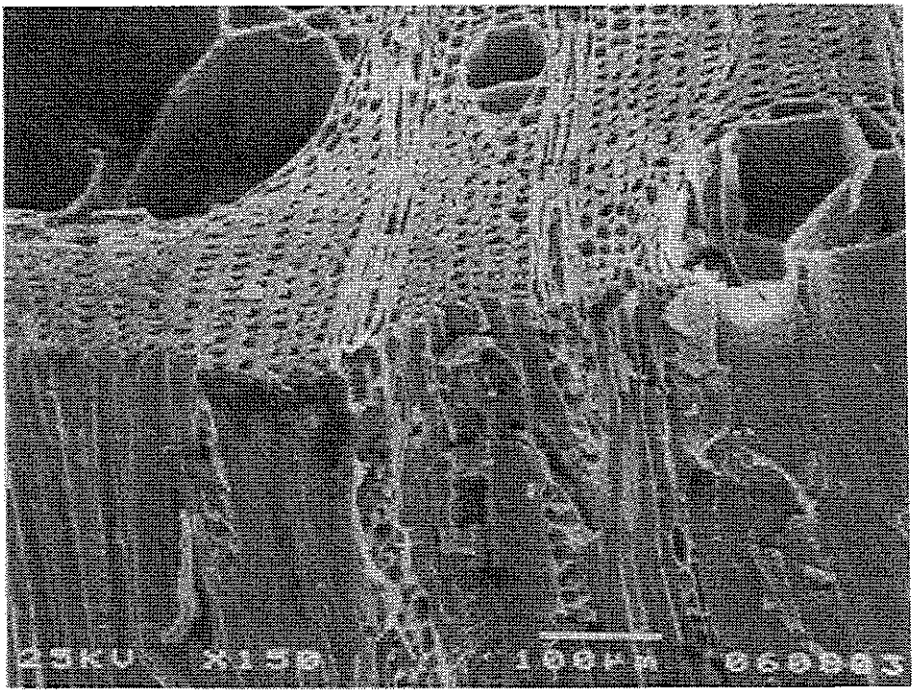

Figure 5. Scanning electron micrograph of Malaysian Nemesu wood (Shorea Pauciflora).

fluid phases contained in a rock. The symbol $V_d(\mathbb{G})$ denotes the d-dimensional *volume* of a set $\mathbb{G} \subset \mathbb{R}^d$. It is defined as

$$V_d(\mathbb{G}) = \int \chi_{\mathbb{G}}(\mathbf{r}) d^d\mathbf{r} \tag{2.3}$$

where $\mathbf{r}$ is a d-dimensional vector, and $d^d\mathbf{r}$ is the d-dimensional Lebesgue measure. Thus V_2 denotes an area, and V_1 is a length. When there is no danger of confusion $V_3(\mathbb{G}) = V(\mathbb{G})$ will be used below. The *characteristic (or indicator) function* of a set $\mathbb{G}$ is defined as

$$\chi_{\mathbb{G}}(\mathbf{r}) = \begin{cases} 1 & \text{for} \quad \mathbf{r} \in \mathbb{G} \\ 0 & \text{for} \quad \mathbf{r} \notin \mathbb{G} \end{cases} \tag{2.4}$$

and it indicates when a point is inside or outside of $\mathbb{G}$. The sets $\partial\mathbb{P}_i$ are the phase boundaries separating the different components. The boundary

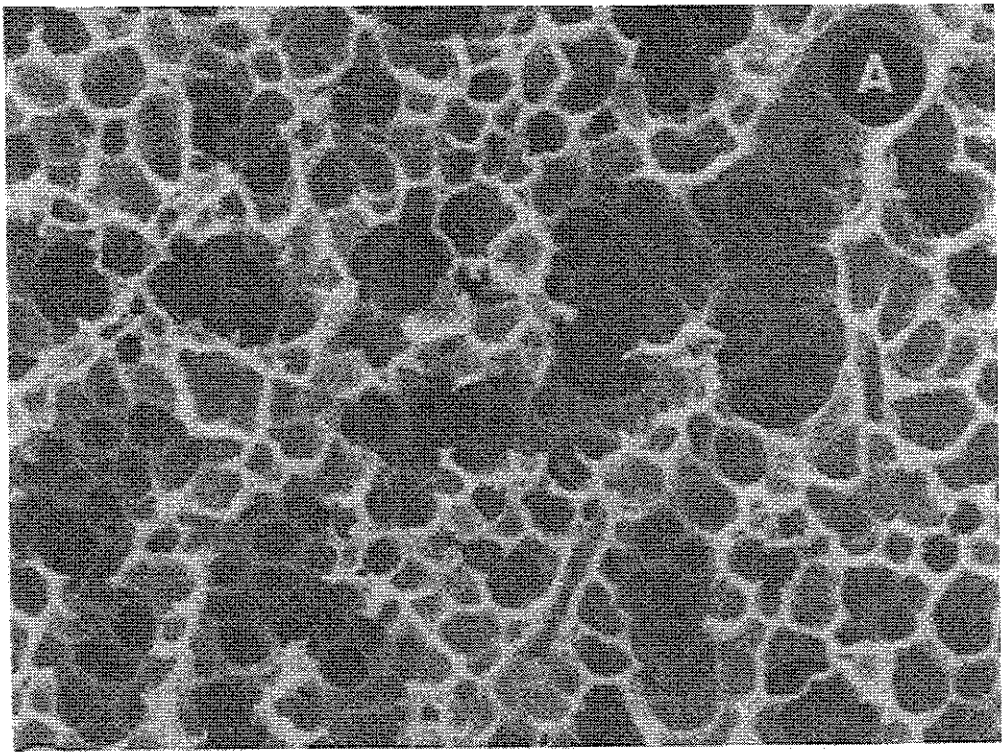

Figure 6. Scanning electron micrograph of air chambers in a lung. (Reproduced with permission from E. Weibel, "The non-statistical nature of biological structure and its implications on sampling for stereology," in *Geometrical Probability and Biological Structures: Buffon's 200th Anniversary*, E. Miles and J. Serra, Eds., Springer, Berlin, 1978, p. 171. Copyright © Springer-Verlag, 1978).

operator ∂ is defined on a general set $\mathbb{G}$ as the difference[1] $\partial\mathbb{G} = \bar{\mathbb{G}} \backslash \mathring{\mathbb{G}}$. The set $\mathring{\mathbb{G}}$, called the *interior* of $\mathbb{G}$, is defined as the union of all open sets contained in $\mathbb{G}$. The set $\bar{\mathbb{G}}$ is called the *closure* of $\mathbb{G}$ and is defined as the intersection of all closed sets containing $\mathbb{G}$. The condition (2.2) excludes fractal boundaries or cases in which a boundary set is dense. By replacing the Lebesgue measure in Eq. (2.3) with Hausdorff measures some of these restrictions may be relaxed [58–61].

[1] The settheoretic difference operation explains the use of the differential symbol ∂, which may also be motivated by the fact that the derivative operator $\nabla\chi_{\mathbb{P}}(\mathbf{r})$ applied to the characteristic function $\chi_{\mathbb{P}}(\mathbf{r})$ of a closed set $\mathbb{P}$ yields the Dirac distribution concentrated on the set $\partial\mathbb{P}$.

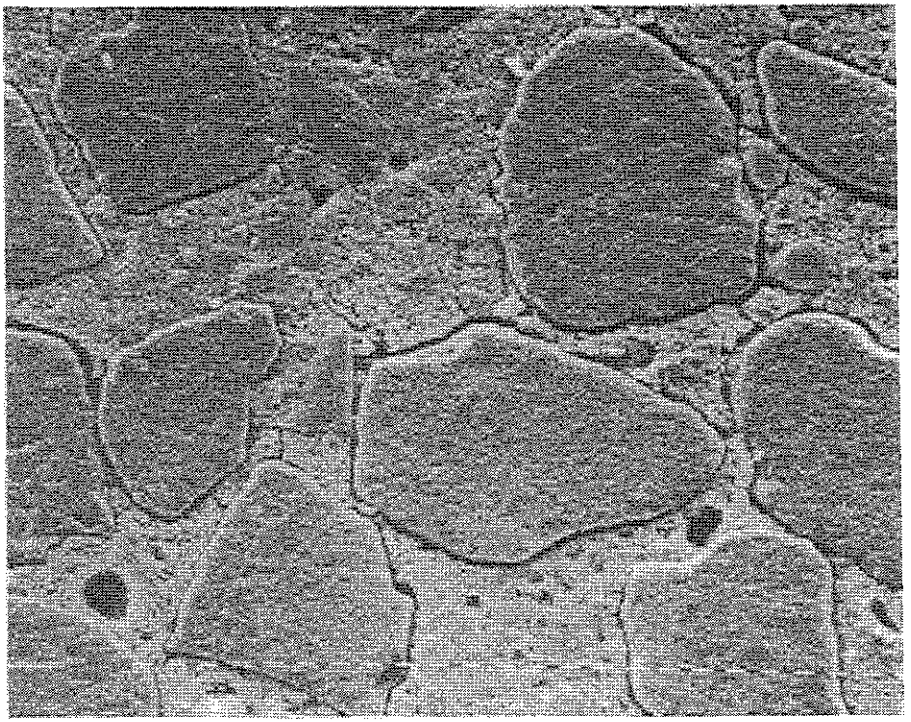

Figure 7. Scanning electron micrograph of a polished surface of mortar (magnification 200×). Reproduced with permisstion from [57].

Frequently, the different phases or components may be classified into solid and fluid phases. An example is a porous rock. In this case, it is convenient to consider the two-component medium in which all the solid phases are collectively denoted as *matrix space* $\mathbb{M}$, and the fluid phases are denoted collectively as *pore space* $\mathbb{P}$. The union of the pore and matrix space $\mathbb{S} = \mathbb{P} \cup \mathbb{M}$ gives the full porous *sample space* $\mathbb{S}$ and the intersection of $\mathbb{P}$ and $\mathbb{M}$ defines the boundary set $\mathbb{P} \cap \mathbb{M} = \partial\mathbb{P} = \partial\mathbb{M}$. It will usually be assumed that the boundary $\partial\mathbb{P}$ of the pore or matrix space is a surface in $\mathbb{R}^3$. This implies that $V_3(\partial\mathbb{P}) = 0$ in agreement with Eq. (2.2).

As an example consider a clean quartz sandstone filled with water. The sets $\mathbb{P}$ and $\mathbb{M}$ can be defined using the density contrast between the density of water $\rho_W \approx 1\ \mathrm{g\,cm^{-3}}$, and that of quartz $\rho_Q \approx 2.65\ \mathrm{g\,cm^{-3}}$ [62].

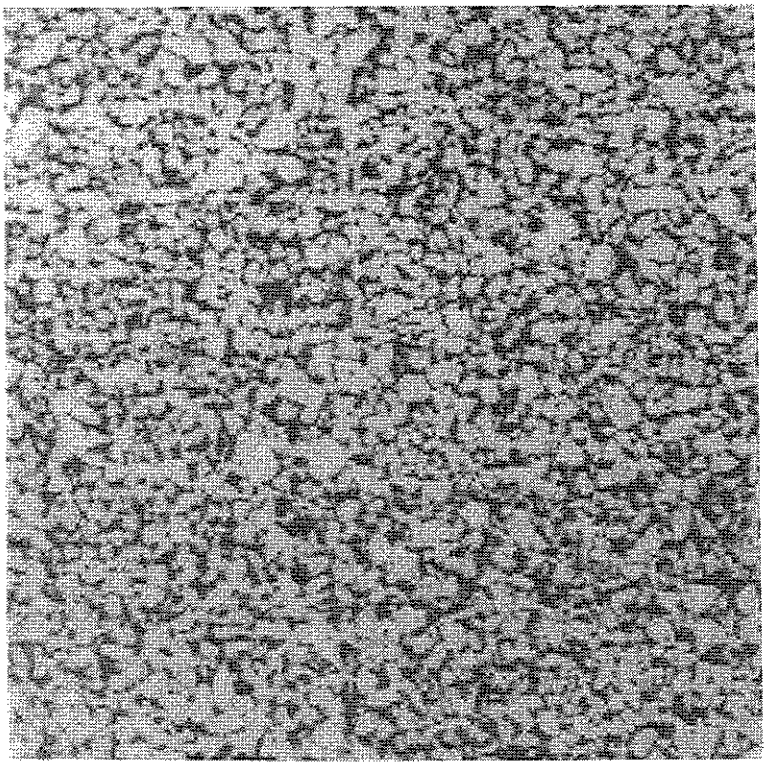

Figure 8. Thin-section micrograph of clastic sandstone from fluvial deposits in the Statfjord formation 3130 m below the bottom of the North Sea. The displayed section measures roughly 2 cm across.

Let $\rho(\mathbf{r}, \varepsilon)$ denote the total density in a small closed ball

$$\mathbb{B}(\mathbf{r}, \varepsilon) = \{\mathbf{q} \in \mathbb{R}^3 : |\mathbf{q} - \mathbf{r}| \leq \varepsilon\} \tag{2.5}$$

of radius ε around $\mathbf{r}$. If $\lim_{\varepsilon \to 0} \rho(\mathbf{r}, \varepsilon)$ exists then the matrix and pore space are defined as $\mathbb{M} = \mathbb{Q}$ and $\mathbb{P} = \mathbb{W}$. Here

$$\mathbb{Q} = \{\mathbf{r} \in \mathbb{S} : |\lim_{\varepsilon \to 0} \rho(\mathbf{r}, \varepsilon) - \rho_{\mathrm{Q}}| < \Delta\rho_{\mathrm{Q}}\} \tag{2.6}$$

$$\mathbb{W} = \{\mathbf{r} \in \mathbb{S} : |\lim_{\varepsilon \to 0} \rho(\mathbf{r}, \varepsilon) - \rho_{\mathrm{W}}| < \Delta\rho_{\mathrm{W}}\} \tag{2.7}$$

are the regions occupied by quartz and water, and $\Delta\rho_Q$, $\Delta\rho_W$ are the uncertainties in the values of their densities ρ_Q and ρ_W. In practice, it may happen that $\mathbb{P} \cup \mathbb{M} \neq \mathbb{S}$ and even the case $\mathbb{P} \cap \mathbb{M} = \emptyset$ is conceivable. An example would be a muscovite overgrowth with a density of $2.82\,\mathrm{g\,cm^{-3}}$ surrounding the quartz grains of the sandstone.

A generalization of the definition above is necessary if the pore space is filled with two immiscible fluids (see Section VI). In this case the fluid–fluid interface is mobile, and thus all the sets above may in general become time dependent. The same applies when the matrix $\mathbb{M}$ is not rigid and represents a deformable medium such as a gel.

Finally, it is of interest to estimate the amount of information contained in a complete specification of a porous geometry according to the definitions above. This will depend on the spatial resolution a and on the size L of the system. Assuming that the resolution is limited by $a \approx 10^{-10}\,\mathrm{m}$ and that $L \approx 10^{-2}\,\mathrm{m}$, the configuration of an n-component medium in d dimensions is completely specified by roughly $(L/a)^d \approx 10^{8d}$ numbers. For $d = 3$ these are $O(10^{24})$ numbers.

2. *Stochastic Geometries*

a. Discrete Space. The irregular geometry of porous media frequently appears to be random or to have random features. This observation suggests the use of probabilistic methods. The idealization underlying the use of statistical methods is that the irregular geometry is a realization drawn at random from an ensemble of possible geometries. It must be emphasized that an idealization is involved in discussing an emsemble rather than individual geometries. It assumes that there exists some form of recognizable statistical regularity in the irregular fluctuations and heterogeneities of the microstructure. This idealization is modeled after statistical mechanics where the microstructure corresponds to a full specification of the positions and momenta of all particles in a fluid while the recognizable regularities are contained in its macroscopic equation of state or thermodynamic potentials. The statistical idealization assumes that the recognizable regularities of porous media can be described by a suitable probability distribution on the space of all possible geometries. Such a description may not always be the most obvious or most advantageous [56], and in fact the merit of the stochastic description does not lie in its improved practicability. The merit of the stochastic description lies in the fact that it provides the necessary framework to define typical or average properties of porous media. The typical or average properties, it is hoped, will provide a more practical geometric characterization of porous media.

Before embarking on the definition of stochastic porous media I wish

to emphasize a recent development in the foundations of statistical mechanics [63–69], which concerns the concept of *stationarity* or *homogeneity*. Stationarity is often invoked in the statistical characterization of porous media, although many media are known to be *heterogenous on all scales*. Heterogeneity on all scales means that the geometrical or physical properties of the medium never approach a large-scale limit but continue to fluctuate as the length scale is increased from the microscopic resolution to some macroscopic length scale. Homogeneity or stationarity assumes the absence of macroscopic fluctuations, and postulates the existence of some intermediate length scale beyond which fluctuations decrease [5]. Recent developments in statistical mechanics [63–69] indicate that the traditional concept of stationarity is too narrow, and that there exists a generalization that describes *stationary but heterogeneous macroscopic* behavior. Although these new concepts are still under development they have already been applied in the context of local porosity theory discussed in Section III.A.5.

Consider a porous sample (e.g., cubically shaped) of extension or side length L, and let a be the microscopic resolution. (For concreteness let $a = 10^{-10}$ m as before.) Then there are $N = (L/a)^d$ volume elements inside the sample space that are conveniently addressed by their position vectors

$$\mathbf{r}_i = \mathbf{r}_{i_1 \cdots i_d} = (ai_1, \ldots, ai_d) \tag{2.8}$$

with integers $1 \leq i_1, \ldots, i_d \leq L/a$. Here $\mathbf{r}_i$ is a shorthand notation for $\mathbf{r}_{i_1 \cdots i_d}$. A random configuration or *random geometry* G of an n-component medium is then given as an N-tuple $G = (X_1, \ldots, X_N) = (X(\mathbf{r}_1), \ldots, X(\mathbf{r}_N))$, where the random variables $X_i \in \mathbb{I}_n = \{\rho_{\mathbb{P}_1}, \ldots, \rho_{\mathbb{P}_n}\}$ defined as

$$X_i = X(\mathbf{r}_i) = \sum_{j=1}^{n} \rho_{\mathbb{P}_j} \chi_{\mathbb{P}_j}(\mathbf{r}_i) \tag{2.9}$$

indicate the presence of phase $\mathbb{P}_i$ for the volume element $\mathbf{r}_i$ as identified from its density value $\rho_{\mathbb{P}_j}$. The set $\mathbb{I}_n = \{\rho_{\mathbb{P}_1}, \ldots, \rho_{\mathbb{P}_n}\}$ is a set of indicators, here the densities, which are used to label the phases. Of course the density could be replaced by other quantities characterizing or labeling the components. The discretization is always chosen such that $\mathbf{r}_i \not\in \partial\mathbb{P}_j$ for all $1 \leq i \leq N$ and $1 \leq j \leq n$.

An n-component *stochastic porous medium* is defined as a discrete

probability density on the set of geometries through

$$\mu(x_1, \ldots, x_N) = \text{Prob}\{G = (x_1, \ldots, x_N)\}$$
$$= \text{Prob}\{(X_1 = x_1) \wedge \cdots \wedge (X_N = x_N)\} \qquad (2.10)$$

where $x_i \in \mathbb{I}_n = \{\rho_{\mathbb{P}_1}, \ldots, \rho_{\mathbb{P}_n}\}$. *Expectation values* of functions $f(G) = f(x_1, \ldots, x_N)$ of the random geometry are defined as

$$\langle f(G) \rangle = \langle f(x_1, \ldots, x_N) \rangle = \sum_{x_1 \in \mathbb{I}_n} \cdots \sum_{x_N \in \mathbb{I}_n} f(x_1, \ldots, x_N) \mu(x_1, \ldots, x_N) \qquad (2.11)$$

where the sum is over all configurations of the geometry. Note the analogy between Eq. (2.11) and expectation values in statistical mechanics. The analogy becomes an equivalence if μ is a finite dimensional normalized Boltzmann–Gibbs measure.

A stochastic porous medium is called *stationary* and *homogeneous* (in the traditional sense) if its distribution $\mu(x_1, \ldots, x_N) = \mu(x(\mathbf{r}_1), \ldots, x(\mathbf{r}_N))$ is translation invariant, that is,

$$\mu(x(\mathbf{r}_1), \ldots, x(\mathbf{r}_N)) = \mu(x(\mathbf{r}_1 + \mathbf{q}), \ldots, x(\mathbf{r}_N + \mathbf{q})) \qquad (2.12)$$

for all $N \in \mathbb{N}$, $\mathbf{q} \in \mathbb{R}^d$. This traditional definition of stationarity is a special case of the more general concept of fractional stationarity [63–69], which is currently being developed to describe macroscopic heterogeneity.

A stochastic porous medium is called *isotropic* if its distribution is invariant under all rigid euclidean motions, that is,

$$\mu(x(\mathbf{r}_1), \ldots, x(\mathbf{r}_N)) = \mu(x(\mathbf{R}\mathbf{r}_1), \ldots, x(\mathbf{R}\mathbf{r}_N)) \qquad (2.13)$$

for all $N \in \mathbb{N}$ where $\mathbf{R}$ denotes a combination of rotation and translation.

The set of possible geometries contains n^N elements. For a two-component porous cube of side length $L = 1$ cm there are $2^{10^{24}}$ possible configurations at the chosen resolution $a = 10^{-10}$ m. Thus the complete specification of a stochastic porous medium through $\mu(x_1, \ldots, x_N)$ is even less practical than specifying all the volume elements of a particular sample. This does not diminish the theoretical importance of the microscopic geometry distribution $\mu(x_1, \ldots, x_N)$. In fact, it is even useful to generalize it to continuous space where the required amount of data to specify the distribution becomes infinite.

b. Continuous Space. Instead of discretizing the space it is possible to

work directly with the notion of random sets in continuous space. The mathematical literature about random sets [10, 70, 71] is based on pioneering work by Choquet [72].

To define random sets, recall first the concepts of a *probability space* and a *random variable* [73–75]. An event $\mathbb{E}$ is a subset of a set $\mathbb{O}$ representing all possible outcomes of some experiment. The probability $\Pr(\mathbb{E})$ of an event is a set function obeying the fundamental rules of probability $\Pr(\mathbb{O}) = 1$, $\Pr(\mathbb{E}) \geq 0$ and $\Pr(\cup_{i=1}^{\infty} \mathbb{E}_i) = \Sigma_{i=1}^{\infty} \Pr(\mathbb{E}_i)$ if $\mathbb{E}_i \cap \mathbb{E}_j = \emptyset$ for $i \neq j$. Formally, the probability Pr is a function on a class $\mathfrak{D}$ of subsets of a set $\mathbb{O}$, called the sample space. If the collection of sets $\mathfrak{D}$ for which the probability is defined is closed under countable unions, complements, and intersections, then the triple $(\mathbb{O}, \mathfrak{D}, \Pr)$ is called a probability space. The family of sets $\mathfrak{D}$ is called a σ algebra. The *conditional probability* of an event $\mathbb{E}$ given the event $\mathbb{G}$ is defined as

$$\Pr(\mathbb{E}|\mathbb{G}) = \frac{\Pr\{\mathbb{E} \cap \mathbb{G}\}}{\Pr\{\mathbb{G}\}}, \qquad \Pr\{\mathbb{G}\} \neq 0 \tag{2.14}$$

A *random variable* is a real valued function on a probability space.

Random sets are generalizations of random variables. The mathematical theory of random sets is based on the "hit-or-miss" idea that a complete characterization of a set can be obtained by intersecting it sufficiently often with an arbitrary compact test set and recording whether the intersection is empty or not [10, 70]. Suppose that $\mathscr{F}$ denotes the family of all closed sets in $\mathbb{R}^d$ including the empty set $\emptyset$. Let $\mathscr{K}$ denote the set of all compact sets. $\mathfrak{F}$ is the smallest σ algebra of subsets of $\mathscr{F}$ that contains all the hitting sets $\mathscr{F}_{\mathbb{K}} = \{\mathbb{F} \in \mathscr{F} : \mathbb{F} \cap \mathbb{K} \neq \emptyset\}$, where $\mathbb{K}$ is a compact test set. An event in this context is the statement whether or not a random set hits a particular countable family of compact subsets.

A *random set* $\mathbb{X}$ (more precisely a random closed set) is defined as a measurable map from a probability space $(\mathbb{O}, \mathfrak{D}, \mu)$ to $(\mathscr{F}, \mathfrak{F})$ [10]. This allows us to assign probabilities to countable unions and intersections of the sets $\mathscr{F}_{\mathbb{K}}$ which are the elements of $\mathfrak{F}$. For example,

$$\Pr(\mathscr{F}_{\mathbb{K}}) = \mu(\mathbb{X}^{-1}(\mathscr{F}_{\mathbb{K}})) \tag{2.15}$$

is the probability that the intersection $\mathbb{X} \cap \mathbb{K}$ is not empty. This probability plays an important role in the geometric characterizations of porous media based on capacity functionals [10, 72] discussed below. Note that there exists no simple mathematical analogue of the expectation value defined for the discrete case in Eq. (2.11). Its definition, which will not

be needed here, requires the introduction of functional integrals on an infinitely dimensional space, or the study of random measures associated with the random set $\mathbb{X}$ [10].

While the expectation value is not readily carried over to the continuous case, the concepts of stationarity and isotropy are straightforwardly generalized. A random set $\mathbb{X}$ is called *stationary* if

$$\Pr\{\mathbb{X} \cap \mathbb{K} \neq \emptyset\} = \Pr\{(\mathbb{X} + \mathbf{r}) \cap \mathbb{K} \neq \emptyset\} \tag{2.16}$$

for all vectors $\mathbf{r} \in \mathbb{R}^d$ and all compact sets $\mathbb{K}$. The notation $\mathbb{G} + \mathbf{r}$ denotes the *translated set* defined as

$$\mathbb{G} + \mathbf{r} = \{\mathbf{q} + \mathbf{r} : \mathbf{q} \in \mathbb{G}\} \tag{2.17}$$

for $\mathbf{r} \in \mathbb{R}^d$ and $\mathbb{G} \subset \mathbb{R}^d$. Using the analogous notation

$$\mathbf{R}\mathbb{G} = \{\mathbf{R}\mathbf{q} : \mathbf{q} \in \mathbb{G}\} \tag{2.18}$$

for $\mathbf{R}$ a rigid euclidean motion allows to define a random set to be *isotropic* if

$$\Pr\{\mathbb{X} \cap \mathbb{K} \neq \emptyset\} = \Pr\{(\mathbf{R}\mathbb{X}) \cap \mathbb{K} \neq \emptyset\} \tag{2.19}$$

for all rigid motions $\mathbf{R}$ and compact sets $\mathbb{K}$. For later reference the notation

$$c\mathbb{G} = \{c\mathbf{q} : \mathbf{q} \in \mathbb{G}\} \tag{2.20}$$

is introduced to denote the multiplication of sets by real numbers. The traditional definition of stationarity presented in Eq. (2.16) is restricted to macroscopically homogeneous porous media. It is a special case of the more general concept of fractional stationarity that describes macroscopic heterogeneity and is currently under development [63–69].

The mathematical definition of random sets in continuous space is even less manageable from a practical perspective than its definition for a discretized space. A complete specification of a random set would require the specification "all" compact or "all" closed subsets of $\mathbb{R}^d$, which is in practice impossible. Nevertheless, the definition is important to clarify the concept of a random set.

III. GEOMETRIC CHARACTERIZATION

A complete specification of the microstructure of a realistic porous medium is impractical. This section discusses possibilities for characteriz-

ing porous media without specifying a porous geometry in all its detail. As emphasized in the introduction, this is the main theoretical task. There are two general approaches: One approach constructs simplified geometric models for each specific porous medium of interest. The other approach attempts to find general characterizations for large classes of porous media that are less specific but more widely applicable. This latter approach will be discussed first.

A. General Geometric Characterization Theories

A general geometric characterization of porous media should satisfy the following requirements:

- It should be well defined in terms of geometric quantities.
- It should involve only parameters that are directly observable or measurable in an experiment independent of the phenomenon of interest.
- It should not require the specification of too many parameters. The required independent experiments should be simple and economical to carry out. What is economical depends on the available data processing technology. With current data processing technology a characterization requiring more than 10^{12} numbers must be considered uneconomical.
- The characterization should be usable in exact or approximate solutions of the equations of motion governing the phenomenon of interest.

The following sections discuss methods based on porosities $\bar{\phi}$, correlation functions $S_n(\mathbf{r})$, $C_n(\mathbf{r})$, local porosity distributions $\mu(\phi)$, pore size distributions $\Pi(r)$, and capacities $T(\mathbb{K})$. Table I collects the advantages and disadvantages of these methods according to the specified criteria.

1. *Porosity and Other Numbers*

a. Porosity. The porosity of a porous medium is its most important geometrical property. Most physical properties are influenced by the porosity.

The *porosity* $\phi(\mathbb{S})$ of a two-component porous medium $\mathbb{S} = \mathbb{P} \cup \mathbb{M}$ consisting of a pore space $\mathbb{P}$ (component one) and a matrix space $\mathbb{M}$ (component two) is defined as the ratio

$$\phi(\mathbb{S}) = \frac{V_3(\mathbb{P})}{V_3(\mathbb{S})} \tag{3.1}$$

TABLE I
Advantages and Disadvantages of Different Geometric Characterization Methods for Porous Media[a]

Characterization	Well Defined	Predictive	Economical	Easily Usable
$\bar{\phi}, \ldots$	Yes	Yes	Yes	Yes
$S_2(\mathbf{r}), \ldots$	Yes	Yes	Yes	Yes
$S_n(\mathbf{r}), \ldots, (n \geq 3)$	Yes	Yes	No	Yes
$\Pi(r)$	No	No	Yes	Yes
$\mu(\phi)$	Yes	Yes	Yes	Yes
$T(\mathbb{K})$	Yes	No	No	No

[a] A geometrical characterization is called economical if it requires the specification of less than 10^{12} numbers. The parameter $\bar{\phi}, \ldots,$ stands for porosity and other numbers defined in Section III.A.1. The correlation functions $S_n(\mathbf{r})$ and $C_n(\mathbf{r})$ are discussed in Section III.A.2. The pore size distribution of mercury porosimetry $\Pi(r)$ is defined in Section III.A.3. The local porosity distributions $\mu(\phi)$ are discussed in Section III.A.5. The capacities $T(\mathbb{K})$ are defined in Section III.A.6.

which gives the volume fraction of pore space. Here $V_3(\mathbb{P})$ denotes the volume of the pore space defined in Eq. (2.3) and $V_3(\mathbb{S})$ is the total sample volume. In the following, the shorthand notation $V(\mathbb{G}) = V_3(\mathbb{G})$ will often be employed.

The definition (3.1) is readily extend to stochastic porous media. In that case $V(\mathbb{P})$ and ϕ are random variables. If the medium is stationary, then one finds using Eqs. (2.3) and (2.11)

$$\begin{aligned}
\langle \phi \rangle &= \frac{\langle V(\mathbb{P}) \rangle}{V(\mathbb{S})} \\
&= \frac{1}{V(\mathbb{S})} \left\langle \int_{\mathbb{S}} \chi_{\mathbb{P}}(\mathbf{r})\, d^3\mathbf{r} \right\rangle \\
&= \frac{1}{V(\mathbb{S})} \int_{\mathbb{S}} \langle \chi_{\mathbb{P}}(\mathbf{r}) \rangle\, d^3\mathbf{r} \\
&= \frac{1}{V(\mathbb{S})} \int_{\mathbb{S}} \Pr\{\mathbf{r} \in \mathbb{P}\}\, d^3\mathbf{r} \\
&= \Pr\{\mathbf{r}_0 \in \mathbb{P}\} = \langle \chi_{\mathbb{P}}(\mathbf{r}_0) \rangle
\end{aligned} \tag{3.2}$$

where the last line holds only if the medium is stationary. The vector $\mathbf{r}_0$ in the last line is an arbitrary point. Although the use of the expectation value $\langle \cdots \rangle$ from Eq. (2.11) requires an underlying discretization, a

continuous notation was used to indicate that the result holds also in the continuous case. If the stochastic porous medium is not only stationary but also *mixing* or *ergodic*, and if it can be thought of as being infinitely extended, then the limit

$$\bar{\phi} = \lim_{R(\mathbb{S})\to\infty} \phi(\mathbb{S}) = \langle \phi \rangle \tag{3.3}$$

exists and equals $\langle \phi \rangle$. Here the *diameter* $R(\mathbb{G})$ of a set $\mathbb{G}$ is defined as $R(\mathbb{G}) = \sup\{|\mathbf{r}_1 - \mathbf{r}_2| : \mathbf{r}_1, \mathbf{r}_2 \in \mathbb{G}\}$, the supremum of the distance between pairs of points. The notation $\bar{\phi} = \overline{\chi_{\mathbb{P}}(\mathbf{r})}$ indicates a spatial average while $\langle \phi \rangle = \langle \chi_{\mathbb{P}}(\mathbf{r}) \rangle$ is a configurational average.

Equation (3.3) always represents an idealization. Geological porous media, for example, are often *heterogeneous on all scales* [5]. This means that their composition or volume fraction $\phi(R(\mathbb{S}))$ does not approach a limit for $R(\mathbb{S}) \to \infty$. Equation (3.3) assumes the existence of a length scale beyond which fluctuations of the porosity decrease. This scale is used traditionally to define so-called "representative elementary volumes" [5, 76]. The problem of macroscopic heterogeneity is related to the remarks in the discussion of stationarity in Section II.B.2. It will be taken up again in Section III.A.5.

The definition of porosity in Eq. (3.1) gives the so-called *total porosity*, which has to be distinguished from the *open porosity* or *effective porosity*. Open porosity is the ratio of accessible pore volume to total volume. Accessible means connected to the surface of the sample.

The porosity of a simple porous medium $\mathbb{S} = \mathbb{P} \cup \mathbb{M}$ is related to the bulk density $\rho_{\mathbb{S}}$, the density of the matrix material $\rho_{\mathbb{M}}$, and the density of the pore space material $\rho_{\mathbb{P}}$ through

$$\phi = \frac{\rho_{\mathbb{M}} - \rho_{\mathbb{S}}}{\rho_{\mathbb{M}} - \rho_{\mathbb{P}}} \tag{3.4}$$

Therefore, porosity is conveniently determined from measuring densities using liquid buoyancy or gas expansion porosimetry [1–3, 77]. Other methods of measuring porosity include small angle neutron, small angle X-ray scattering, and quantitative image analysis for total porosity [2, 43, 44, 77, 78]. Open porosity may be obtained from xylene and water impregnation, liquid-metal impregnation, nitrogen adsorption, and air or helium penetration [44, 77].

Porosity in rocks originates as *primary porosity* during sedimentation or organogenesis and as *secondary porosity* at later stages of the geological development [1]. In sedimentary rocks the porosity is further classified as intergranular porosity between grains, intragranular or

intercrystalline porosity within grains, fracture porosity caused by mechanical or chemical processes, and cavernous porosity caused by organisms or chemical processes.

b. Specific Internal Surface Area. Similar to the porosity the specific internal surface area is an important geometric characteristic of porous media. In fact, a porous medium may be loosely defined as a medium with a large "surface to volume" ratio. The specific internal surface area is a quantitative measure for the surface/volume ratio. Often this ratio is so large that it has been idealized as infinite [43, 78–85] and the application of fractal concepts has found much recent attention [42, 58, 84, 86–91].

The *specific internal surface* S of a two-component porous medium is defined as

$$S = \frac{V_2(\partial \mathbb{P})}{V_3(\mathbb{S})} \tag{3.5}$$

where $V_2(\partial \mathbb{P})$ is the surface area, defined in Eq. (2.3), of the boundary set $\partial \mathbb{P}$. The surface area $V_2(\partial \mathbb{P})$ exists only if the internal surface or interface $\partial \mathbb{P}$ fulfills suitable smoothness requirements. Fractal surfaces would have $V_2(\partial \mathbb{P}) = \infty$ and in such cases it is necessary to replace the Lebesgue measure in Eq. (2.3) with the Hausdorff measure or another suitable measure of the "size" of $\partial \mathbb{P}$ [58–61].

The specific internal surface is a characteristic inverse length giving the surface/volume ratio of a porous medium. Typical values for unconsolidated sand are $2 \times 10^4\ \mathrm{m}^{-1}$, and range from 10^5 to $10^7\ \mathrm{m}^{-1}$ for sandstones [3, 92]. A piece of sandstone measuring 10 cm on each side and having a specific internal surface of $10^7\ \mathrm{m}^{-1}$ contains the same area as a sports arena of dimensions 100×100 m. This illustrates the importance of surface effects for all physical properties of porous media.

Specific internal surface area can be measured by similar techniques as porosity. Some commonly employed methods are given in Fig. 1 together with their ranges of applicability. Particularly important methods are based on physisorption isotherms [93, 94]. The interpretation of the BET-method [93] is restricted to certain types of isotherms, and its interpretation requires considerable care. In particular, if micropores are present these will be filled spontaneously and application of the BET-analysis will lead to wrong results [44]. Other methods to determine S measure the two-point correlation function. As discussed further in Section II.A.2 the specific internal surface area can for statistically

homogeneous media be deduced from the slope of the correlation function at the origin [95].

2. *Correlation Functions*

Porosity and specific internal surface area are merely two numbers characterizing the geometric properties of a porous medium. Obviously, these two numbers are not sufficient for a full statistical characterization of the system. A full characterization can be given in terms of multipoint correlation functions [6, 8, 96–112].

The average porosity $\langle \phi \rangle$ of a stationary two-component porous medium is given by Eq. (3.2) as

$$\langle \phi \rangle = \langle \chi_{\mathbb{P}}(\mathbf{r}_0) \rangle = \Pr\{\mathbf{r}_0 \in \mathbb{P}\} \tag{3.6}$$

in terms of the expectation value of the random variable $\chi_{\mathbb{P}}(\mathbf{r}_0)$ taking the value 1 if the point $\mathbf{r}_0$ lies in the pore space and 0 if not. This is an example of a so-called one-point function. An example of a two-point function is the *covariance function* $C_2(\mathbf{r}_0, \mathbf{r})$, defined as the covariance of two random variables $\chi_{\mathbb{P}}(\mathbf{r})$ and $\chi_{\mathbb{P}}(\mathbf{r}_0)$ at two points $\mathbf{r}_0$ and $\mathbf{r}$,

$$C_2(\mathbf{r}_0, \mathbf{r}) = \langle [\chi_{\mathbb{P}}(\mathbf{r}_0) - \langle \chi_{\mathbb{P}}(\mathbf{r}_0) \rangle][\chi_{\mathbb{P}}(\mathbf{r}) - \langle \chi_{\mathbb{P}}(\mathbf{r}) \rangle] \rangle \,. \tag{3.7}$$

For a stationary medium the covariance function depends only on the difference $\mathbf{r} - \mathbf{r}_0$, which allows to set $\mathbf{r}_0 = \mathbf{0}$ without loss of generality. This gives

$$C_2(\mathbf{r}) = \langle \chi_{\mathbb{P}}(\mathbf{0}) \chi_{\mathbb{P}}(\mathbf{r}) \rangle - \langle \phi \rangle^2 \tag{3.8}$$

Because $\chi^2_{\mathbb{P}}(\mathbf{r}) = \chi_{\mathbb{P}}(\mathbf{r})$ it follows that $C_2(\mathbf{0}) = \langle \phi \rangle (1 - \langle \phi \rangle)$. The *correlation coefficient* of two random variables X and Y is in general defined as the ratio of the covariance $\mathrm{cov}(X, Y)$ to the two standard deviations of X and Y [73, 74]. It varies between 1 and -1 corresponding to complete correlation or anticorrelation. The covariance function is often normalized analogous to the correlation coefficient by division with $C_2(\mathbf{0})$ to obtain the *two-point correlation function*

$$G_2(\mathbf{r}) = \frac{C_2(\mathbf{r})}{C_2(\mathbf{0})} = \frac{C_2(\mathbf{r})}{\langle \phi \rangle (1 - \langle \phi \rangle)} \tag{3.9}$$

An illustration of a two-point correlation function can be seen in Fig. 14. The porosity in Eq. (3.6) is an example of a moment function. The

general nth *moment function* is defined as

$$S_n(\mathbf{r}_1, \ldots, \mathbf{r}_n) = \left\langle \prod_{i=1}^{n} [\chi_{\mathbb{P}}(\mathbf{r}_i)] \right\rangle \tag{3.10}$$

where the average is defined in Eq. (2.11) with respect to the probability density of microstructures given in Eq. (2.10). The covariance function in Eqs. (3.7) or (3.8) is an example of a *cumulant function* (also known as Ursell or cluster functions in statistical mechanics). The nth cumulant function is defined as

$$C_n(\mathbf{r}_1, \ldots, \mathbf{r}_n) = \left\langle \prod_{i=1}^{n} [\chi_{\mathbb{P}}(\mathbf{r}_i) - \langle \chi_{\mathbb{P}}(\mathbf{r}_i) \rangle] \right\rangle = \left\langle \prod_{i=1}^{n} [\chi_{\mathbb{P}}(\mathbf{r}_i) - \langle \phi \rangle] \right\rangle \tag{3.11}$$

where the second quality assumes stationarity. The cumulant functions are related to the moment functions. For $n = 1$, 2, or 3 one has the relations

$$C_1(\mathbf{r}_1) = 0 \tag{3.12}$$

$$C_2(\mathbf{r}_1, \mathbf{r}_2) = S_2(\mathbf{r}_1, \mathbf{r}_2) - S_1(\mathbf{r}_1) S_1(\mathbf{r}_2) \tag{3.13}$$

$$\begin{aligned} C_3(\mathbf{r}_1, \mathbf{r}_2, \mathbf{r}_3) = {} & S_3(\mathbf{r}_1, \mathbf{r}_2, \mathbf{r}_3) - S_2(\mathbf{r}_1, \mathbf{r}_2) S_1(\mathbf{r}_3) - S_2(\mathbf{r}_1, \mathbf{r}_3) S_1(\mathbf{r}_2) \\ & - S_2(\mathbf{r}_2, \mathbf{r}_3) S_1(\mathbf{r}_1) + 2 S_1(\mathbf{r}_1) S_1(\mathbf{r}_2) S_1(\mathbf{r}_3) \end{aligned} \tag{3.14}$$

The analogous moment functions may be defined for the matrix space $\mathbb{M}$ by replacing $\chi_{\mathbb{P}}$ in all formulas with $\chi_{\mathbb{M}}$. These functions have been called n-point matrix probability functions [105, 107] or simply correlation functions [111]. From Eqs. (2.10), (2.11) and (3.10) the probabilistic meaning of the moment functions is found as

$$S_n(\mathbf{r}_1, \ldots, \mathbf{r}_n) = \langle \chi_{\mathbb{P}}(\mathbf{r}_1) \cdot \ldots \cdot \chi_{\mathbb{P}}(\mathbf{r}_n) \rangle = \Pr\{\mathbf{r}_1 \in \mathbb{P}, \ldots, \mathbf{r}_n \in \mathbb{P}\} \tag{3.15}$$

Therefore $S_n(\mathbf{r}_1, \ldots, \mathbf{r}_n)$ is the probability that all the points $\mathbf{r}_1, \ldots, \mathbf{r}_n$ fall into the pore space.

The case $n = 2$ of the second moment is of particular interest. If the pore space is stationary and isotropic then $S_2(\mathbf{r}) = S_2(|\mathbf{r}|)$ and one has $S_2(0) = \langle \phi \rangle$. If the porous medium is also mixing then $S_2(\infty) = \langle \phi \rangle^2$. If the pore space $\mathbb{P}$ is three dimensional, and does not contain flat two-dimensional surfaces of zero thickness, then its derivative at the origin is

related to the specific internal surface area S through

$$S_2'(0) = \frac{dS_2(r)}{dr}\bigg|_{r=0} = -\frac{S}{4} \tag{3.16}$$

In two dimensions an analogous formula holds in which S is replaced with a "specific internal length" and the denominator 4 is replaced with π.

The practical measurement of two-point correlation functions is based on Minkowski addition and subtraction of sets [10, 37]. The *Minkowski addition* of two sets $\mathbb{A}$ and $\mathbb{B}$ in $\mathbb{R}^d$ is defined as the set

$$\mathbb{A} \oplus \mathbb{B} = \{\mathbf{q} + \mathbf{r} : \mathbf{q} \in \mathbb{A}, \mathbf{r} \in \mathbb{B}\} \tag{3.17}$$

Note that $\mathbb{A} \oplus \{\mathbf{r}\} = \mathbb{A} + \mathbf{r}$ is the translation defined in Eq. (2.17). Therefore $\mathbb{A} \oplus \mathbb{B} = \cup_{\mathbf{q} \in \mathbb{B}} (\mathbb{A} + \mathbf{q}) = \cup_{\mathbf{r} \in \mathbb{A}} (\mathbb{B} + \mathbf{r})$ is the union of the translates $(\mathbb{B} + \mathbf{r})$ as $\mathbf{r}$ runs through $\mathbb{A}$. The dual operation to Minkowski addition is *Minkowski subtraction* defined as

$$\mathbb{A} \ominus \mathbb{B} = \bigcap_{\mathbf{q} \in \mathbb{B}} (\mathbb{A} + \mathbf{q}) = C(C\mathbb{A} \oplus \mathbb{B}) \tag{3.18}$$

where $C\mathbb{A}$ denotes the complement of $\mathbb{A}$. With these definitions the two-point function is given as

$$S_2(\mathbf{r}) = \Pr\{\mathbf{0} \in \mathbb{P}, \mathbf{r} \in \mathbb{P}\} = \Pr\{\mathbf{0} \in \mathbb{P} \ominus (-\mathbb{B})\} \tag{3.19}$$

where $\mathbb{B} = \{\mathbf{0}, \mathbf{r}\}$ is the set consisting of the origin and the point $\mathbf{r}$. This formula is the basis for the statistical estimation of $S_2(\mathbf{r})$ and $G_2(\mathbf{r})$ in image analyzers from the area of the "eroded" set $\mathbb{P} \ominus (-\mathbb{B})$. The operation $\mathbb{P} \rightarrow \mathbb{P} \ominus (-\mathbb{B})$ is called *erosion* of the set $\mathbb{P}$ with the set $\mathbb{B}$ and it has been used in methods to define pore size distributions, which will be discussed in Section III.A.3. An example for the erosion of a pore space image by a set $\{\mathbf{0}, \mathbf{r}\}$ is shown in Fig. 9. The original image (shown Fig. 12) is obtained from a cross-section micrograph of a Savonnier oolithic sandstone. Two copies of the image are displaced relative to each other by a vector $\mathbf{r}$ as indicated in Fig. 3.1. The two images are rendered in gray, and their intersection is colored black. The area of the intersection is an estimate for $S_2(\mathbf{r})$.

The main advantage of the correlation function method for characterizing porous media is that it provides a set of well-defined functions of increasing complexity for the geometric description. In practice, one truncates the hierarchy of correlation functions at the two-point functions. While this provides much more information about the geometry than the porosity and specific surface area alone, many important

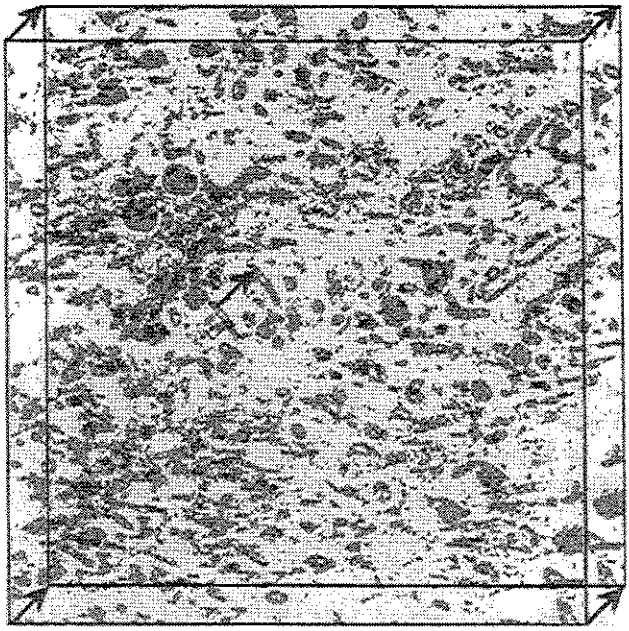

Figure 9. Erosion of a pore space image by the set $\{\mathbf{0}, \mathbf{r}\}$ consisting of the origin $\mathbf{0}$ and a vector $\mathbf{r}$. The vector $-\mathbf{r}$ is shown as an arrow in the image. The overlap of the two images is rendered darker than the rest.

properties of the medium (such as its connectivity) are buried in higher order functions.[2] Depending on the required accuracy a simple two-point function for a three-dimensional stationary but anisotropic two-component medium could be specified by 10^6–10^9 data points, which would be economical according to the criterion adopted previously. An n point function with the same accuracy would require $10^{6(n-1)}$–$10^{9(n-1)}$ data points. Specifying five or higher point functions quickly becomes just as impractical as specifying a given geometry completely.

3. *"Pore Size" Distributions*

In certain porous materials, such as wood (see Fig. 5), it is natural to identify cylindrically shaped pores and to represent their disorder through a distribution of pore diameters. In other media, such as systems with

[2] Two points are called connected if there exists a path between them that lies completely inside the pore space. Therefore the probabilistic description of connectedness properties requires multipoint correlation functions involving all the points that make up the path.

cavernous or oomoldic porosity, it is possible to identify roughly convex pore bodies analogous to convex sand grains dispersed in a uniform background. If the radius R of the cylindrical capillaries or spherical pore bodies in such media is randomly distributed, then the *pore size distribution* $\Pi(r)$ can be defined as

$$\Pi(r) = \Pr\{R \leq r\} \tag{3.20}$$

giving the probability that the random radius R of the cylinders or spheres is smaller than r. For general porous microstructures, however, it is difficult to define "pores" or "pore bodies," and the concept of pore size distribution remains ill defined.

Nevertheless many authors have introduced a variety of well-defined probability distributions of length for arbitrary media which intended to overcome the stated difficulty [2, 3, 113–119]. The concept of pore size distributions enjoys continued popularity in most fields dealing with porous materials. Recent examples can be found in chromatography [120, 121], membranes [122–124], polymers [125], ceramics [126–129], silica gels [130–132], porous carbon [133, 134], cements [135–137], rocks and soil science [138–143], fuel research [144], separation and adhesion technology [30, 145], or food engineering [146]. The main reasons for this popularity are adsorption measurements [30, 147, 148] and mercury porosimetry [149–152].

a. Mercury Porosimetry. The "pore size distribution" of mercury porosimetry is not a geometric but a physical characteristic of a porous medium. Mercury porosimetry is a transport and relaxation phenomenon [43, 153], and its discussion would find a more appropriate place in Section V. On the other hand "pore size distributions" are routinely measured in practice using mercury porosimetry, and many readers will expect its discussion in a section on pore size distributions. Therefore, pore size distributions from mercury porosimetry are discussed already here together with other definitions of this important concept.

Mercury porosimetry is based on the fact that mercury is a strongly nonwetting liquid on most substrates, and that it has a high surface tension. To measure the "pore size distribution" a porous sample $\mathbb{S}$ with pore space $\mathbb{P}$ is evacuated inside a pycnometer pressure chamber at elevated temperatures and low pressures [43]. Subsequently, the sample is immersed into mercury and an external pressure is applied. As the pressure is increased, mercury is injected into the pore space occupying a subset $\mathbb{P}_{\mathrm{Hg}}(P)$ of the pore space which depends on the applied external pressure P. The experimenter records the injected volume of mercury

$V(\mathbb{P}_{Hg}(P))$ as a function of the applied external pressure. If the volume of the pore space $V(\mathbb{P})$ is known independently then this gives the saturation $S_{Hg}(P) = V(\mathbb{P}_{Hg}(P))/V(\mathbb{P})$ as a function of pressure. The cumulative "pore size" distribution function $\Pi_{Hg}(r) = \Pr\{R \leq r\}$ of mercury porosimetry is now defined by

$$\Pi_{Hg}(r) = 1 - S_{Hg}\left(\frac{2\sigma_{Hg}\cos\theta}{r}\right) \tag{3.21}$$

For rocks a contact angle $\theta_{Hg} \approx 135°$ and surface tension with a vacuum of $\sigma_{Hg} \approx 0.48\,\mathrm{Nm}^{-1}$ are commonly used [1, 43, 153]. The definition of $\Pi_{Hg}(r)$ is based on the equation

$$P_{cap} = \frac{2\sigma_{Hg}\cos\theta}{r} \tag{3.22}$$

for the capillary pressure P_{cap}, which expresses the force balance in a single cylindrical capillary tube. Equation (3.21) follows from Eq. (3.22) if it is assumed that the saturation history $S_{Hg}(P)$ is identical to that obtained from the so-called capillary tube model discussed in Section III.B.1. The capillary tube model is a hypothetical porous medium consisting of parallel nonintersecting cylindrical capillaries of random diameter.

The fact that $\Pi_{Hg}(r)$ is not a geometrical quantity but a capillary pressure function for drainage is obvious from its definition. It depends on physical properties such as the nature of the injected fluid or wetting properties of the walls. For a suitable choice of tube diameter the function $S_{Hg}(P)$ of pressure could equally well be translated into a distribution of the wetting angles θ. The parameter $S_{Hg}(P)$ shows hysteresis implying that the pore size distribution $\Pi_{Hg}(r)$ is process dependent.

Although $\Pi_{Hg}(r)$ is not a geometrical quantity, it contains much useful information about the microstructure of the porous sample. An example for the information obtained from mercury porosimetry is shown in Fig. 10 together with an image of the rock for which it was measured [1].[3] The rock is an example of a medium with hollow pores. The correct interpretation of the saturation history $S_{Hg}(P)$ obtained from mercury porosimetry continues to be an active research topic [154–160].

b. Random Point Methods. Several authors [3, 113, 116] suggest defining the "pore size" by first choosing a point $\mathbf{r} \in \mathbb{P}$ at random in the pore

[3] 1 MPa = 10 bar = 10^7 dyn cm^{-2} = 9.869 atm = 145.04 psi.

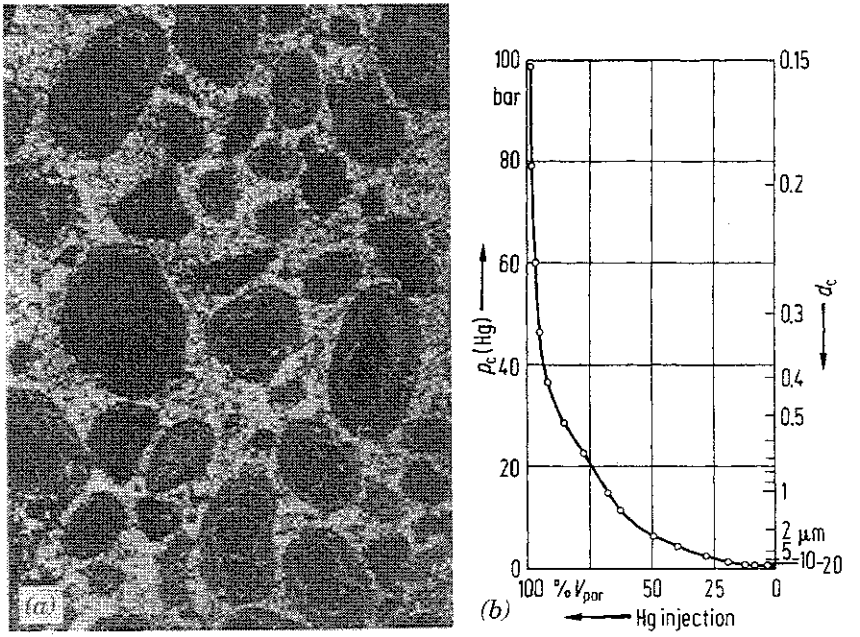

Figure 10. (*a*) Crossed nicols image of Dolomite oncolithe. The image width corresponds to 2.3 mm. The porosity is 11%, the permeability 11 md. (*b*) Capillary pressure curve for the rock shown in the image. The right axis shows the "pore size" scale. (Reproduced with permission from J. Schopper, "Porosität und Permeabilitat," in *Landolt–Börnstein: Physikalische Eigenschaften der Gesteine*, K.-H. Hellwege, Ed., Vol. V/1a, Springer, Berlin, 1982, p. 184. Copyright © Springer-Verlag, 1982.)

space, then choosing a compact set $\mathbb{K}$ containing $\mathbf{r}$, and finally enlarging $\mathbb{K}$ until it first intersects the matrix space $\mathbb{M}$. In its simplest version [3, 116] the set $\mathbb{K}$ is chosen as a small sphere $\mathbb{B}(\mathbf{r}, \varepsilon)$ of radius ε [see Eq. (2.5)]. Then the pore size distribution $\Pi_{rp}(x)$ of the random point method is defined as the distribution function $\Pi_{rp}(x) = \Pr\{R(\mathbf{r}) \leq x\}$ of the random variable $R(\mathbf{r})$ defined as

$$R(\mathbf{r}) = \inf\{\varepsilon : \mathbb{B}(\mathbf{r}, \varepsilon) \cap \mathbb{M} \neq \emptyset\} \tag{3.23}$$

In a deterministic porous medium, R is a random variable because $\mathbf{r} \in \mathbb{P}$ is chosen at random.

In a more sophisticated version of the same idea the set $\mathbb{K}$ is chosen as a small coordinate cross whose axes are then increased independently until they first touch the matrix space [2, 113]. This gives direction dependent pore size distributions.

The main weakness of such a definition is that it is imprecise. This

becomes apparent from the fact that the randomness of the pore sizes $R(\mathbf{r})$ does not arise from the irregularities of the pore space, but from the random placement of $\mathbf{r}$. Consider a regular pore space consisting of nonintersecting spheres of equal radii R_0 centered at the vertices of a simple (hyper)cubic lattice. Assuming that the points $\mathbf{r}$ are chosen at random with a uniform distribution it follows that the pore size distribution Π_{rp} is not given by a δ function at R_0 but instead as a uniform distribution on the interval $[0, R_0]$. More dramatically, exactly the same pore size distribution is obtained for every pore space made from nonintersecting spheres of equal radii, regardless of whether they are placed randomly or not. In addition, $\Pi_{rp}(x)$ can be changed arbitrarily by changing the distribution function governing the random placement of $\mathbf{r}$.

A more precise formulation of the same idea is possible in terms of conditional probabilities. In Section III.A.4 it will be seen that the vague ideas underlying random point methods are given a precise definition in the form of contact and chord length distributions [10, 37].

c. Erosion Methods. Another approach to the definition of a geometrical pore size distribution [117–119] is borrowed from the erosion operation in image processing [161, 162]. Erosion is defined in terms of Minkowski addition and subtraction of sets introduced above in Eqs. (3.17) and (3.18). The *erosion* of a set $\mathbb{A}$ by a set $\mathbb{B}$ is defined as the map $\mathbb{A} \to \mathbb{A} \ominus (-\mathbb{B}) = \cap_{\mathbf{q} \in \mathbb{B}} (\mathbb{A} - \mathbf{q})$. The erosion was illustrated in Fig. 9 for a pore space image and a set $\mathbb{B} = \{\mathbf{0}, \mathbf{r}\}$.

The method for locating "pore chambers," "pore channels," and "pore throats" suggested in [117] is based on eroding the matrix space $\mathbb{M}$ of a two component porous medium. A ball $\mathbb{B}(\mathbf{0}, \varepsilon)$ is chosen as the structuring element. The erosion $\mathbb{M} \ominus (-\mathbb{B}(\mathbf{0}, \varepsilon))$ shrinks the matrix space $\mathbb{M}$. The erosion operation is repeated until the matrix space decomposes into disconnected fragments. By continuing the erosion the pieces may either fragment again or become convex. If a piece becomes convex it is called a "grain." The centroid of the convex grain is called a "grain center." Reversing the erosion process allows one to locate the point of respectively first last contact of two fragments. Connecting neighboring grain centers by a path through their last contact point produces a network model of the grain space. After having defined a network of grain centers and last contact points, the authors of [117] and their followers [118, 119] suggest to erect contact "surfaces" in each contact point. A contact plane is defined as a "minimum area cross section" of $\mathbb{M}$. Subsequently, a ball is placed at each grain center and continually enlarged. When the enlargement encounters a surface plane the ball is truncated at the surface plane and only its nontruncated pieces continue

to grow until the sample space is completely filled with the inflated grains. The intersection points of three or more planes in the resulting tesselation of space are defined to be *pore chambers*. The intersection lines of two planes are called *pore channels*, and "minimal-area cross sections" of the pore space $\mathbb{P}$ along the pore channels are called *pore throats*. The pore throats are not unique and are sensitive to details of the local geometry. The pore chambers and channels will in general not lie in the pore space.

A drawback of this procedure is that it is less unique than it seems at first sight. The network constructed from eroding the pore space is not unique because the erosion operation involves the set $\mathbb{B}$ as a structuring element, and hence there are infinitely many erosions possible. The resulting grain network depends on the choice of the set $\mathbb{B}$, a fact that is not discussed in [117, 119]. Figure 11 shows an example where erosion with a sphere produces three grains while erosion with an ellipsoid produces only two grains. The original set consists of the gray and black region, the eroded part is coloured gray, and the residual set is colored black. The theoretically described procedure for determining the network was not carried out in practice [117]. Instead "subjective human preprocessing" ([117], p. 4158) was used to determine the network.

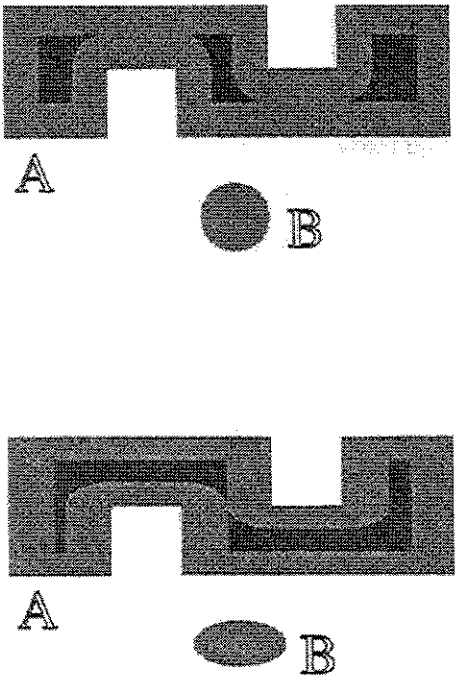

Figure 11. Erosion $\mathbb{A} \oplus (-\mathbb{B})$ of a set $\mathbb{A}$ by a set $\mathbb{B}$ for the cases where $\mathbb{B}$ is a sphere or an ellipsoid. For a sphere the eroded set (shown in black) has three components while for an ellipsoid it consists of only two connected components.

d. Hydraulic Radius Method. The hydraulic radius method [2, 114, 115] for determining pore size distributions is based on the idea of "symbolically closing pore throats." The definition of pore throats is given in terms of "cross sections" of the pore space. A cross-section $\mathbb{C}$ could be defined as the intersection of a plane $\mathbb{E}(\mathbf{q}, \mathbf{r}_0)$, characterized by its unit normal $\mathbf{q} \in \partial\mathbb{B}(\mathbf{0}, 1)$ and a point $\mathbf{r}_0$ in the plane, with the pore space $\mathbb{P}$ and some suitable set $\mathbb{G}(\mathbf{q}, \mathbf{r}_0)$ that represents the region of interest and could depend on the choice of plane. In symbols $\mathbb{C}(\mathbf{q}, \mathbf{r}_0) = \mathbb{P} \cap \mathbb{E}(\mathbf{q}, \mathbf{r}_0) \cap \mathbb{G}(\mathbf{q}, \mathbf{r}_0)$. A *pore throat containing the point* $\mathbf{r}_0$ is then defined as

$$\mathbb{C}^*(\mathbf{r}_0) = \min_{\mathbf{q} \in \partial\mathbb{B}(\mathbf{0},1)} \frac{V_2(\mathbb{C}(\mathbf{q}, \mathbf{r}_0))}{V_1(\partial\mathbb{C}(\mathbf{q}, \mathbf{r}_0))} \tag{3.24}$$

where the minimum is taken over the unit sphere of orientations of the planes. A *pore throat* is now defined as a local minimum of the function $\mathbb{C}^*(\mathbf{r}_0)$ as $\mathbf{r}_0$ is varied over the pore space. This ideal definition has in practice been replaced with a subjective choice of orientations based on the assumption of isotropy [2, 114, 115]. After constructing all pore throats of a medium the pore space becomes divided into separate compartments called "pore bodies" whose "size" can then be measured by a suitable measure such as the volume to the power one-third.

The definition of pore throats in hydraulic radius methods is very sensitive to surface roughness. This is readily seen from an idealized spherical pore with a few spikes. Another problem as remarked in [115], page 586, is that "the size of a pore body is not readily related in a unique manner to any measurable physical quantity."

4. *Contact and Chord Length Distributions*

Chord length distributions [163–166] are special cases of so-called contact distributions [10, 37]. Consider the random matrix space $\mathbb{M}$ of a two component stochastic porous medium and choose a compact set $\mathbb{K}$ containing the origin $\mathbf{0}$. Then the *contact distribution* is defined as the conditional probability

$$\begin{aligned} \Pi_{\mathbb{K}}(x) &= 1 - \Pr\{\mathbf{0} \notin \mathbb{M} \oplus (-x\mathbb{K}) | \mathbf{0} \notin \mathbb{M}\} \\ &= 1 - \frac{\Pr\{\mathbf{0} \notin \mathbb{M} \oplus (-x\mathbb{K})\}}{1 - \phi} \end{aligned} \tag{3.25}$$

for $x \geq 0$. Here ϕ denotes the bulk porosity as usual. Two special choices of the compact set $\mathbb{K}$ are of particular importance. These are the unit sphere $\mathbb{K} = \mathbb{B}(\mathbf{0}, 1) \subset \mathbb{R}^3$ and the unit interval $\mathbb{K} = [0, 1] \subset \mathbb{R}$.

For a unit sphere $\mathbb{K} = \mathbb{B}(\mathbf{0}, 1)$ the quantity $1 - \Pi_{\mathbb{B}(\mathbf{0},1)}(x)$ is the

conditional probability that a fixed point in the pore space is the center of a sphere of radius x contained completely in the pore space, under the condition that the chosen point does not belong to $\mathbb{M}$. If $\mathbb{M}$ is isotropic and its boundary is sufficiently smooth, then the specific internal surface S can be obtained from the derivative at the origin as [37]

$$S = \phi \frac{d}{dx} \Pi_{\mathbb{B}(0,1)}(x)\Big|_{x=0} \tag{3.26}$$

The spherical contact distribution $\Pi_{\mathbb{B}(0,1)}(x)$ provides a more precise formulation of the random point generation methods for pore size distributions [3, 116] discussed in Section III.A.3.b.

For the unit interval $\mathbb{K} = [0, 1]$ the contact distribution $\Pi_{[0,1]}(x)$ is related to the *chord length distribution* $\Pi_{cl}(x)$ giving the probability that an interval in the intersection of $\mathbb{P}$ with a straight line containing the unit interval has a length smaller than x. This provides a more precise formulation of the random point generation ideas in [2, 113]. The relation between the contact distribution and the chord length distribution is given by the equation

$$\Pi_{[0,1]}(x) = 1 - \frac{\int_x^\infty (y - x)\, d\Pi_{cl}(y)}{\int_0^\infty y\, d\Pi_{cl}(y)} \tag{3.27}$$

where the denominator on the right-hand side gives the mean chord length $\bar{\ell} = \int_0^\infty y\, d\Pi_{cl}(y)$. The mean chord length is related to the specific internal surface area through $\bar{\ell} = 4\phi/S$. In Section III.A.2 it was mentioned that the specific internal surface area can be obtained from the two-point function [see Eq. (3.16)]. Therefore the mean chord length can also be related to the correlation function through

$$\bar{\ell} = -\frac{\phi}{S_2'(0)} \tag{3.28}$$

Along these lines it has been suggested in [167] that the full chord length distribution can be obtained directly from small-angle scattering experiments.

Contact and chord length distributions provide much more geometrical information about the porous medium than the porosity and specific surface area, and are at the same time not as unnecessarily detailed as the complete specification of the deterministic or stochastic geometry. Depending on the demands on accuracy a contact or chord length distribution may be specified by 10–1000 numbers irrespective of the

microscopic resolution. This should be compared with 10^{24} or $2^{10^{24}}$ numbers for a fully deterministic or stochastic characterization.

5. *Local Geometry Distributions*

a. Local Porosity Distribution. Local porosity distributions, or more generally local geometry distributions, provide a well-defined general geometric characterization of stochastic porous media [168–175]. Local porosity distributions were mainly developed as an alternative to pore size distributions (see Section III.A.3). They are intimately related with the theory of finite size scaling in statistical physics [64, 176–178]. Although fluctuations in the porosities have been frequently discussed [2, 5, 10, 37, 76, 179–182], the concept of local porosity distributions and its relation with correlation functions was developed only recently [168–175]. More applications are being developed [183, 184].

Local porosity distributions can be defined for deterministic as well as for stochastic porous media. For a single deterministic porous medium consider a partitioning $\mathcal{K} = \{\mathbb{K}_1, \ldots, \mathbb{K}_M\}$ of the sample space $\mathbb{S}$ into M mutually disjoint subsets, called *measurement cells* $\mathbb{K}_j$. Thus $\cup_{j=1}^{M} \mathbb{K}_j = \mathbb{S}$ and $\mathbb{K}_i \cap \mathbb{K}_j = \emptyset$ if $i \neq j$. A particular partitioning was used in the original publications [169–171, 178], where the $\mathbb{K}_j$ are unit cells centered at the vertices of a Bravais lattice superimposed on $\mathbb{S}$. This has the convenient feature that the $\mathbb{K}_j$ are translated copies of one and the same set, and they all have the same shape. An example is illustrated in Fig. 12 showing a quadratic lattice as the measurement grid in two dimensions superposed on a thin section of an oolithic sandstone. The *local porosity* inside a measurement cell $\mathbb{K}_j$ is defined as

$$\phi(\mathbb{K}_j) = \frac{V(\mathbb{P} \cap \mathbb{K}_j)}{V(\mathbb{K}_j)} = \frac{1}{M_j} \sum_{\mathbf{r}_i \in \mathbb{K}_j} \chi_{\mathbb{P}}(\mathbf{r}_i) \tag{3.29}$$

where the second equality applies in case of discretized space and M_j denotes the number of volume elements or voxels in $\mathbb{K}_j$. Thus the *empirical one-cell local porosity density function* is defined as

$$\tilde{\mu}(\phi; \mathcal{K}) = \frac{1}{M} \sum_{j=1}^{M} \delta(\phi - \phi(\mathbb{K}_j)) \tag{3.30}$$

where $\delta(x)$ is the Dirac δ distribution. Obviously, the distribution depends on the choice of partitioning the sample space. Two extreme partitions are of immediate interest. The first arises from setting $M = N$, and thus each $\mathbb{K}_j$ contains only one individual volume element $\mathbb{K}_j = \{\mathbf{r}_j\}$ with $1 \leq j \leq M = N$. In this case $\phi(\mathbb{K}_j) = 0$ or $\phi(\mathbb{K}_j) = 1$, depending on

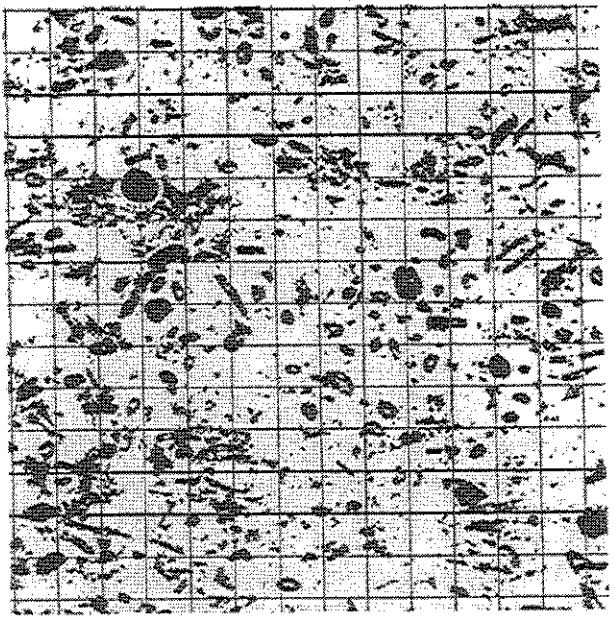

Figure 12. Measurement lattice of squares superimposed on the discretized thin section image of a sandstone. The pore space $\mathbb{P}$ is colored black, the matrix space is rendered white.

whether the volume element falls into matrix space (0), or pore space (1). This immediately gives

$$\tilde{\mu}(\phi; \{\{\mathbf{r}_1\}, \ldots, \{\mathbf{r}_N\}\}) = \phi(\mathbb{S})\delta(\phi - 1) + (1 - \phi(\mathbb{S}))\delta(\phi) \quad (3.31)$$

where $\phi(\mathbb{S})$ is the total porosity. The other extreme arises for $M = 1$. In this case $\mathbb{K}_1 = \mathbb{S}$ and the measurement cell coincides with the sample space. Hence

$$\tilde{\mu}(\phi; \{\mathbb{S}\}) = \delta(\phi - \phi(\mathbb{S})) \quad (3.32)$$

Note that in both extreme cases the local porosity density is completely determined by the total porosity $\phi(\mathbb{S})$, which equals $\phi(\mathbb{S}) = \bar{\phi}$ if the sample is sufficiently large and mixing or ergodicity Eq. (3.3) holds.

For a stochastic porous medium the *one-cell local porosity density function* is defined for each measurement cell as

$$\mu(\phi; \mathbb{K}_j) = \langle \delta(\phi - \phi(\mathbb{K}_j)) \rangle \quad (3.33)$$

where $\mathbb{K}_j \in \mathcal{K}$ is an element of the partitioning of the sample space. For the finest partition with $M = N$ and $\mathbb{K}_j = \{\mathbf{r}_j\}$ one finds now using Eq. (3.2)

$$\begin{aligned}\mu(\phi; \{\mathbf{r}_j\}) &= \Pr\{X(\mathbf{r}_j) = 1\}\delta(\phi - 1) + \Pr\{X(\mathbf{r}_j) = 0\}\delta(\phi) \\ &= \langle \phi \rangle \delta(\phi - 1) + (1 - \langle \phi \rangle)\delta(\phi) \end{aligned} \tag{3.34}$$

independent of j. If mixing Eq. (3.3) holds, then $\phi(\mathbb{S}) = \langle \phi \rangle = \bar{\phi}$ if the sample becomes sufficiently large, and the result becomes identical to Eq. (3.31) for deterministic media. In the other extreme of the coarsest partition one finds

$$\mu(\phi; \mathbb{S}) = \langle \delta(\phi - \phi(\mathbb{S})) \rangle \tag{3.35}$$

which may in general differ from Eq. (3.32) even if the sample becomes sufficiently large, and mixing holds. This is an important observation because it emphasizes the necessity to consider more carefully the infinite volume limit $\mathbb{S} \to \mathbb{R}^d$.

If a large deterministic porous medium is just a realization of a stochastic medium obeying the mixing property, and if the sets $\mathbb{K}_j$ are chosen such that the random variables $\phi(\mathbb{K}_j)$ are independent, then Gliwenkos theorem [185] of mathematical statistics guarantees that the empirical one-cell distribution approaches $\mu(\phi; \mathbb{K})$ in the limit $M \to \infty$. In symbols

$$\lim_{M \to \infty} \tilde{\mu}(\phi; \mathcal{K}) = \mu(\phi; \mathbb{K}_j) \tag{3.36}$$

where the right-hand side is independent of the choice of $\mathbb{K}_j$. Therefore μ and $\tilde{\mu}$ are identified in the following. This identification emerges also from considering average and variance as shown next.

Define the *average local porosity* $\bar{\phi} = \int_0^1 \phi \mu(\phi)\, d\phi$ as the first moment of the local porosity distribution. For a stationary (=homogeneous) porous medium the definitions (3.33) and (3.29) immediately yield

$$\begin{aligned}\overline{\phi(\mathbb{K}_j)} &= \int_0^1 \phi \mu(\phi; \mathbb{K}_j)\, d\phi \\ &= \langle \phi(\mathbb{K}_j) \rangle \\ &= \frac{1}{M_j} \sum_{\mathbf{r}_i \in \mathbb{K}_j} \langle \chi_{\mathbb{P}}(\mathbf{r}_i) \rangle \\ &= \langle \phi \rangle \end{aligned} \tag{3.37}$$

where $\mathbb{K}_j$ is a measurement cell. Similarly, the variance of local porosities reads

$$\begin{aligned}\overline{(\phi(\mathbb{K}_j)-\overline{\phi(\mathbb{K}_j)})^2} &= \int_0^1 [\phi-\overline{\phi(\mathbb{K}_j)}]^2 \mu(\phi;\mathbb{K}_j)\,d\phi \\ &= \int_0^1 \phi^2 \langle \delta(\phi-\phi(\mathbb{K}_j))\rangle\,d\phi - \bar{\phi}^2 \\ &= \langle \phi(\mathbb{K}_j)^2\rangle - \langle \phi(\mathbb{K}_j)\rangle^2 \\ &= \frac{1}{M_j^2}\left\langle \left[M_j\phi - \sum_{i=1}^{M_j} \chi_{\mathbb{P}}(\mathbf{r}_i)\right]^2 \right\rangle \\ &= \frac{\langle\phi\rangle}{M_j}(1-\langle\phi\rangle) + \frac{2}{M_j^2} \sum_{\substack{i\neq k \\ r_i,r_k\in\mathbb{K}_j}} C_2(\mathbf{r}_i-\mathbf{r}_k)\,.\end{aligned} \tag{3.38}$$

This result is important for two reasons. First, it relates local porosity distributions to correlation functions discussed in Section III.A.2. Second, it shows that the variance depends inversely on the volume M_j of the measurement cell. This observation reconciles Eq. (3.35) for stochastic media with Eq. (3.32) for deterministic media because it shows that $\mu(\phi;\mathbb{K}_j)$ approaches a degenerate δ distribution in the limit $M_j\to\infty$. Together with Eq. (3.37) and $M_j = N$ and $M = 1$ for $\mathbb{K}_j = \mathbb{S}$ this shows that Eqs. (3.35) and (3.32) become equivalent.

The *n-cell local porosity density function* $\mu_n(\phi_1,\ldots,\phi_n;\mathbb{K}_1,\ldots,\mathbb{K}_n)$ is the probability density to find local porosity ϕ_1 in measurement cell $\mathbb{K}_1$, ϕ_2 in $\mathbb{K}_2$, and so on, until n. Formally, it is defined by generalizing Eq. (3.33) to read

$$\mu_n(\phi_1,\ldots,\phi_n;\mathbb{K}_1,\ldots,\mathbb{K}_n) = \langle \delta(\phi_1-\phi(\mathbb{K}_1))\cdot\cdots\delta(\phi_n-\phi(\mathbb{K}_n))\rangle \tag{3.39}$$

where the sets $\mathbb{K}_1,\ldots,\mathbb{K}_n \in \mathcal{K}$ are a subset of measurement cells in the partition $\mathcal{K}$. Note that the n-cell functions μ_n are only defined for $M > n$, that is, if there are a sufficient number of cells. In particular, for the extreme case $M = 1$ only the one-cell function is defined. In the extreme case $M = N$ of highest resolution ($\mathbb{K}_j = \{\mathbf{r}_j\}$) the moments of the n-cell local porosity distribution reproduce the moment functions (3.10) of the

correlation function approach (Section III.A.2) as

$$\begin{aligned}\overline{\phi_{i_1}\cdot\cdots\cdot\phi_{i_m}} &= \int_0^1\cdots\int_0^1 \phi_{i_1}\cdot\cdots\cdot\phi_{i_m}\mu_n(\phi_1,\ldots,\phi_n;\{\mathbf{r}_1\},\ldots,\{\mathbf{r}_n\})\\ &\quad\times d\phi_1\cdots d\phi_n\\ &= \langle\chi_{\mathbb{P}}(\mathbf{r}_{i_1})\cdot\cdots\cdot\chi_{\mathbb{P}}(\mathbf{r}_{i_m})\rangle\\ &= S_m(\mathbf{r}_{i_1},\ldots,\mathbf{r}_{i_m})\end{aligned}\tag{3.40}$$

where $m\le n$ must be fulfilled. This provides a connection between local porosity approaches and correlation function approaches. Simultaneously, it shows that the local porosity distributions are significantly more general than correlation functions. Already the one-cell function μ contains more information than the two-point correlation functions S_2 or C_2 as demonstrated on test images in [171].

The most important practical aspect of local porosity distributions is that they are easily measurable in an independent experiment. Experimental determinations of local porosity distributions have been reported in [173–175, 186]. They were obtained from two-dimensional sections through a sample of sintered glass beads. An example from [175] is shown in Fig. 13. The porous medium was made from sintering glass beads of roughly 250 μm diameter. Scanning electron migrographs obtained from the specimen were then digitized with a spatial resolution of 4.1 μm per pixel. The pore space is represented by black in Fig. 13 and the total porosity is $\bar{\phi}=10.7\%$. The pixel–pixel correlation function of the pore space image is shown in Fig. 14. The local porosity distribution was then measured using a square lattice with lattice constant L. The results are shown in Fig. 15 for measurement cell sizes of $L=40$, 50, 60 and $L=80$ pixels.

Measurements of the local porosity distribution from three-dimensional pore space images are currently carried out [183]. The pore space is reconstructed from serial sections that are a standard, but costly, technique to obtain three-dimensional pore space representations [2, 113, 114, 117, 162, 183, 188]. The advent of synchrotron microtomography [4, 119, 188a] promises to reduce the cost and effort.

b. Local Geometry Entropies. The linear extension L of the measurement cells is the length scale at which the pore space geometry is described. The length L can be taken as the side length of a hypercubic measurement cell, or more generally as the diameter $R(\mathbb{K})=\sup\{|\mathbf{r}_1-\mathbf{r}_2|:\mathbf{r}_1,\mathbf{r}_2\in\mathbb{K}\}$ of a cell $\mathbb{K}$ defined as the supremum of the distance

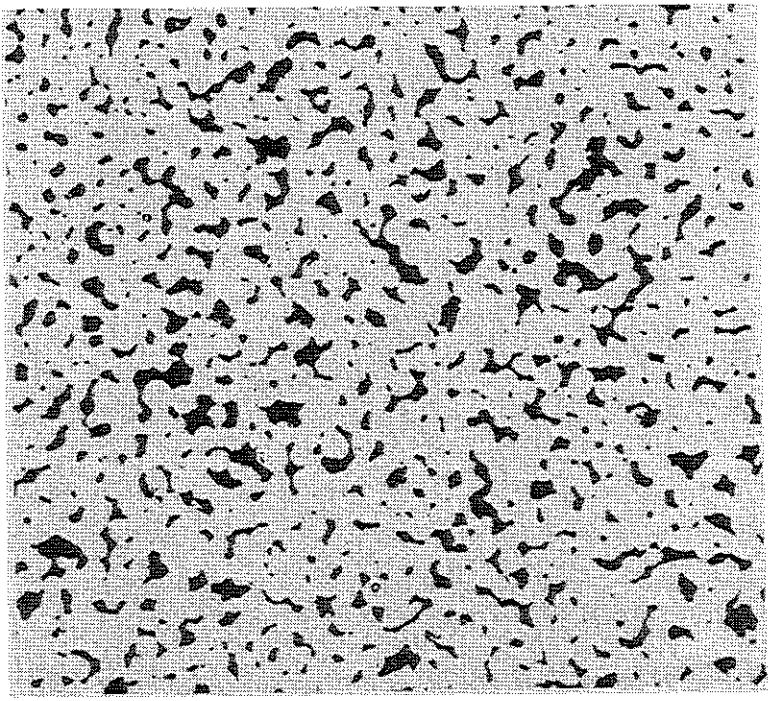

Figure 13. Pore space image of sintered 250-μm glass beads with total porosity of 10.7%. The pore space is rendered in black, the matrix space in white.

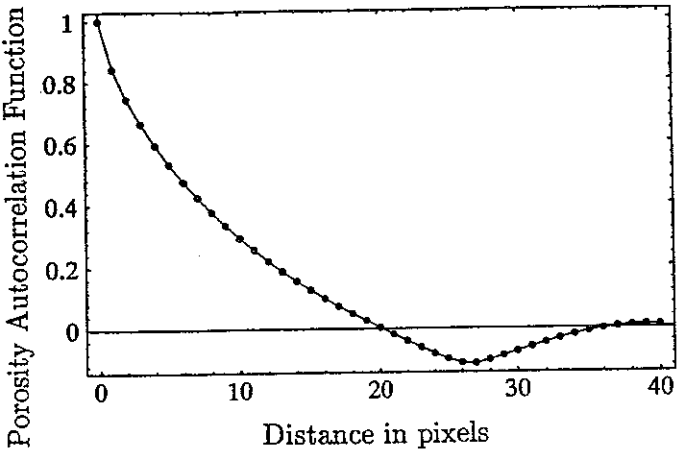

Figure 14. Pixel–pixel porosity correlation function $G_2(r)$ for the image shown in Fig. 13. The distance r is measured in pixels corresponding to 4.1 μm per pixel [175].

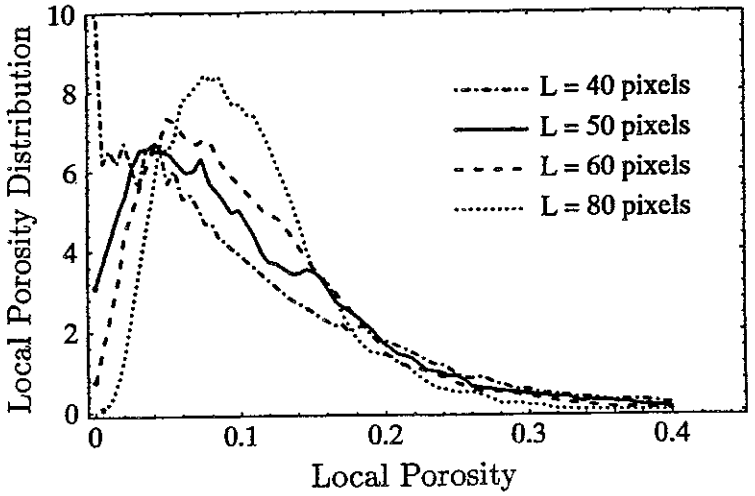

Figure 15. Local porosity probability density function $\mu(\phi; L)$ measured from square shaped measurement cells from the image shown in Fig. 13. The dash–dotted line corresponds to $L = 40$ pixels, the solid line to $L = 50$, the dashed line to $L = 60$ and the dotted line to $L = 80$ pixels. One pixels corresponds to 4.1 μm [175]

between pairs of points. As $L \to \infty$ the local porosity distribution approaches a δ distribution concentrated at $\bar{\phi}$ according to Eqs. (3.32) and (3.35). On the other hand, for $\ell \to 0$ it approaches two δ distributions concentrated at 0 and 1 according to Eqs. (3.31) and (3.34). In both limits the local porosity distribution contains only the bulk porosity $\bar{\phi} = \langle \phi \rangle = \phi(\mathbb{S})$ as a geometric parameter. At intermediate scales the distribution contains additional information, such as the variance of the porosity fluctuations. This suggests a search for an intermediate scale L^*, which provides an optimal description. Several criteria for determining L^* were discussed in [171]. One interesting possibility is to optimize an information measure or entropy associated with $\mu(\phi; L)$ and to define the entropy function

$$I(L) = \int_0^1 \mu(\phi; L) \log \mu(\phi; L)\, d\phi \tag{3.41}$$

relative to the conventional a priori uniform distribution. The so-called entropy length is then obtained from the extremality condition

$$\left. \frac{d\mu(\phi; L)}{dL} \right|_{L=L^*} = 0 \tag{3.42}$$

That the entropy length L^* exists and is well defined was first demon-

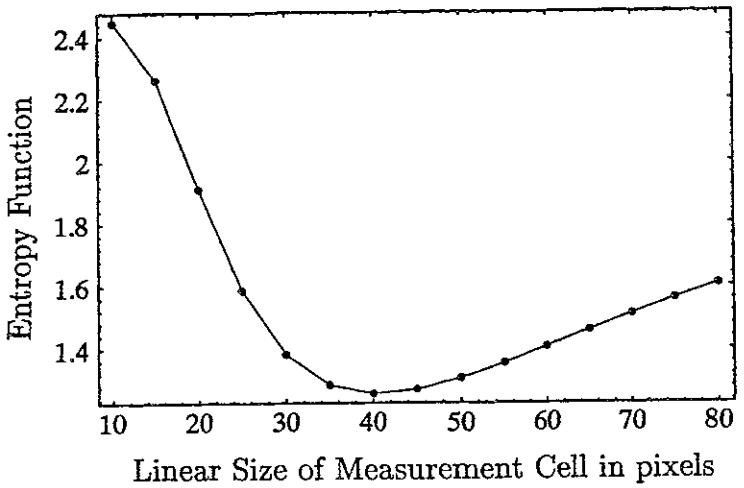

Figure 16. Entropy function as a function of the linear size of the measurement cell in pixels for the local porosity probability density functions obtained from the image shown in Fig. 13. One pixel corresponds to 4.1 μm [175].

strated in [171] using synthetic computer generated images. Figure 16 shows the function $I(L)$ calculated for the image displayed in Figure 13. A clear minimum appears at $L \approx 40$ pixels corresponding to 164 μm.

A similar entropy analysis was recently discussed in [189] for thin-film morphologies of composites. The entropy function $H^*(L)$ defined in [189] is not equivalent to $I(L)$ above because it is not additive. Nevertheless, it was recently found [184] that $H^*(L)$ and $I(L)$ give the same value of L^*.

c. Local Specific Internal Surface Distributions. Local specific internal surface area distributions are a natural generalization of local porosity distributions. They were first introduced in [171] in the study of fluid transport in porous media. Define the local specific internal surface area in a cell $\mathbb{K}_j$ as

$$S(\mathbb{K}_j) = \frac{V_2(\partial\mathbb{P} \cup \mathbb{K}_j)}{V_3(\mathbb{K}_j)} = \frac{1}{M_j} \sum_{\mathbf{r}_i \in \mathbb{K}_j} \chi_{\partial\mathbb{P}}(\mathbf{r}_i) \tag{3.43}$$

which is analogous to Eq. (3.29). Generalizing Eqs. (3.30) and (3.33) the *local specific internal surface area probability density* is defined as

$$\mu(S; \mathbb{K}_j) = \langle \delta(S - S(\mathbb{K}_j)) \rangle \tag{3.44}$$

in analogy with Eq. (3.33). The joint probability density $\mu(\phi, S; \mathbb{K}_j)$ to find a local porosity ϕ and local specific internal surface areas in the range ϕ to $\phi + d\phi$ and S to $S + dS$ will be called *local geometry distribution*. It is defined as the probability density

$$\mu(\phi, S; \mathbb{K}_j) = \langle \delta(\phi - \phi(\mathbb{K}_j))\, \delta(S - S(\mathbb{K}_j)) \rangle \tag{3.45}$$

The average specific internal surface area in a measurement region $\mathbb{K}$ is then obtained from the local geometry distribution as

$$\overline{S(\mathbb{K})} = \int_0^\infty \int_0^\infty S\mu(\phi, S; \mathbb{K})\, d\phi\, dS \tag{3.46}$$

and it represents an important local length scale.

Of course, local geometry distributions can be extended to include other well-defined geometric characteristics such as mean curvature or topological invariants. The definition of the generalized local geometry distribution is then obtained by generalizing Eq. (3.45).

d. Local Percolation Probability. In addition to the local porosity distributions and local specific internal surface area distributions it is necessary to characterize the geometrical connectivity properties of a porous medium. This is important for discussing transport properties that depend critically on the connectedness of the pore space, but are less sensitive to its overall porosity or specific internal surface.

Two points inside the pore space $\mathbb{P}$ of a two-component porous medium are called *connected* if there exists a path contained entirely within the pore space which connects the two points. By using this connectivity criterion a cubic measurement cell $\mathbb{K}$ is called percolating if there exist two points on opposite surfaces of the cell which are connected to each other. The *local percolation probability* $\lambda(\phi, S; \mathbb{K})$ is defined as the probability to find a percolating geometry in a measurement cell $\mathbb{K}$ whose local porosity is ϕ and whose local specific internal surface area is S. In practice, the estimator for $\lambda(\phi, S; \mathbb{K})$ is the fraction of percolating measurement cells which have the prescribed values of ϕ and S.

The average local percolation probability defines an important global geometric characteristic

$$p(\mathbb{K}) = \int_0^\infty \int_0^1 \lambda(\phi, S; \mathbb{K})\mu(\phi, S; \mathbb{K})\, d\phi\, dS \tag{3.47}$$

which gives the *total fraction of percolating local geometries*. It will be

seen in Sections V.B.4 and V.C.6 that $p(\mathbb{K})$ is an important control parameter for the connectivity of the porous medium.

e. Large-Scale Local Porosity Distributions. This section reviews the application of recent results in statistical physics [63–69, 178, 190] to the problem of describing the *macroscopic heterogeneity on all scales*. The original definition (3.33) of the local porosity distributions depends on the size and shape of the measurement cells, that is, on the partitioning $\mathcal{K}$ of the sample space. This dependence on the choice of a test set or "structuring element" is characteristic for many methods of mathematical morphology [10, 37, 71], and many of those discussed in Sections III.A.3 and III.A.4. On the other hand, Section III.A.5.a has shown that in the limit of large measurement cells $\mathcal{R}(\mathbb{K}) \to \infty$ the form of the local porosity distribution $\mu(\phi; \mathbb{K})$ becomes independent of $\mathbb{K}$ and approaches one and the same universal limit given by $\delta(\phi - \bar{\phi})$. This behavior is an expression of the central limit theorem. Local porosity distributions have support in the unit interval, hence their second moment is always finite, and the average local porosities must become sharp in the limit. It will be seen now that this behavior is indeed characteristic for *macroscopically homogeneous* porous media, while other limiting distributions may arise for *macroscopically heterogeneous* media.

Consider a convex measurement cell $\mathbb{K}$ of volume V_0. Let b be the random scale factor at which the pore space volume $V(\mathbb{P} \cap b\mathbb{K})$ of the inflated measurement cell $b\mathbb{K}$ first exceeds V_0, that is, define b as

$$b = \inf\{c \geq 1 : V(\mathbb{P} \cap c\mathbb{K}) \geq V_0\} \tag{3.48}$$

Consider N mutually disjoint measurement cells $\mathbb{K}_i$ $(1 \leq i \leq N)$ all having the same volume $V(\mathbb{K}_i) = V_0$. Let b_i denote the scale factors associated with the cells, and let $V_i = V(\mathbb{P} \cap b_i\mathbb{K}_i)$ be the N values of the pore space volumes. If the medium is homogeneous there exists a finite correlation length beyond which fluctuations decrease. Then the nonoverlapping cells $\mathbb{K}_i$ can be chosen such that the inflated cells remain nonoverlapping, and such that they are separated more than the correlation length. Then, the N local porosities $\phi(\mathbb{K}_i) = V_0/V_i$ are uncorrelated random variables. For macroscopically heterogeneous media the correlation length may be infinite, and thus it is necessary to consider the limit $V_0 \to \infty$ of infinitely large cells to obtain uncorrelated porosities. In [63–65, 178, 190] the resulting *ensemble limit* $N, V_0 \to \infty$ has been defined and studied in detail. In the present context the ensemble limit can be used to study the limiting

distribution of the N-cell porosity

$$\phi(\mathbb{K}_1, \ldots, \mathbb{K}_N) = \frac{NV_0}{V_1 + \cdots + V_N} = N\left[\sum_{i=1}^{N} (\phi(\mathbb{K}_i))^{-1}\right]^{-1} \tag{3.49}$$

obtained from the N measurements. In the ensemble limit the N porosities $\phi(\mathbb{K}_i)$ become independent but ill defined, because $V(\mathbb{K}_i) \to \infty$. This suggests that one instead considers the limiting behavior of the renormalized sums of positive random variables

$$\varphi_N = \frac{1}{D_N}\left(\sum_{i=1}^{N} (\phi(\mathbb{K}_i))^{-1} - C_N\right) \tag{3.50}$$

where $D_N > 0$ and C_N are renormalization constants. Note that $\phi(\mathbb{K}_i)^{-1} \geq 1$ for all i.

If the sequence of distribution functions of the random variables φ_N converges in the ensemble limit $N \to \infty$ and $V_0 \to \infty$, then the limiting distribution is given by a stable law [74]. The existence of this limit is an indication of fractional stationarity [63–65, 68, 69, 178]. The limiting probability density function for the variables φ_N is obtained along the lines of [64] as

$$h(\varphi; \varpi, C, D) = \frac{1}{\varpi(\varphi - C)} H_{11}^{10}\left(\frac{D^{1/\varpi}}{\varphi - C}\,\middle|\, \begin{matrix}(0,1)\\(0,1/\varpi)\end{matrix}\right) \tag{3.51}$$

where $\varphi \geq C$ and the parameters obey the restrictions $0 < \varpi < 1$, $D \geq 0$ and $C \geq 1$. The function H_{11}^{10} appearing on the left-hand side is a generalized hypergeometric function that can be defined through a Mellin–Barnes contour integral [191]. The limiting local porosity density is obtained as the distribution of the random variable $\phi = 1/\varphi$, and reads

$$\mu(\phi; \varpi, C, D) = \frac{1}{\varpi\phi(1 - C\phi)} H_{11}^{10}\left(\frac{D^{1/\varpi}\phi}{1 - C\phi}\,\middle|\, \begin{matrix}(0,1)\\(0,1/\varpi)\end{matrix}\right) \tag{3.52}$$

for $0 \leq \phi \leq 1/C$ and $\mu(\phi) = 0$ for $\phi > 1/C$. The universal limiting local porosity distributions $\mu(\phi; \varpi, C, D)$ depend on only three parameters, and are independent of the diameter or size of the measurement cells $\mathbb{K}_i$. It is plausible that the limiting distributions will also be independent of the shape of the measurement cells, at least for the classes and sequences of convex measurement sets usually employed in studying the thermodynamic limit [192].

Because the limiting distributions have their support in the interval $0 \leq \phi \leq 1/C$ all its moment exist, and one has $\phi^n = \phi^n(\varpi, C, D)$. If the

moments for $n = 1, 2, 3$ can be inverted, then the parameters ϖ, C, D can be written as

$$\varpi = \varpi(\bar{\phi}, \overline{\phi^2}, \overline{\phi^3}) \qquad C = C(\bar{\phi}, \overline{\phi^2}, \overline{\phi^3}) \qquad D = D(\bar{\phi}, \overline{\phi^2}, \overline{\phi^3}) \tag{3.53}$$

in terms of the first three integer moments. Figure 17 displays the form of $\mu(\phi; \frac{1}{2}, 2, D)$ for various values of D. In the limit of small porosities $\phi \to 0$ the result (3.52) behaves as a power law

$$\mu(\phi) \propto \phi^{\varpi - 1} \tag{3.54}$$

Within local porosity theory this behavior can give rise to scaling laws in transport and relaxation properties of porous media [170]. The importance of universal limiting local geometry distributions arises from the fact that there exists a class of limit laws which remains broad even after taking the macroscopic limit $N \to \infty$, $V_0 \to \infty$. This is the signature of *macroscopic heterogeneity*, and it occurs for $\varpi < 1$. Macroscopically homogeneous systems, corresponding to $\varpi = 1$, converge instead towards a δ distribution concentrated at the bulk porosity $\bar{\phi}$.

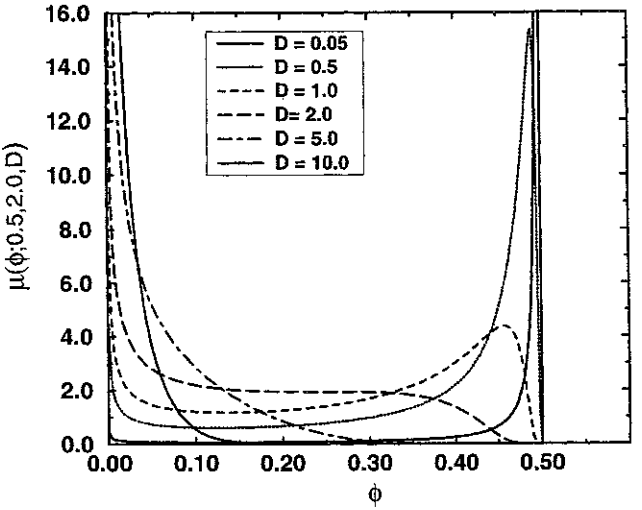

Figure 17. Universal limiting local porosity density (3.52) for $\varpi = 0.5$, $C = 2$, and $D = 0.05, 0.5, 1.0, 2.0, 5.0, 10.0$. For $D \to 0$ the density function is concentrated at $\phi = 1/C$, and it vanishes generally for $\phi > 1/C$.

6. *Capacities*

While local porosity distributions (in their one-cell form) give a useful practical characterization of stochastic porous media they do not characterize the medium completely. A complete characterization of a stochastic medium is given by the so-called Choquet capacities [10, 72]. Although this characterization is very important for theoretical and conceptual purposes it is not practical because it requires to specify the set of "all" compact subsets (see discussion in Section II.B.2).

Consider the pore space $\mathbb{P}$ of a stochastic two-component porous medium as a random set. Let $\mathcal{F}$ denote the family of all closed sets and $\mathcal{K}$ the set of all compact sets as in Section II.B.2. For any $\mathbb{K} \in \mathcal{K}$ the "hitting function" or *capacity functional* is defined as

$$T(\mathbb{K}) = \Pr\{\mathcal{F}_{\mathbb{K}}\} = \Pr\{\mathbb{P} \cap \mathbb{K} \neq \emptyset\} \tag{3.55}$$

where Pr is the probability law governing the random set $\mathbb{P}$. Then T has the following properties: (1) $T(\emptyset) = 0$ and $0 \leq T(\mathbb{K}) \leq 1$. (2) If $\mathbb{K}_1, \ldots, \mathbb{K}_n, \ldots$ is a sequence of compact subset, then $\mathbb{K}_1 \downarrow \mathbb{K}$ implies $T(\mathbb{K}_n) \downarrow \mathbb{K}$. (3) For all n the numbers $S_n(\mathbb{K};\ \mathbb{K}_1, \ldots, \mathbb{K}_n) \geq 0$ are nonnegative where the S_n are determined by the recursion relation

$$\begin{aligned} S_n(\mathbb{K}; \mathbb{K}_1, \ldots, \mathbb{K}_n) &= S_{n-1}(\mathbb{K}; \mathbb{K}_1, \ldots, \mathbb{K}_{n-1}) \\ &\quad - S_{n-1}(\mathbb{K} \cup \mathbb{K}_n; \mathbb{K}_1, \ldots, \mathbb{K}_{n-1}) \end{aligned} \tag{3.56}$$

and $S_0(\mathbb{K}) = 1 - T(\mathbb{K})$. The number $S_n(\mathbb{K};\ \mathbb{K}_1, \ldots, \mathbb{K}_n)$ give the probability that $\mathbb{P} \cap \mathbb{K}$ is empty, but $\mathbb{P} \cap \mathbb{K}_i$ is not empty for all i. The functional $T(\mathbb{K})$ is called an *alternating Choquet capacity of infinite order* [10, 71].

Choquet's theorem says that the converse is also true. Explicitly, if T is a functional on $\mathcal{K}$, then there exists a necessarily unique distribution Pr in $\mathfrak{F}$ with

$$\Pr(\mathcal{F}_{\mathbb{K}}) = T(\mathbb{K}) \tag{3.57}$$

for all $\mathbb{K} \in \mathcal{K}$, if and only if T is an alternating Choquet capacity of infinite order. This theorem shows that capacity functionals play the same defining role for random sets in continuous space as do the numbers $\mu(x_1, \ldots, x_N)$ in Eq. (2.10) in the discrete case.

The main problem with this theoretically important result is that the family of hitting sets $\mathcal{F}_{\mathbb{K}}$ is much too large for both practical and theoretical purposes.

B. Specific Geometric Models

1. *Capillary Tubes and Slits*

A simple model for porous media is the capillary tube model in which the pore space is represented as an array of cylindrical tubes. The crucial assumption of the model is that the tubes do not intersect each other. Often it is also assumed that the tubes are straight or parallel to each other. Consider a cubic sample $\mathbb{S}$ with side length L and volume $V(\mathbb{S}) = L^3$. If there are N tubes of length L_i that have circular cross sections of radii a_i $(i = 1, \ldots, N)$ the porosity becomes

$$\phi = \frac{\pi}{L^3} \sum_{i=1}^{N} L_i a_i^2 \tag{3.58}$$

The specific internal surface on the other hand is given as

$$S = \frac{2\pi}{L^3} \sum_{i=1}^{N} L_i a_i \tag{3.59}$$

In a stochastic model the radii a_i and tube lengths L_i are chosen at random according to a joint probability density $\Pi(a, L)$.

Several special cases are of particular interest. If the random radii a_i and tube lengths L_i are chosen statistically independently, then the joint density $\Pi(a, L)$ factorizes as $\Pi(a, L) = \Pi_a(a)\Pi_L(L)$ into a "pore width distribution" $\Pi_a(a)$ and a "pore length distribution" $\Pi_L(L)$. The average porosity and average specific internal surface area become in this case

$$\langle S \rangle = 2\pi \langle \mathcal{T} \rangle \langle a \rangle \frac{N}{L^2} \tag{3.60}$$

$$\langle \phi \rangle = \pi \langle \mathcal{T} \rangle \langle a^2 \rangle \frac{N}{L^2} \tag{3.61}$$

where N/L^2 is the number of capillaries per unit area, and $\langle \mathcal{T} \rangle = \langle L \rangle / L$ is the *average tortuosity* factor obtained by averaging the dimensionless *tortuosity* $\mathcal{T}_i$ defined for each tube as

$$\mathcal{T}_i = \frac{L_i}{L} \tag{3.62}$$

Moreover, in this case the ratio

$$\frac{\langle \phi \rangle}{\langle S \rangle} = \frac{\langle a^2 \rangle}{2\langle a \rangle} \tag{3.63}$$

is a characteristic length independent of the tortuosity and sample size. Two further special cases arise from setting all radii equal to each other, $a_i = a$ or all lengths to the system size, $L_i = L$. If $L_i = L$ the tortuosity factor in Eqs. (3.60) and (3.61) is unity, and Eq. (3.63) holds unchanged. If the a_i are chosen statistically independently, then for large N the average porosity is related to the variance of the specific internal surface according to

$$\langle \phi \rangle = \frac{L^2}{4\pi}(\langle S^2 \rangle - \langle S \rangle^2) \tag{3.64}$$

In the case where all radii are equal, $a_i = a$, the relation (3.63) simplifies to

$$\frac{\langle \phi \rangle}{\langle S \rangle} = \frac{a}{2} \tag{3.65}$$

Although this relation holds only in a special case it has become the basis for defining the so-called *hydraulic radius*

$$R_H = \frac{\phi}{S} = \frac{\text{area of cross section}}{\text{perimeter of cross section}} \tag{3.66}$$

as a characteristic length scale of porous media [1, 2]. The hydraulic radius concept was used in Section III.A.3.d for defining pore size distributions. The capillary tube model and the hydraulic radius concept play an important role for fluid flow through porous media, and will be discussed further in Section V.C.2.

A model that is closely related to the capillary tube model is obtained by considering N slits, that is, N parallel planes of width b_i, instead of tubes. All slits are assumed to be parallel, and hence nonintersecting. The resulting capillary slit model has a porosity

$$\phi = \frac{1}{L}\sum_{i=1}^{N} b_i \tag{3.67}$$

and specific internal surface area

$$S = \frac{2N}{L} \tag{3.68}$$

independent of the widths of the slits. Here the specific internal surface is independent of the distribution of widths. As in the capillary tube model one also finds a relation

$$\frac{\langle \phi \rangle}{S} = \frac{\langle b \rangle}{2} \tag{3.69}$$

similar to Eq. (3.65) for the model of capillary slits. The model may be generalized by allowing small undulations and smooth fluctuations of the slits.

2. *Grain Models*

Grain models of various sorts have long been studied in optics [179, 193], colloids [194, 195], phase transitions [196], and disordered systems [197]. An important class of grain models are random bead packs [198–204], which provide a reasonable starting point for modeling unconsolidated sediments. In grain models, either the pore or the matrix space are represented as an array of convex grains [107–109, 205–209]. The grains could be regularly shaped such as spheres, cubes or ellipoids, or more irregularly shaped convex sets. They may be positioned randomly or regularly in space, and they may have equal or varying diameters. If the grains are placed randomly their centroids are assumed to form a stochastic point process. For a *Poisson point process* the centers or centroids of the grains are placed randomly and independently in space such that the number $N(\mathbb{B})$ of points inside a set $\mathbb{B}$ is Poisson distributed with point density ϱ. For a Poisson point process the whole distribution is determined by its density ϱ. If $\mathbb{B}_1, \ldots, \mathbb{B}_n$ are n disjoint bounded sets, then the numbers $N(\mathbb{B}_1), \ldots, N(\mathbb{B}_n)$ are independent Poisson random variables with joint probability distribution

$$\Pr\{N(\mathbb{B}_1) = N_1, \ldots, N(\mathbb{B}_n) = N_n\} = \frac{\varrho^{N_1+\cdots+N_n} V_d(\mathbb{B}_1)^{N_1} \cdots V_d(\mathbb{B}_n)^{N_n}}{N_1! \cdots N_n!} \exp(-\varrho(V_d(\mathbb{B}_1) + \cdots + V_d(\mathbb{B}_n))) \tag{3.70}$$

The Poisson point process with constant density is stationary and isotropic. The contact distribution $H_{\mathbb{K}}(x)$, defined in Section III.A.4, for the Poisson point process can be obtained from the so-called void probability that there is no point inside $\mathbb{K}$ as

$$H_{\mathbb{K}}(x) = 1 - \Pr\{N(x\mathbb{K}) = 0\} = 1 - \exp(-\varrho V_d(x\mathbb{K})) \tag{3.71}$$

A simple class of grain models is obtained by attaching compact sets to the points of a Poisson point process. The compact sets are called *primary grains*. Spheres of constant radius are examples. Important generalizations are obtained by randomizing the primary grains. An example would be spherical grains with random radii. More generally, it is possible to use as grains independent realizations of a random compact set as defined in Section II.B.2.b. If $\mathbb{G}_i$ denote the independent realizations of the grains and $\mathbf{r}_i$ the points of a Poisson point process, then a grain model is obtained as the set

$$\mathbb{P} = \bigcup_{i=1}^{\infty} (\mathbb{G}_i + \mathbf{r}_i) \tag{3.72}$$

if the grains are interpreted as pores. If the grains are matrix then $\mathbb{P}$ has to be replaced by $\mathbb{M}$. The grain model is uniquely characterized by its capacity functional $T(\mathbb{K}) = \Pr\{\mathbb{P} \cap \mathbb{K} \neq \emptyset\}$ defined in Section III.A.6. If $\mathbb{G}_0$ denotes an independent realization of the primary grains, and $\mathbb{K}$ a compact set, then the capacity functional can be shown to have the form [10, 37]

$$T(\mathbb{K}) = 1 - \exp[-\varrho \langle V_d((-\mathbb{G}_0) \oplus \mathbb{K}) \rangle] \tag{3.73}$$

where $\langle \cdots \rangle$ denotes the expectation value with respect to the distribution of primary grains, and the Minkowski addition $\oplus$ of sets was defined in Eq. (3.17). The porosity of a grain model is obtained as

$$\langle \phi \rangle = 1 - \exp[-\varrho \langle V_d(\mathbb{G}_0) \rangle] \tag{3.74}$$

where $\mathbb{G}_0$ is again a typical primary grain. The covariance function defined in Eqs. (3.7) and (3.8) reads

$$C_2(\mathbf{r}) = 2\langle \phi \rangle - 1 + (1 - \langle \phi \rangle)^2 \exp[\varrho \langle V_d(\mathbb{G}_0 \cap (\mathbb{G}_0 - \mathbf{r})) \rangle] \tag{3.75}$$

and it determines the specific internal surface according to Eqs. (3.16) and (3.13). The contact distribution $\Pi_{\mathbb{K}}(x)$ for a compact set $\mathbb{K}$ is given as

$$\Pi_{\mathbb{K}}(x) = 1 - \exp[-\varrho(\langle V_d(\mathring{\mathbb{G}}_0 \oplus x\mathbb{K}) \rangle - \langle V_d(\mathbb{G}_0) \rangle)] \tag{3.76}$$

where the interior $\mathring{\mathbb{G}}$ of a set was defined in Section II.B.1 and $x \geq 0$.

Two simple classes of grain models are obtained by randomly placing penetrable or impenetrable spheres of radius R and number density ρ. Specializing Eq. (3.74) to spherical grains of equal diameter one obtains

$$\langle \phi \rangle = \exp(-4\pi R^3 \varrho / 3) \tag{3.77}$$

for the porosity of fully penetrating spheres. The relation

$$\langle \phi \rangle = 1 - 4\pi R^3 \varrho / 3 \tag{3.78}$$

applies to hard spheres of radius R [108]. The specific internal surface area of overlapping spheres reads

$$S = 4\pi R^2 \varrho \exp(-4\pi R^3 \varrho / 3) \tag{3.79}$$

and for hard spheres

$$S = 4\pi R^2 \varrho \tag{3.80}$$

is obtained [108].

A basic question of stereology concerns the "unfolding" of three-dimensional information from planar sections [210]. For a stationary Poisson distributed grain model with spherical grains of random diameter the problem of calculating the probability density $p_3(r)$ of the diameters of spheres from the probability density $p_2(r)$ of section circles was solved long ago [211, 212]. The spatial and planar distributions are related through an Abel integral equation

$$p_2(r) = \frac{r}{a} \int_r^\infty \frac{p_3(x)}{\sqrt{(x^2 - r^2)}} dx \tag{3.81}$$

where the mean-sphere diameter a is given by

$$a = \frac{\pi}{2} \left[\int_0^\infty \frac{1}{r} p_2(r)\, dr \right]^{-1} \tag{3.82}$$

The solution to this equation is

$$p_3(r) = -\frac{2ar}{\pi} \int_r^\infty \frac{1}{\sqrt{(x^2 - r^2)}} \frac{d}{dx} \left[\frac{p_2(x)}{x} \right] dx \tag{3.83}$$

for $r \geq 0$. In the special case where all spheres have the same constant diameter a the probability density of section circle diameters is given as

$$p_2(r) = \frac{r}{a\sqrt{(a^2 - r^2)}} \tag{3.84}$$

with $0 \leq r \leq a$. The average diameter of the section circles is $a_2 = \pi a/4$, and its variance is $\sigma^2 = (32 - 3\pi^2)a^2/48$. Another interesting special case

is when the diameters of the spheres are distributed according to

$$p_3(r) = \frac{r}{b^2} \exp\left[-\frac{r^2}{(2b^2)} \right] \tag{3.85}$$

for $r \geq 0$, which gives a mean-sphere diameter $a = b\sqrt{\pi/2}$. In this case, the distribution reproduces itself, that is, $p_3(r) = p_2(r)$.

Even the simplest grain model with penetrable spheres of equal diameter and Poisson distributed centers still poses unsolved problems. At low-dimensionless densities $\rho = (4\pi/3)R^3\varrho$ the grains form isolated bounded sets. Here R is the radius of the spheres and ϱ their number density. As the dimensionless density is increased the grains begin to overlap and ultimately "percolate," which means that an unbounded connected component appears. This *continuum percolation transition* between a state without unbounded connected component and a state where the strains percolate to infinity is a phase transition of order larger than 2 in the sense of statistical mechanics [64, 213]. It continues to be the subject of much research in recent years [214–219].

A different parallel with statistical mechanics emerges if the grains are identified with the particles in statistical mechanics [6–8, 208]. This identification suggests generalizations of the underlying uncorrelated Poisson point process, which corresponds to an ideal gas of noninteracting particles, by adding interactions between the points. A large variety of new models such as hard-sphere models or Gibbs point fields [34, 37] emerges from this generalization.

3. *Network Models*

Network models represent the most important and widely used class of geometric models for porous media [155, 157, 187, 220–233]. They are not only used in theoretical calculations but also in the form of micromodels in experimental observations [157, 234–238]. For random bead packs a random network model has recently been derived starting from the microstructure [200, 204]. Network models arise generally and naturally from discretizing the equations of motion using finite difference schemes. As such they will be discussed in more detail in Section V.

A network is a graph consisting of a set of vertices or sites connected by a set of bonds. The vertices or sites of the network could, for example, represent the grain centers of a grain model. If the grains represent pore bodies the bonds represent connections between them. The vertices can be chosen deterministically as for the sites of a regular lattice or randomly as in the realization of a Poisson or other stochastic point process. Similarly, the bonds connecting different vertices may be chosen accord-

ing to some deterministic or random procedure. Finally, the vertices are "dressed" with convex sets such as spheres representing pore bodies, and the bonds are dressed with tubes providing a connecting path between the pore bodies. A simple ordered network model consists of a regular lattice with spheres of equal radius centered at its vertices that are connected through cylindrical tubes of equal diameter. Very often the diameters of spheres and tubes in a regular network model are chosen at random. If a finite fraction of the bond diameters is zero, one obtains the *percolation model*.

4. *Percolation Models*

The purpose of this section is not to review percolation theory but to introduce the concept of a percolation transition, and to collect for later reference the values of percolation thresholds. The name "percolation" derives from fluid flow through a coffee percolator, and it has been used extensively to model various aspects of flow through porous media [41, 113, 153, 154, 156, 226, 239–243]. Invasion percolation has become a frequently studied model for displacement processes in porous media [42, 244–246, 246a]. Percolation theory itself is a well-developed branch in the theory of disordered systems and critical phenomena, and the reader is referred to [197, 213, 247, 248] for thorough information on the subject.

Percolation as a geometrical model for porous media is closely related both to grain models and to network models. The model of spherical grains attached to the points of a Poisson process is also known as continuum percolation or the "swiss cheese" model [213]. Site percolation is an abstract version of a grain model, while bond percolation may be seen as an abstraction from network models. The distinguishing feature of percolation theory from other models is its focus on a sudden phase transition associated with the connectivity of random media.

The simplest model of percolation is bond percolation on a lattice. In *bond percolation* the bonds of a regular (e.g., simple cubic) lattice are occupied randomly with connecting (=conducting) elements (e.g., tubes) with a certain occupation probability p. Alternatively, one removes a fraction $1-p$ of bonds at random from a fully occupied infinite lattice. Two lattice sites are called *connected* if there exists a path between them traversing only bonds occupied by connecting elements. A set of connected bonds is called a *cluster*. In an infinitely large system there exists a critical occupation probability p_{bc} above which there exists an unbounded connected cluster, while below p_{bc} all clusters are finite and bounded. If the connecting elements are cylindrical tubes of fixed or variable diameter, then the resulting network model of a porous medium would be permeable above p_{bc} and impermeable below p_{bc}.

Similarly, *site percolation* may be viewed as a lattice version of a grain model. In site percolation the sites of the underlying regular lattice are occupied randomly with spherical pore bodies of radius at least one-half the lattice constant. Two nearest-neighbor sites are called connected if they are both occupied. As in bond percolation there exists a critical occupation probability p_{sc} separating a permeable connected regime from an impermeable regime.

These basic bond and site percolation models may be modified in many ways. The underlying lattice may be replaced with an arbitrary regular or random graph. The radii of tubes and pores may be randomized, and the connectivity criterion may be changed. Table II shows the values of the critical occupation probabilities (thresholds) for bond and site percolation for some common two- and three-dimensional lattices [213]. The table also lists the coordination number of each lattice defined as the number of bonds meeting at an interior lattice site.

The transition between the permeable and impermeable regime becomes a phase transition in the limit of an infinitely large lattice. The role of the order parameter is played by the *percolation probability* $P(p)$ defined as the probability that a given point belongs to an infinite cluster. The correlation length $\xi(p)$ is defined from the correlation function giving the probability that a site at distance r from a given site is occupied and connected to the given site. The correlation length measures the typical size of a cluster, and it diverges as p approaches p_c.

Similar to network models percolation arises naturally in the study of transport and relaxation phenomena. Effective medium theories dis-

TABLE II
Values of the Bond p_{bc} and Site p_{sc} Percolation Thresholds for Various Two- and Three-Dimensional Lattices[a]

Lattice Type	Dimension	Coordination	p_{bc}	p_{sc}
Honeycomb	2	3	$1-2\sin(\pi/18)\approx 0.6527$	0.6962
Square	2	4	$\frac{1}{2}$	0.592746
Triangular	2	6	$2\sin(\pi/18)\approx 0.3473$	$\frac{1}{2}$
Diamond	3	4	0.3886	0.4299
Simple cubic	3	6	0.2488	0.3116
Body centered cubic	3	8	0.180	0.246
Face centered cubic	3	12	0.119	0.198

[a] Also given is the coordination number defined as the number of bonds meeting at an interior lattice site.

cussed in Sections V.B.3 or V.C.6 contain an underlying percolation transition.

5. *Filtering and Reconstruction*

Recently, a new type of geometric models has appeared [118, 171, 249–252], which is based on image processing techniques. These models attempt to reconstuct a porous medium with prespecified statistical characteristics such as its porosity $\bar{\phi}$ and two-point correlation function $S_2(\mathbf{r})$ [249, 250]. This is achieved through real space or Fourier space filtering of random fields. To this end a two- or three-dimensional random function assigning an independent random number to each point in space is convoluted with a smoothing kernel. Alternatively, the Fourier transforms of the two functions are multiplied and backtransformed to obtain the smoothed image. In [249, 250, 252] it has been argued that such reconstructed images resemble the structures observed in sedimentary rocks or Vycor glass. In [171] such models have been used to test the microstructural sensitivity of local porosity distributions (discussed in Section III.A.5) on models with identical two-point correlation functions.

The motivation for studying reconstructed porous media is to generate precisely known microgeometries whose transport properties can then be calculated numerically [249, 252]. As shown in [171] two media with the same porosity and correlation function may still show significant differences in their geometric characteristics. More importantly, the porosity and two-point correlation function are not sufficient to determine the connectivity of a medium. The connectivity controls the transport, and therefore it is unclear to what extent reconstructed porous media are useful for predicting transport or relaxation properties.

6. *Process Models*

The geometric models discussed in the previous sections do not account for the fact that the pore space configuration is often the result of a physical process. This suggests the use of dynamic *process models* that describe the formation of the porous medium. While such models are employed routinely for unconsolidated bead packs [199, 201, 202, 253] they are relatively rare for consolidated porous media. The so-called *bond shrinkage model* [254] was developed for sedimentary rocks. In this model one starts from a random resistor network on a simple cubic lattice in d dimensions. Each resistor in the model represents a cylindrical tube with radius r_i in a corresponding network model on the lattice. Next, a tube element is randomly chosen and its radius is reduced by a fixed factor x with $0 < x < 1$. The radius of the shrunk element is then xr_i. The shrinkage process may be repeated as often as necessary to reach a

specified porosity or until some other criterion is satisfied depending on the modeling purpose. The condition $x > 0$ guarantees that the model remains connected at all times if the shrinkage is repeated a finite number of times. Because $x > 0$ the bond shrinkage model does not give rise to a percolation threshold.

The so-called grain consolidation model [255, 256] does give rise to a percolation threshold. In the grain consolidation model one starts from a grain model with nonoverlapping grains $\mathbb{G}_i$. The grains are then allowed to grow. In the simplest version [255] the grains form a regular cubic lattice of spheres. As the grains grow the porosity is reduced and more and more narrow constrictions between grains are closed. Thus the system becomes impenetrable at a finite porosity. For a regular simple cubic lattice of spheres the percolation threshold appears at a critical porosity of $\phi_c = 0.0349$ [255]. This value is much smaller than the values $p_{sc} \approx 0.2488$ or $p_{bc} \approx 0.3116$ in Table II for bond and site percolation. If the grains are grown from a random bead pack the critical porosity is found to be $\phi_c \approx 0.03$. This value is again much smaller than the threshold $\phi_c \approx 0.17$ in continuum percolation [257, 258].

Another process model, called *local porosity reduction model*, was introduced in [170]. Consider a simple regular lattice (e.g., simple cubic) with lattice constant L superimposed on a porous medium as shown in Fig. 12. The lattice cells are the measurement cells of local porosity theory defined in Section III.A.5. In the simplest example, one may assume that all measurement cells have the same initial porosity ϕ_0 and specific internal surface area S_0. The consolidation process is modeled by picking at random a particular cell and reducing its porosity by a factor r, and its specific surface by a factor s. This operation is repeated until a desired average porosity $\bar{\phi}$ has been reached. It is assumed that the local percolation probability function $\lambda(\phi, S)$ is unaffected by the consolidation operations. The final state of the porous medium can be described by assigning to each cell the random integer n giving the number of times a local consolidation operation was performed on that cell. The random variable n is Poisson distributed, and this observation allows one to find the local porosity distribution as [170]

$$\mu(\phi, L) = \frac{1}{\Gamma(\ln(r\phi/\phi_0)/\ln r)} \left(\frac{\phi}{\phi_0}\right)^{\ln \bar{n}/\ln r} \exp(-\bar{n}) \tag{3.86}$$

where

$$\bar{n} = \frac{\ln \bar{\phi} - \ln \phi_0}{r - 1} \tag{3.87}$$

and $\Gamma(x)$ denotes Eulers gamma function. A similar consideration could be performed for the specific internal surface distribution. In many consolidation processes the reduction factors are not independent. For grain consolidation models this is illustrated by Eqs. (3.77)–(3.80), relating the porosity and specific surface through the sphere radius. Similarly, if a crack is closed by an applied external pressure this will reduce the porosity but not the surface area, as long as the possibility of crushing the crack profile is neglected. Therefore, in this case $s = r^0 = 1$. Similarly, if a void space is uniformly cemented by precipitation of minerals from the pore fluids this implies the relation $s = r^{2/3}$ between the reduction factors. The simple relation

$$s = r^{\alpha} \tag{3.88}$$

summarizes several idealized processes such as crack compaction, $\alpha = 0$, shrinkage of capillaries, $\alpha = \frac{1}{2}$, shrinkage of voids, $\alpha = \frac{2}{3}$, and void filling, $\alpha = 1$.

IV. DEFINITION AND EXAMPLES OF TRANSPORT

A. Examples

This section begins the discussion of physical processes in porous media involving the transport or relaxation of physical quantities, such as energy, momentum, mass, or charge. As discussed in the introduction, physical properties require equations of motion describing the underlying physical processes. Recurrent examples of experimental, theoretical, and practical importance include:

- The disordered *diffusion equation*

$$\frac{\partial T(\mathbf{r}, t)}{\partial t} = \nabla^T \cdot (\mathbf{D}(\mathbf{r}) \nabla T(\mathbf{r}, t)) \tag{4.1}$$

where $\mathbf{r} \in \mathbb{S}$, $\mathbf{D}(\mathbf{r}) = \kappa(\mathbf{r})/(c_p(\mathbf{r})/\rho(\mathbf{r})) > 0$ is the thermal diffusivity tensor, $T(\mathbf{r}, t)$ is the space–time dependent temperature field, $\rho(\mathbf{r})$ is the density, $\kappa(\mathbf{r})$ the thermal conductivity, and $c_p(\mathbf{r})$ the specific heat at constant pressure. The superscript T denotes transposition. If the tensor field $\mathbf{D}(\mathbf{r})$ is sufficiently often differentiable the equations are completed with boundary conditions at the sample boundary $\partial\mathbb{S}$. For the microscopic description of diffusion in a two-component porous medium $\mathbb{S} = \mathbb{P} \cup \mathbb{M}$ whose components have diffusivities $\mathbf{D}_{\mathbb{P}}$ and $\mathbf{D}_{\mathbb{M}}$ the diffusivity field $\mathbf{D}(\mathbf{r})$ has the form $D(r) = D_{\mathbb{P}}\chi_{\mathbb{P}}(r) + D_{\mathbb{M}}\chi_{\mathbb{M}}(r)$, which is not differentiable at $\partial\mathbb{P}$. In such cases, additional

boundary conditions are required at the internal interface $\partial\mathbb{P}$, and the equation is interpreted in the sense of distributions [259]. Typical values for sedimentary rocks are $\kappa_{\mathbb{M}} \approx 1 \ldots 6\ \mathrm{Wm^{-1}\,K^{-1}}$, $\rho_{\mathbb{M}} \approx 1 \ldots 3\ \mathrm{g\,cm^{-3}}$, and $c_{p\mathbb{M}} \approx 0.8 \ldots 1.2\ \mathrm{kJ\,kg^{-1}\,K^{-1}}$.

- The Laplace equation with variable coefficients

$$\nabla^T \cdot (\mathbf{C}(\mathbf{r})\nabla u(\mathbf{r})) = 0 \tag{4.2}$$

where $\mathbf{C}(\mathbf{r})$ is again a second rank tensor field of local transport coefficients, $u(\mathbf{r})$ is a scalar field, $\mathbf{r} \in \mathbb{S}$, and the same remarks apply as for the diffusion equation with respect to differentiability of $\mathbf{C}(\mathbf{r})$ and boundary conditions. For constant $\mathbf{C}(\mathbf{r})$ the equation reduces to the Laplace equation $\Delta u = 0$. If the medium is random the coefficient matrix $\mathbf{C}$ is a random function of $\mathbf{r}$. Equation (4.2) is the basic equation for Section IV.B. It is frequently obtained as the steady-state limit of the time-dependent equations such as the diffusion equation (4.1). Other examples of Eq. (4.2) occur in fluid flow, dielectric relaxation, or dispersion in porous media. In dielectric relaxation u is the electric potential and $\mathbf{C}$ is the matrix of local (spatially varying) dielectric permittivity. In diffusion problems or heat flow u is the concentration field or temperature, and $\mathbf{C}$ the local diffusivity. In Darcy flow through porous media u is the pressure and $\mathbf{C}$ is the tensor of locally varying absolute permeabilities.

- The elastic wave equation is a system of equations for the three components $u_i(\mathbf{r}, t)$ $(i = 1, 2, 3)$ of a vector displacement field

$$\frac{\partial^2 u_i(\mathbf{r}, t)}{\partial t^2} = v_s^2\, \Delta u_i(\mathbf{r}, t) + (v_p^2 - v_s^2) \frac{\partial}{\partial r_i} \left(\sum_{j=1}^{3} \frac{\partial u_j(\mathbf{r}, t)}{\partial r_j} \right) \tag{4.3}$$

where v_p is the compressional and v_s the shear wave velocity of the material.

- Maxwells equations in SI units for a medium with real dielectric constant ε', magnetic permeability μ', real conductivity σ' and charge density ρ

$$\nabla \cdot (\varepsilon' \varepsilon_0 \mathbf{E}(\mathbf{r}, t)) = \rho(\mathbf{r}, t) \tag{4.4}$$

$$\nabla \cdot (\mu' \mu_0 \mathbf{H}(\mathbf{r}, t)) = 0 \tag{4.5}$$

$$\nabla \times \mathbf{E}(\mathbf{r}, t) = -\frac{\partial}{\partial t}(\mu' \mu_0 \mathbf{H}(\mathbf{r}, t)) \tag{4.6}$$

$$\nabla \times \mathbf{H}(\mathbf{r}, t) = \sigma' \mathbf{E}(\mathbf{r}, t) + \frac{\partial}{\partial t}(\varepsilon' \varepsilon_0 \mathbf{E}(\mathbf{r}, t)) \tag{4.7}$$

for the electric field $\mathbf{E}(\mathbf{r}, t)$, magnetic field $\mathbf{H}(\mathbf{r}, t)$ supplemented by boundary conditions and the continuity equation

$$\frac{\partial \rho(\mathbf{r}, t)}{\partial t} + \nabla \cdot \sigma' \mathbf{E}(\mathbf{r}, t) = 0 \tag{4.8}$$

Here $\varepsilon_0 = 8.8542 \times 10^{-12}\,\mathrm{F\,m^{-1}}$ is the permittivity and $\mu_0 = 4\pi \times 10^{-7}\,\mathrm{H\,m^{-1}}$ is the magnetic permeability of empty space.

- The Navier–Stokes equations for the velocity field $\mathbf{v}(\mathbf{r}, t)$ and the pressure field $P(\mathbf{r}, t)$ of an incompressible liquid flowing through the pore space

$$\rho \frac{\partial \mathbf{v}}{\partial t} + \rho(\mathbf{v}^T \cdot \nabla)\mathbf{v} = \eta\, \Delta \mathbf{v} + \rho g \nabla z - \nabla P \tag{4.9}$$

$$\nabla^T \cdot \mathbf{v} = 0 \tag{4.10}$$

where ρ is the density and μ the viscosity of the liquid. The coordinate system was chosen such that the acceleration of gravity g points in the z direction. These equations have to be supplemented with the no-slip boundary condition $\mathbf{v} = 0$ on the pore-space boundary.

In the following, mainly the equations for fluid transport and Maxwells equation for dielectric relaxation will be discussed in more detail. Combining fluid flow and diffusion into convection–diffusion equations yields the standard description for solute and contaminant transport [21, 24, 26, 260–262].

B. General Formulation

Transport and relaxation processes in a three-dimensional two-component porous medium $\mathbb{S} = \mathbb{P} \cup \mathbb{M}$ (defined above in Section II) may be

formulated very broadly as a system of partial differential equations

$$F_{\mathbb{P}}\left(r_1, r_2, \ldots, u_1(\mathbf{r}), u_2(\mathbf{r}), \ldots, \frac{\partial u_i(\mathbf{r})}{\partial r_j}, \ldots, \frac{\partial^2 u_i(\mathbf{r})}{\partial r_j \partial r_k}, \ldots\right) = 0 \quad \mathbf{r} \in \mathbb{P}$$

$$F_{\mathbb{M}}\left(r_1, r_2, \ldots, u_1(\mathbf{r}), u_2(\mathbf{r}), \ldots, \frac{\partial u_i(\mathbf{r})}{\partial r_j}, \ldots, \frac{\partial^2 u_i(\mathbf{r})}{\partial r_j \partial r_k}, \ldots\right) = 0 \quad \mathbf{r} \in \mathbb{M}$$

$$F_{\partial\mathbb{P}}\left(r_1, r_2, \ldots, u_1(\mathbf{r}), u_2(\mathbf{r}), \ldots, \frac{\partial u_i(\mathbf{r})}{\partial r_j}, \ldots, \frac{\partial^2 u_i(\mathbf{r})}{\partial r_j \partial r_k}, \ldots\right) = 0 \quad \mathbf{r} \in \partial\mathbb{P} \tag{4.11}$$

for n unknown functions $u_i(\mathbf{r})$ with $i = 1, \ldots, n$ and $\mathbf{r} = (r_1, \ldots, r_d) \in \mathbb{R}^d$. Here the unknown functions u_i describe properties of the physical process (such as displacements, velocities, temperatures, pressures, electric fields, etc.), and the given functions $F_{\mathbb{P}}$, $F_{\mathbb{M}}$, and $F_{\partial\mathbb{P}}$ depend on a finite number of its derivatives. The function $F_{\partial\mathbb{P}}$ provides a coupling between the processes in the pore and matrix space. The main difficulty arises from the irregular structure of the boundary. The formulation may be generalized to porous media with more than two components. For a stochastic porous medium the solutions $u_i(\mathbf{r})$ of Eq. (4.11) depend on the random realization, and one is usually interested in the averages $\langle u_i(\mathbf{r})\rangle$. Some authors [2, 41] have recently emphasized the difference between continuum descriptions such as Eq. (4.11) and discrete descriptions such as network models. Section V will show that discrete formulations arise as approximations and reduce to the continuum description of the same phenomenon in an appropriate limit.

V. TRANSPORT AND RELAXATION IN TWO COMPONENT MEDIA

The calculation of effective macroscopic physical properties from a geometrical characterization of the microstructure is the second subproblem of the central question discussed in the introduction. This section will focus on single-phase fluid transport and dielectric relaxation in porous media as representative examples for this general problem. The third subproblem of passage between microscopic and macroscopic length scales that has played an important role in Section III.A.5 will become more prominent in this and Section VI. The upscaling problem appears in the present section as the need to find effective macroscopic equations of motion from averaging the underlying microscopic equations of motion.

Successive spatial averaging allows passage to larger and larger length scales, and it can be carried out using systematic expansions in the ratio of length scales or self-consistent effective medium theories. The idea of a self-consistently determined homogeneous reference medium is cental to the definition of an effective macroscopic physical property. Asymptotic expansions in the ratio of a microscopic length scale to a macroscopic scale are known as homogenization theory, and will be discussed in Sections V.C.3 and V.C.4. Their purpose is to provide a systematic method of identifying useful macroscopic reference properties. Once a useful macroscopic description is identified, a generalized form of effective medium theory can be employed to calculate the effective macroscopic properties.

A. Effective Transport Coefficients

1. *Definition*

A large number of transport and relaxation processes in porous media are governed by the disordered Laplace equation (4.2) with variable coefficients $\mathbf{C}(\mathbf{r})$ for a scalar field $P(\mathbf{r})$

$$\nabla^T \cdot (\mathbf{C}(\mathbf{r})\nabla P(\mathbf{r})) = 0 \tag{5.1}$$

within the sample region $\mathbb{S} = \mathbb{P} \cup \mathbb{M}$. This "equation of motion" for P must be supplemented with suitable boundary conditions on the sample boundary $\partial\mathbb{S}$, and, if $\mathbf{C}(\mathbf{r})$ is discontinuous across $\partial\mathbb{P}$, also on the internal boundary $\partial\mathbb{P}$. By introducing the vector field $\mathbf{v}(\mathbf{r})$, Eq. (5.1) may be rewritten as

$$\begin{aligned} \mathbf{v}(\mathbf{r}) &= -\mathbf{C}(\mathbf{r})\nabla P(\mathbf{r}) \\ \nabla^T \cdot \mathbf{v}(\mathbf{r}) &= 0 \end{aligned} \tag{5.2}$$

These equations can be used as the microscopic starting point although, as shown in Section V.C.3 for the case of fluid flow, they may hold only in a macroscopic limit starting from a different underlying microscopic description. Equations (5.1) or (5.2) appear in many transport and relaxation problems for porous and heterogeneous media. For Darcy flow in porous media P is the pressure, $\mathbf{C} = \mathbf{K}/\eta$ is the quotient of absolute hydraulic permeability and fluid viscosity, and $\mathbf{v}$ is the fluid velocity field. For dielectric relaxation P becomes the electrostatic potential, $\mathbf{v}$ becomes the dielectric displacement, and $\mathbf{C}$ becomes the dielectric permittivity tensor. In diffusion or dispersion problems P is the concentration field, $\mathbf{v}$

TABLE III
Quantities Corresponding to P, $\mathbf{v}$, and $\mathbf{C}$ in Eq. (5.2) for Different Transport and Relaxation Problems in Porous Media

Problem Type	P	$\mathbf{v}$	$\mathbf{C}$
Fluid flow	Pressure	Velocity	Permeability/viscosity
Electrical conduction	Voltage	Current	Conductivity
Dielectric relaxation	Potential	Displacement	Dielectric permittivity
Diffusion (dispersion)	Concentration	Particle flux	Diffusion constant

corresponds to the diffusion flux, and $\mathbf{C}$ becomes the diffusivity. Table III summarizes the translation of P, $\mathbf{v}$, and $\mathbf{C}$ into various problems.

For a homogeneous and isotropic medium the transport coefficients $\mathbf{C}(\mathbf{r}) = C\mathbf{1}$, where $\mathbf{1}$ denotes the identify, are independent of $\mathbf{r}$, and Eq. (5.1) reduces to a Laplace equation for the field P. For a random medium the transport coefficients are random functions of $\mathbf{r}$ and the solutions $P(\mathbf{r})$ and $\mathbf{v}(\mathbf{r})$ depend on the realization of $\mathbf{C}(\mathbf{r})$. The averaged solutions $\langle P(\mathbf{r})\rangle$ and $\langle \mathbf{v}(\mathbf{r})\rangle$ are therefore of primary interest. The tensor of *effective transport coefficients* is $\bar{\mathbf{C}}$ defined as

$$\langle \mathbf{v}(\mathbf{r})\rangle = -\bar{\mathbf{C}}\nabla\langle P(\mathbf{r})\rangle \tag{5.3}$$

and it provides a relation between the average fields. The ensemble averages $\langle f(\mathbf{r})\rangle$ in the definition can be replaced with spatial averages defined by

$$\bar{f} = \frac{1}{V(\mathbb{S})}\int f(\mathbf{r})\chi_{\mathbb{S}}(\mathbf{r})\, d^3\mathbf{r} \tag{5.4}$$

where f stands for P or $\mathbf{v}$. Both the ensemble and the spatial average depend on the averaging region $\mathbb{S}$, and a residual variation of $\bar{f}$ or $\langle f\rangle$ is possible on scales larger than the size of $\mathbb{S}$. In the following it will always be assumed that $\bar{f} = \langle f\rangle$ if $\mathbb{S}$ is sufficiently large. The ensemble average notation will be preferred because it is notationally more convenient.

The purpose of introducing effective macroscopic transport coefficients is to replace the heterogeneous medium described by $\mathbf{C}(\mathbf{r})$ with an equivalent homogeneous medium described by $\bar{\mathbf{C}}$. If $\bar{\mathbf{C}}$ is known, then all the knowledge accumulated for the homogeneous problem can be utilized immediately, and, for example, the average field $\mathbf{v}$ can be obtained simply from solving a Laplace equation for P.

2. *Discretization and Networks*

If the function $\mathbf{C}(\mathbf{r})$ is known, then Eq. (5.1) can be solved to any desired accuracy using standard finite difference approximation schemes. To this end the sample space $\mathbb{S}$ of linear extension $\mathscr{L}$ is partitioned into cubes $\mathbb{K}_j$. The cubes are centered on the sites $\mathbf{r}_i$ of a simple cubic lattice with lattice spacing L. Other lattices may also be employed. The lengths L and $\mathscr{L}$ obey $L \ll \mathscr{L}$. The total number of cubes is $N = (\mathscr{L}/L)^d$.

For a stationary and isotropic medium with $\mathbf{C}(\mathbf{r}) = c(\mathbf{r})\mathbf{1}$ the discretization of Eq. (5.1) gives a system of linear equations for the pressure variables at the cube centers $P_i = P(\mathbf{r}_i)$

$$\sum_j c_{ij}(P_i - P_j) = 0 \tag{5.5}$$

for cubes $\mathbf{r}_i$ not located at the sample boundary. The boundary conditions at the sample boundary give rise to a nonvanishing right-hand side of the linear system if $\mathbf{r}_i$ is the center of a cube located close to $\partial\mathbb{S}$. The local transport coefficients c_{ij} are given as

$$c_{ij}(L) = c((\mathbf{r}_i + \mathbf{r}_j)/2) \tag{5.6}$$

if $\mathbf{r}_i$ and $\mathbf{r}_j$ are nearest neighbors. If $\mathbf{r}_i$ and $\mathbf{r}_j$ are not nearest neighbors the local coefficient vanishes, $c_{ij} = 0$. Because the location of the cube centers $\mathbf{r}_i$ depends on the resolution L the coefficients c_{ij} in the network equations depend on L and on the shape of the measurement cells $\mathbb{K}_i$.

The numerical solution of the discretized equations (5.5) can be obtained by many methods including relaxation, successive overrelaxation, or conjugate gradient schemes, transfer matrix calculations, series expansions, or recursion methods [40, 248, 263–267]. If the function $c(\mathbf{r})$ is known, then the solution to Eq. (5.1) is recovered in the limit $L \to 0$ to any desired accuracy. Within a certain class of lattices the limit is known to be independent of the choice of the approximating discrete lattice. To actually perform this limit, however, the function $c(\mathbf{r})$ must be known to arbitrary accuracy.

In most experimental and practical problems the function $c(\mathbf{r})$ is either completely unknown or not known to arbitrary accuracy. Therefore, it is necessary to have a theory for the *local transport coefficients* $c_{ij}(L)$ as a function of the resolution L of the discretization. At present, the only resolution dependent theories seem to be local porosity theory [168–175] and homogenization theory [38, 268–271], which will be discussed in more detail below. The basic idea of local porosity theory is to use the local geometry distributions defined in Section III.A.5 and to express the

local transport coefficients in terms of the geometrical quantities characterizing the local geometry. The basic idea of homogenization theory is a double scale asymptotic expansion in the small parameter $L/\mathscr{L}$.

The discretized equations (5.5) are network equations. This explains the great importance and popularity of network models. In the more conventional *network models* [155, 157, 187, 220, 223, 225–233] the resolution dependence is neglected altogether. Instead one assumes a specific model for the local transport coefficients c_{ij} such that the *global* geometric characteristics (porosity, etc.) are reproduced by the model. Three immediate problems arise from this assumption:

- The connection with the underlying *local* geometry is lost, although the local value of the transport property depends on it.
- In the absence of an independent measurement of the local transport coefficients they become free fit parameters. Popular stochastic network models assume log normal or binary distributions for the local transport coefficients.
- Without a model for the local geometry an independent experimental or calculational determination of the local transport coefficients for one transport problem (say fluid flow) cannot be used for another transport problem (say diffusion) although the equations of motion [Eq. (5.1)] have the same mathematical form for both cases.

All of these problems are alleviated in local porosity theory or homogenization theory, which attempt to keep the connection with the underlying local geometry.

3. *Simple Expressions for Effective Transport Coefficients*

While a numerical solution of the network equations (5.5) is of great practical interest, its value for a scientific understanding of heterogeneous media is limited. Analytical expressions, be they exact or approximate, are better suited for developing the theory because they allow to extract the general model independent aspects. Unfortunately, only very few exact analytical results are available [272–275]. The one-dimensional case can be solved exactly by a change of variable. The exact result is the harmonic average

$$\bar{c} = \langle c^{-1} \rangle^{-1} \tag{5.7}$$

where the average denotes either an average with respect to $w(c)$, the probability density of local transport coefficients, or a spatial average as

defined in Eq. (5.4). In two dimensions the geometric average

$$\bar{c} = \exp\langle \log c \rangle = \frac{\langle c \rangle^{1/2}}{\langle c^{-1} \rangle^{1/2}} \tag{5.8}$$

has been obtained exactly using duality in harmonic function theory [272] if the microstructure is homogeneous, isotropic, and symmetric. It was later rederived under less stringent conditions [273] and generalized to isomorphisms between associated microstructures [274].

Most analytical expressions for effective transport properties are approximate. In general dimensions, approximation formulas such as [275–277]

$$\bar{c} = \frac{\langle c \rangle^{(d-1)/d}}{\langle c^{-1} \rangle^{1/d}} \tag{5.9}$$

or [278, 279]

$$\bar{c} = \langle c^{(1-2/d)} \rangle^{1/(1-2/d)} \tag{5.10}$$

have been suggested, which reduce to the exact results for $d = 1$ and $d = \infty$. Various mean-field theories also provide approximate estimates for the effective permeabilities. The simplest mean-field theory

$$\bar{c} = \langle c \rangle \tag{5.11}$$

is obtained from Eqs. (5.9) or (5.10) by letting $d \to \infty$. Another very important approximation is the self-consistent effective medium approximation which reads

$$\left\langle \frac{c - \bar{c}}{c + (d-1)\bar{c}} \right\rangle = 0 \tag{5.12}$$

for a d-dimensional hypercubic lattice. For other regular lattices the factor $d - 1$ in the denominator has to be replaced with $(z/2) - 1$, where z is the coordination number of the lattice. Note that for $d = 1$ and $d \to \infty$ the effective medium approximation reproduces the exact result.

To distinguish the quality of these approximations it is instructive to consider a probability density $w(c)$ of local transport coefficients which has a finite fraction $p = 1 - \lim_{\varepsilon \to 0} \int_0^\varepsilon w(c)\, dc$ of blocking bonds. In dimension $d > 1$ this implies the existence of a percolation threshold $0 < p_c < 1$ below which $\bar{c} = 0$ vanishes identically (see Table II for values of p_c). Among the expressions (5.7)–(5.12) only the effective medium

approximation (5.12) is able to predict the existence of a transition. The predicted critical value $p_c = 1/d$, however, is not exact as seen by comparison with Table II.

Another method for calculating the effective transport coefficient $\bar{c}$ will be discussed in homogenization theory in Section V.C.4. The resulting expression appears in Eq. (5.87) if one sets $\mathbf{K} = c\mathbf{1}$. It is given as a correction to the simplest mean-field expression (5.11). The correction involves the fundamental solution of the local transport problem [Eq. (5.88)]. In practice, the use of Eq. (5.87) is restricted to simple periodic microstructures [268, 280]. If the microstructure is periodic it suffices to obtain the fundamental solutions within the basic period, and to extend the average in Eq. (5.87) over that period. If the microstructure is not periodic then the solution of Eq. (5.88) and averaging in Eq. (5.87) quickly become as impractical as solving the original problem, because $c(\mathbf{r})$ is then unknown.

B. Dielectric Relaxation

1. *Maxwell Equations in the Quasistatic Approximation*

Consider a two component medium $\mathbb{S} = \mathbb{P} \cup \mathbb{M}$. The substances filling the sets $\mathbb{P}$ and $\mathbb{M}$ are assumed to be electrically homogeneous and characterized by their real frequency dependent conductivity $\sigma'(\omega)$ and dielectric function $\varepsilon'(\omega)$. The real dielectric function $\varepsilon'(\mathbf{r}, \omega)$ and conductivity $\sigma'(\mathbf{r}, \omega)$ of the composite are then given as

$$\varepsilon'(\mathbf{r}, \omega) = \varepsilon'_{\mathbb{P}}(\omega)\chi_{\mathbb{P}}(\mathbf{r}) + \varepsilon'_{\mathbb{M}}(\omega)\chi_{\mathbb{M}}(\mathbf{r}) \tag{5.13}$$

$$\sigma'(\mathbf{r}, \omega) = \sigma'_{\mathbb{P}}(\omega)\chi_{\mathbb{P}}(\mathbf{r}) + \sigma'_{\mathbb{M}}(\omega)\chi_{\mathbb{M}}(\mathbf{r}) \tag{5.14}$$

in terms of the functions $\varepsilon'_{\mathbb{P}}(\omega)$, $\varepsilon'_{\mathbb{M}}(\varepsilon)$ and $\sigma'_{\mathbb{P}}(\omega)$, $\sigma'_{\mathbb{M}}(\omega)$ characterizing the dielectric response of the constituents.

The propagation of electromagnetic waves in the composite medium is described by the macroscopic Maxwell equations (4.4)–(4.8). In the following, the magnetic permeabilities are assumed to be unity to simplify the analysis. The time variation of the fields is taken to be proportional to $\exp(-i\omega t)$. Fourier transforming and inserting Eq. (4.8) into Eq. (4.4) yields $\nabla \cdot \mathbf{D}(\mathbf{r}, \omega) = 0$, where the frequency-dependent displacement field

$$\mathbf{D}(\mathbf{r}, \omega) = \left(\varepsilon'(\mathbf{r}, \omega)\varepsilon_0 + \frac{i\sigma'(\mathbf{r}, \omega)}{\omega}\right)\mathbf{E}(\mathbf{r}, \omega) \tag{5.15}$$

combines the free current density and the polarization current. In the quasistatic approximation one assumes that the frequency is small enough

such that the inductive term on the right-hand side of Faradays law (4.6) can be neglected. By introducing the complex frequency dependent dielectric function

$$\varepsilon(\mathbf{r}, \omega) = \varepsilon'(\mathbf{r}, \omega) + i\varepsilon''(\mathbf{r}, \omega) = \varepsilon'(\mathbf{r}, \omega)\varepsilon_0 + i\frac{\sigma'(\mathbf{r}, \omega)}{\omega} \tag{5.16}$$

the electric field and the displacement are found to satisfy the equations

$$\nabla \cdot \mathbf{D}(\mathbf{r}, \omega) = 0 \tag{5.17}$$

$$\nabla \times \mathbf{E}(\mathbf{r}, \omega) = 0 \tag{5.18}$$

$$\mathbf{D}(\mathbf{r}, \omega) = \varepsilon(\mathbf{r}, \omega)\mathbf{E}(\mathbf{r}, \omega) \tag{5.19}$$

in the quasistatic approximation. If the electric field is replaced by the potential these equations assume the same form as Eq. (5.2), and hence the methods discussed in Section V.A can be employed in their analysis.

The neglect of the induced electromagnetic force is justified if the wavelength or penetration depth of the radiation is large compared to the typical linear dimension of the scatterers. If the scattering is caused by heterogeneities on the micrometer scale, as in many examples of interest, the approximation will be valid well into the infrared region.

2. *Experimental Observations for Rocks*

The electrical conductivity of rocks fully or partially saturated with brine is an important quantity for the reconstruction of subsurface geology from borehole logs [281, 282]. The main contribution to the total conductivity $\sigma'_{\mathbb{S}}$ of a sample $\mathbb{S} = \mathbb{P} \cup \mathbb{M}$ of brine-filled rock comes from the electrolyte. The contribution $\sigma'_{\mathbb{M}}$ from the rock matrix is usually negligible.[4] The electrolyte filling the pore space contributes through its intrinsic electrolytic conductivity $\sigma_{\mathbb{P}}$ as well as through electrochemical interactions at the interface. The total dc conductivity of the sample is written as

$$\sigma'_{\mathbb{S}}(0) = \frac{1}{F}\sigma'_{\mathbb{P}}(0) + \sigma'_{\partial\mathbb{P}}(0) \tag{5.20}$$

where $\sigma'_{\mathbb{P}}(0)$ is the dc conductivity of the electrolyte (usually salt water) filling the pore space $\mathbb{P}$ and $\sigma'_{\partial\mathbb{P}}(0)$ denotes the conductivity resulting from the electrochemical boundary layer at the internal surface [283]. The surface conductivity $\sigma'_{\partial\mathbb{P}}(0)$ correlates well with the specific internal surface S and indirectly with other quantities related to it. The factor F is

[4] Nonvanishing matrix conductivity does, however, occur in veinlike ores.

called *electrical formation factor*. If the salinity of the pore water is high or electrochemical effects are absent, the second term in Eq. (5.20) can be neglected and the formation factor becomes identical with the dimensionless resistivity of the sample normalized by the water resistivity. In the following, the formation factor will be used synonymously for the dimensionless inverse dc conductivity $F = [\sigma'(0)]^{-1}$.

The formation factor is usually correlated with the bulk porosity $\bar{\phi}$ in a relation known as "Archie's first equation" [284]

$$F = \bar{\phi}^{-m} \tag{5.21}$$

where the so-called cementation index m scatters widely and often obeys $1.3 \leq m \leq 2.5$ [281, 282]. Smaller values of m are associated empirically with loosely packed media, while higher values are associated with more consolidated and compacted media. Equation (5.21) implies not only an algebraic correlation between a purely geometric quantity $\bar{\phi}$ and a transport coefficient F, but it also states that porous rocks do not show a conductor–insulator transition at any finite porosity.

The experimental evidence for the postulated algebraic correlation (5.21) between conductivity and porosity is weak. The available range of the porosity rarely spans more than a decade. The corresponding conductivity data scatter widely for measurements on porous rocks and other media [188, 254, 281, 285–288]. The most reliable tests of Archies law have been performed on artificial porous media made from sintering glass beads [254, 285, 287]. These media have a microstructure very similar to sandstone and are at the same time free from electrochemical effects. A typical experimental result for glass beads is shown in Fig. 18 [287]. Note the small range of porosities in the figure. The existence of nontrivial power law relations in such samples is better demonstrated by correlating the conductivity with the permeability [170, 284]. In other experiments on artificial media a mixture of rubber balls and water is successively compressed while monitoring its conductivity [217, 289]. These experiments show deviations from the pure algebraic behavior postulated by Eq. (5.21). If the cementation "exponent" in Eq. (5.21) is assumed to depend on $\bar{\phi}$, then it increases at low porosities in agreement with the general trend that higher values correspond to a higher degree of compaction.

A much better confirmed observation on natural and artificial porous rocks is dielectric enhancement caused by the disorder in the microstructure [89, 287, 290–295]. Dielectric enhancement due to disorder has been studied extensively in percolation theory and experiment [40, 296,

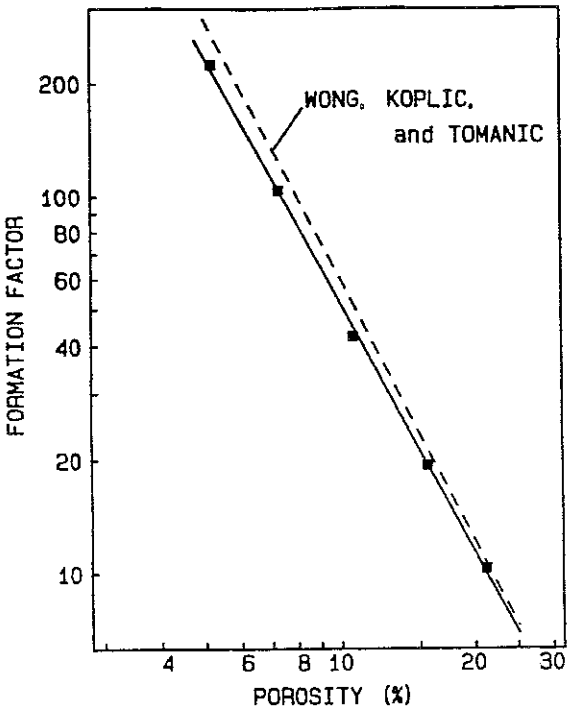

Figure 18. Log–log plot of formation factor versus porosity for sintered glass beads with 200–300-μm diameter. The solid line is a fit to $F = a\phi^{-m}$ with $a = 0.33$ and a cementation exponent $m = 2.2$ while the dashed line represents the results $a = 0.30$ and $m = 2.3$ on the same system in [254]. (Reproduced with permission from [287].)

297]. An example is shown in Fig. 19 for the sintered glass bead media containing thin-glass plates. In these media interfacial conductivity and other electrochemical effects can be neglected [287]. The frequency is plotted in units of $\omega_W = \sigma'_W/(\varepsilon_0\varepsilon'_W)$ the relaxation frequency of water. Although salt water and glass are essentially dispersion free in the frequency range shown in Fig. 19 their mixture shows a pronounced dispersion, which exceeds the values of the dielectric constants of both components. Similar results can be found in [287]. In [295] the dielectric response of a large number of sandstones and carbonates is given in terms of the empirical Cole–Cole formula [298]. Interestingly, the corresponding temporal relaxation function appears within the recent theory of nonequilibrium systems [64], which is the same theory on which the macroscopic local porosity distributions in Section III.A.5 were based.

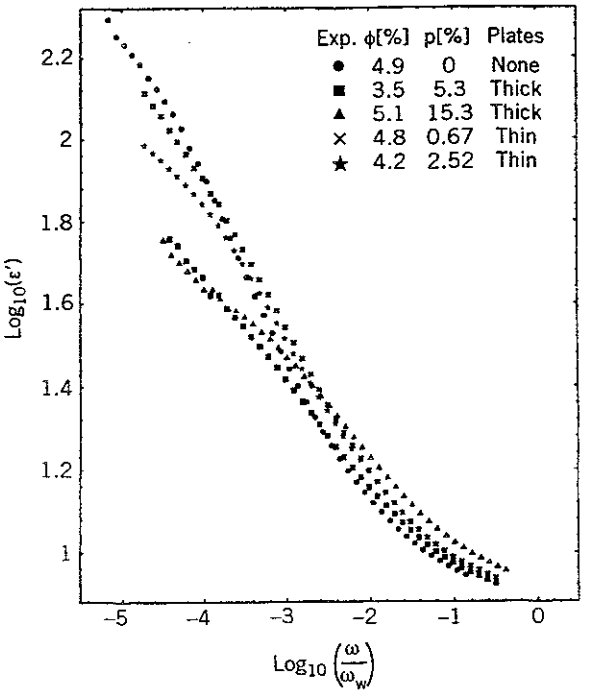

Figure 19. Log–log plot of the real part of the dielectric function versus normalized frequency ω/ω_w where $\omega_w = \sigma_w'/(\varepsilon_0\varepsilon_w')$ is the relaxation frequency of water for samples with porosities close to 5%. The different symbols denote different concentrations of thin glass plates p defined as the ratio of the mass of the glass plates divided by the total mass of glass in the sample [362].

3. *Theoretical Mixing Laws*

a. Spectral Theories. Dielectric mixing laws express the frequency dependent dielectric function or conductivity of a two-component mixture in terms of the dielectric functions of the constituents [31, 35, 40, 46]. Spectral theories express the effective dielectric function in terms of an abstract pole spectrum which is independent of the dielectric functions $\varepsilon_{\mathbb{P}}$ and $\varepsilon_{\mathbb{M}}$ of the two constituents filling the pore and matrix space [293, 299–309]. Theoretically, the effective dielectric function may be written as

$$\bar{\varepsilon} = \varepsilon_{\mathbb{M}}\left(1 - \sum_{n=1}^{\infty} \frac{a_n}{s - b_n}\right) \tag{5.22}$$

where

$$s = \left(1 - \frac{\varepsilon_{\mathbb{P}}}{\varepsilon_{\mathbb{M}}}\right)^{-1} \tag{5.23}$$

The constants a_n and b_n are the strength and location of the poles and they reflect the influence of the microgeometry. Unfortunately, these parameters do not have a direct geometrical interpretation, although under the assumption of stationarity and isotropy two sum rules are known that connect integrals of the pole spectrum with the bulk porosity [40].

b. Geometric Theories. The simplest geometric theories for the effective dielectric function $\bar{\varepsilon}$ are mean-field theories. In these approximations, a small spherical cell with a randomly valued dielectric constant ε is embedded into a homogeneous host medium of dielectric constant ε_h. Then the electrical analogue of Eq. (5.3) becomes

$$\bar{\varepsilon} = \varepsilon_h \left(1 + 2\left\langle \frac{\varepsilon - \varepsilon_h}{\varepsilon + 2\varepsilon_h} \right\rangle\right)\left(1 - \left\langle \frac{\varepsilon - \varepsilon_h}{\varepsilon + 2\varepsilon_h} \right\rangle\right)^{-1} \tag{5.24}$$

where the average denotes an ensemble average using the probability density $w(\varepsilon)$ of ε. A two-component medium $\mathbb{S} = \mathbb{P} \cup \mathbb{M}$ can be represented by the binary probability density

$$w(\varepsilon) = \bar{\phi}\delta(\varepsilon - \varepsilon_{\mathbb{P}}) + (1 - \bar{\phi})\delta(\varepsilon - \varepsilon_{\mathbb{M}}) \tag{5.25}$$

containing $\bar{\phi}$ as the only geometrical input parameter. The *Clausius–Mossotti approximation* [46, 310] for a two-component medium is obtained by setting $\varepsilon_h = \varepsilon_{\mathbb{M}}$ in the limit $\bar{\phi} \to 0$ or $\varepsilon_h = \varepsilon_{\mathbb{P}}$ in the limit $\bar{\phi} \to 1$ in Eq. (5.24). In the former case one obtains

$$\frac{\bar{\varepsilon} - \varepsilon_{\mathbb{M}}}{\bar{\varepsilon} + 2\varepsilon_{\mathbb{M}}} = \bar{\phi}\,\frac{\varepsilon_{\mathbb{P}} - \varepsilon_{\mathbb{M}}}{\varepsilon_{\mathbb{P}} + 2\varepsilon_{\mathbb{M}}} \tag{5.26}$$

which will be a good approximation at low porosities. Note that the Clausius–Mossotti approximation is not symmetrical under exchanging pore and matrix. A symmetrical and also self-consistent approximation is obtained from Eq. (5.24) by setting $\varepsilon_h = \bar{\varepsilon}$. This leads to the symmetrical *effective medium approximation* for a two-component medium

$$\bar{\phi}\,\frac{\varepsilon_{\mathbb{P}} - \bar{\varepsilon}}{\varepsilon_{\mathbb{P}} + 2\bar{\varepsilon}} + (1 - \bar{\phi})\,\frac{\varepsilon_{\mathbb{M}} - \bar{\varepsilon}}{\varepsilon_{\mathbb{M}} + 2\bar{\varepsilon}} = 0 \tag{5.27}$$

which also could have been derived from using Eq. (5.25) in Eq. (5.12). The effective medium approximation is a very good approximation for microstructures consisting of a small concentration of nonoverlapping spherical grains embedded in a host. Recently, much effort has been expended to show that the effective medium approximation (EMA) becomes exact for certain pathological microstructures [311]. The so-called *asymmetrical* or *differential effective medium approximation* is obtained by iterating the Clausius–Mossotti equation, which gives the effective conductivity to lowest order in $\bar{\phi}$ [285, 312, 313]. One finds the result

$$\left(\frac{\bar{\varepsilon}-\varepsilon_{\mathbb{M}}}{\varepsilon_{\mathbb{P}}-\varepsilon_{\mathbb{M}}}\left(\frac{\varepsilon_{\mathbb{P}}}{\bar{\varepsilon}}\right)^{1/3}=\bar{\phi}\right) \tag{5.28}$$

for spherically shaped inclusions.

The symmetric and asymmetric effective medium approximations can be generalized to ellipoidal inclusions because the electric field and polarization inside the ellipsoid remain uniform in an applied external field [40, 310, 312]. For aligned oblate spheroids whose quadratic form is $(x/b_2)^2+(y/b_2)^2+(z/b_1)^2=1$ with $b_1 \le b_2$ the effective medium theory for a two-component composite results in two coupled equations

$$\bar{\phi}\frac{\varepsilon_{\mathbb{P}_i}-\bar{\varepsilon}_i}{1+\Lambda_i(\varepsilon_{\mathbb{P}_i}-\bar{\varepsilon}_i)}+(1-\bar{\phi})\frac{\varepsilon_{\mathbb{M}_i}-\bar{\varepsilon}_i}{1+\Lambda_i(\varepsilon_{\mathbb{M}_i}-\bar{\varepsilon}_i)}=0 \tag{5.29}$$

where the index $i=1$ denotes vertical conductivities and the index $i=2$ denotes horizontal conductivities. The two equations in Eq. (5.29) are coupled through

$$\Lambda=\frac{L_i}{\bar{\varepsilon}_i} \tag{5.30}$$

$$2L_2=(-L_1) \tag{5.31}$$

$$L_1=(e^{-3}+e^{-1})(e-\arctan e) \tag{5.32}$$

$$e=\sqrt{\frac{b_2^2\bar{\varepsilon}_1}{b_1^2\bar{\varepsilon}_2}-1} \tag{5.33}$$

with $\frac{1}{3} \le L_1 \le 1$. The generalization of the asymmetric effective medium theory [Eq. (5.28)] to aligned spheroids with depolarization factor L was

given in [285] as

$$\frac{\bar{\varepsilon} - \varepsilon_{\mathbb{M}}}{\varepsilon_{\mathbb{P}} - \varepsilon_{\mathbb{M}}} \left(\frac{\varepsilon_{\mathbb{P}}}{\bar{\varepsilon}} \right)^{L} = \bar{\phi} \tag{5.34}$$

For spheroids with identical shape but isotropically distributed orientations

$$\frac{\bar{\varepsilon} - \varepsilon_{\mathbb{M}}}{\varepsilon_{\mathbb{P}} - \varepsilon_{\mathbb{M}}} \left(\frac{\varepsilon_{\mathbb{P}}}{\bar{\varepsilon}} \right)^{[3L(1-L)/(1+3L)]} \times \left(\frac{(5-3L)\varepsilon_{\mathbb{P}} + (1+3L)\varepsilon_{\mathbb{M}}}{(5-3L)\bar{\varepsilon} + (1+3L)\varepsilon_{\mathbb{M}}} \right)^{[2(1-3L)^2/(1+3L)(5-3L)]} = \bar{\phi} \tag{5.35}$$

was obtained in [205, 292, 314]. Equation (5.34) will be referred to as the Sen–Scala–Cohen model (SSC) and Eq. (5.35) will be called the uniform spheroid model (USM).

Recently, local porosity theory has been proposed as an alternative generalization of effective medium theories [168–175]. The simplest mean-field theories [Eqs. (5.26)–(5.28)] are based on the simplest geometric characterization theories of Section III.A.1. The theories are usually interpreted geometrically in terms of grain models (see Section III.B.2) with spherical grains embedded into a homogeneous host material. The generalizations (5.29), (5.34), and (5.35) are obtained by generalizing the interpretation to more general grain models. Local porosity theory on the other hand is based on generalizing the geometric characterization by using local geometry distributions (see Section III.A.5) rather than simply porosity or specific surface area alone. In Section III.A.5 two different types of local geometry distributions were introduced: Macroscopic distributions with infinitely large measurement cells defined in Eq. (3.52), and mesoscopic distributions with measurement cells of finite volume defined in Eq. (3.33). For a mesoscopic partitioning $\mathcal{H}$ of the sample using a simple cubic lattice with cubic unit cell $\mathbb{K}$ the self-consistency equation of local porosity theory for $\bar{\varepsilon}$ reads

$$\int_0^1 \left[\frac{\varepsilon_C(\phi) - \bar{\varepsilon}}{\varepsilon_C(\phi) + 2\bar{\varepsilon}} \lambda(\phi; \mathbb{K}) + \frac{\varepsilon_B(\phi) - \bar{\varepsilon}}{\varepsilon_B(\phi) + 2\bar{\varepsilon}} (1 - \lambda(\phi; \mathbb{K})) \right] \mu(\phi; \mathbb{K})\, d\phi = 0 \tag{5.36}$$

where $\lambda(\phi; \mathbb{K})$ is the local percolation probability defined in Section III.A.5.d, and $\varepsilon_C(\phi)$ and $\varepsilon_B(\phi)$ are the local dielectric functions of

percolating or conducting (index C) and nonpercolating or blocking (index B) measurement cells. In Eq. (5.40) it is assumed that the local dielectric response depends only on the porosity, but this may be generalized to include other geometrical characteristics.

Equation (5.36) has two interesting special cases. For a cubic measurement lattice ($z = 6$) in the limit $L \to 0$ in which the side length L of the cubic cells is small the one-cell local porosity distribution is given by Eq. (3.31) or (3.34) if the medium is mixing. Inserting Eq. (3.31) or (3.34) into Eq. (5.36) and using $\lambda(0) = 0$, $\lambda(1) = 1$, $\varepsilon_C(0) = \varepsilon_B(0) = \varepsilon_{\mathbb{M}}$, and $\varepsilon_C(1) = \varepsilon_B(1) = \varepsilon_{\mathbb{P}}$ yields Eq. (5.27) for traditional effective medium theory. Note, however, that in the limit $L \to 0$ the local porosities become *highly correlated* rendering a description of the geometry in terms of the one-cell function $\mu(\phi; \mathbb{K})$ more and more inadequate. This argument does not apply in the opposite limit $L \to \infty$ in which the measurement cells $\mathbb{K}$ become very large. For stationary media, the local porosities in nonoverlapping measurement cells are uncorrelated in the limit $L \to \infty$. For stationary and mixing media the local porosity distribution

$$\lim_{b \to \infty} \mu(\phi; b\mathbb{K}) = \delta(\phi - \bar{\phi}) \tag{5.37}$$

becomes concentrated at a single point according to Eq. (3.32) or (3.35). Assuming, as before, that the limit is independent of the shape of $\mathbb{K}$ Equation (5.36) reduces to

$$\lambda(\bar{\phi}) \frac{\varepsilon_C(\bar{\phi}) - \bar{\varepsilon}}{\varepsilon_C(\bar{\phi}) + 2\bar{\varepsilon}} + (1 - \lambda(\bar{\phi})) \frac{\varepsilon_B(\bar{\phi}) - \bar{\varepsilon}}{\varepsilon_B(\bar{\phi}) + 2\bar{\varepsilon}} = 0 \tag{5.38}$$

which is identical to Eq. (5.27) except for the replacement of $\bar{\phi}$ by $\lambda(\bar{\phi})$, $\varepsilon_{\mathbb{M}}$ by $\varepsilon_B(\bar{\phi})$, and $\varepsilon_{\mathbb{P}}$ by $\varepsilon_C(\bar{\phi})$. Repeating the same differential replacement arguments [285] that lead to Eq. (5.28) for $\lambda(\bar{\phi})$ instead of $\bar{\phi}$ gives a differential version of mesoscopic local porosity theory in the limit $L \to \infty$

$$\frac{\bar{\varepsilon} - \varepsilon_B(\bar{\phi})}{\varepsilon_C(\bar{\phi}) - \varepsilon_B(\bar{\phi})} \left(\frac{\varepsilon_C(\bar{\phi})}{\bar{\varepsilon}} \right)^{1/3} = \lambda(\bar{\phi}) \tag{5.39}$$

Note that the limiting equations (5.38) and (5.39) for $L \to \infty$ contain geometric information about the pore space that goes beyond the bulk porosity and is contained in the function $\lambda(\bar{\phi})$.

As discussed in Section III.A.5.e the δ distribution is not the only possible macroscopic limit. Macroscopically heterogeneous media are described by the limiting macroscopic local porosity densities

$\mu(\phi; \varpi, C, D)$ defined in Eq. (3.52). The δ distribution $\delta(\phi - \bar{\phi})$ is obtained in the limit $\varpi \to 1$ or in the degenerate case arising for $D = 0$. The macroscopic form of local porosity theory for the effective dielectric constant is given by the integral equation

$$\int_0^1 \left[\frac{\varepsilon_C(\phi) - \bar{\varepsilon}}{\varepsilon_C(\phi) + 2\bar{\varepsilon}} \lambda(\phi) + \frac{\varepsilon_B(\phi) - \bar{\varepsilon}}{\varepsilon_B(\phi) + 2\bar{\varepsilon}} (1 - \lambda(\phi)) \right] \times \mu(\phi; \varpi, C, D)\, d\phi = 0 \tag{5.40}$$

with $\mu(\phi; \varpi, C, D)$ defined in Eq. (3.52) and $\varpi \neq 1$ and $D \neq 0$. If the parameters $\varpi = \varpi(\bar{\phi}, \overline{\phi^2}, \overline{\phi^3})$, $D = D(\bar{\phi}, \overline{\phi^2}, \overline{\phi^3})$, and $C = C(\bar{\phi}, \overline{\phi^2}, \overline{\phi^3})$, are expressed in terms of the moments according to Eq. (3.53) the resulting effective dielectric function $\bar{\varepsilon} = \bar{\varepsilon}(\bar{\phi}, \overline{\phi^2}, \overline{\phi^3})$ is found to be a function of the bulk porosity and its fluctuations. This observation indicates the possibility to study Archie's law within the framework of local porosity theory.

4. *Archie's Law*

Archie's law [Eq. (5.21)] concerns the effective dc conductivity, $\sigma'(0)$, and can be studied by replacing ε with $\sigma'(0)$ in all the formulas of Section V.B.3. For notational convenience the shorthand notation $\sigma'(0) = \sigma$ will be employed in this section. Archie's law can then be discussed by replacing ε with σ throughout and setting $\sigma_{\mathbb{M}} = 0$. From the Clausius–Mossotti formula (5.26) one obtains the relation

$$\bar{\sigma} = \sigma_{\mathbb{P}} \frac{2\bar{\phi}}{3 - \bar{\phi}} \tag{5.41}$$

which reproduces Archie's law (5.21) with a cementation exponent $m = 1$. The symmetrical effective medium approximation (5.27) gives

$$\bar{\sigma} = \frac{\sigma_{\mathbb{P}}}{2} (3\bar{\phi} - 1) \tag{5.42}$$

for $\bar{\phi} > \frac{1}{3}$ and $\bar{\sigma} = 0$ for $\bar{\phi} \leq \frac{1}{3}$. Thus the symmetrical effective medium theory predicts a percolation transition at $\bar{\phi}_c = \frac{1}{3}$ and does not agree with Archie's law (5.21) in this respect. The same conclusion holds for the anisotropic generalization of the symmetric theory to nonspherical inclusions given in Eq. (5.29).

For the asymmetric effective medium theory in its simplest form (5.28)

one finds

$$\bar{\sigma} = \sigma_{\mathrm{p}} \bar{\phi}^{3/2} \tag{5.43}$$

consistent with Archies law (5.21) with cementation exponent $m = \frac{3}{2}$. This expression has found much attention because it yields $m \neq 1$ [205, 285, 312, 314, 315]. There are, however, several problems with Eq. (5.43). Its derivation implies that the solid component is not connected [312]. The experimentally observed behavior is often not algebraic, and if a power law is nevertheless assumed its exponent is often very different from $\frac{3}{2}$. Most importantly, the frequency dependent theory does not predict sufficient dielectric enhancement. The first problem can be circumvented by generalizing to a three-component medium [313, 316], the second can be overcome by considering nonspherical inclusions [205, 285, 312, 314, 315]. As an example the generalization to nonspherical grains [Eq. (5.34)] gives

$$\bar{\sigma} \approx \sigma_{\mathrm{p}} \bar{\phi}^{1/(1-L)} \tag{5.44}$$

with $\frac{1}{3} \leq L \leq 1$, and the uniform spheroid model gives a similar result. The most serious problem, however, is the fact pointed out in [285, 292] that Eq. (5.28) cannot reproduce the frequency dependence of $\bar{\sigma}$ and the observed dielectric enhancement. This will be discussed further in Section V.B.5.

Local porosity theory contains geometrical information above and beyond the average porosity $\bar{\phi}$. Consequently, it predicts more general relationships between porosity and conductivity. In its simplest form Eq. (5.38) leads to

$$\bar{\sigma} = \frac{\sigma_C(\bar{\phi})}{2} (3\lambda(\bar{\phi}) - 1) \tag{5.45}$$

which may or may not have a percolation transition depending on whether the equation

$$\lambda(\bar{\phi}_c) = \tfrac{1}{3} \tag{5.46}$$

has a solution $0 < \bar{\phi}_c < 1$ that can be interpreted as a critical porosity. Therefore, the percolation threshold can arise at any porosity including $\bar{\phi}_c = 0$. This fact reconciles percolation theory with Archie's law. Note

also that the behavior is nonuniversal[5] and depends on the local percolation probability function $\lambda(\phi)$, and the local response $\sigma_C(\bar{\phi})$. Similarly, the differential form (5.39) of local porosity theory yields

$$\bar{\sigma} = \sigma_C(\bar{\phi})\lambda(\bar{\phi})^{3/2} \tag{5.47}$$

which is more versatile than Eq. (5.44). The preceding results hold for large measurement cells when $\mu(\phi) \approx \delta(\phi - \bar{\phi})$. For general local porosity distributions equation (5.36) gives the result [168]

$$\bar{\sigma} \approx \sigma_0(p - p_c) \tag{5.48}$$

where $p_c = \frac{1}{3}$,

$$\frac{1}{\sigma_0} = \int_0^1 \frac{\lambda(\phi; \mathbb{K})\mu(\phi; \mathbb{K})}{\sigma_C(\phi)}\, d\phi \tag{5.49}$$

and p is the control parameter of the percolation transition

$$p = \int_0^1 \lambda(\phi; \mathbb{K})\mu(\phi; \mathbb{K})\, d\phi \tag{5.50}$$

giving the total fraction of percolating local geometries. The result [Eq. (5.48)] applies if $\bar{\phi} \to 0$ for all values of p, and also if $p \to p_c$ at arbitrary $\bar{\phi}$. It holds universally as long as

$$\int_0^1 \frac{1}{\phi}\, \lambda(\phi; \mathbb{K})\mu(\phi; \mathbb{K})\, d\phi < \infty \tag{5.51}$$

the inverse first moment is finite [317]. This condition is violated for the macroscopic distributions $\mu(\phi; \varpi, C, D)$ if all cells are percolating, $\lambda(\phi) = 1$. In such a case if $\lambda(\phi)\mu(\phi) \propto \phi^{-\alpha}$ as $\phi \to 0$, then Eq. (5.48) is replaced with [317]

$$\bar{\sigma} \propto (p - p_c)^{1/[1-\alpha(\bar{\phi}, \overline{\phi^3}, \overline{\phi^3})]} \tag{5.52}$$

where α depends on the moments $\overline{\phi^n}$ because ϖ depends on them through Eq. (3.53).

Compaction and consolidation processes will in general change the local porosity distribution $\mu(\phi)$ where its dependence on $\mathbb{K}$ or the parameters ϖ, C, D has been suppressed. Assume that it is possible to

[5] The statement in [41] that local porosity theory predicts Archies law with a universal exponent is incorrect.

describe the consolidation process as a one parameter family $\mu_q(\phi)$ of local porosity distributions depending on a parameter q, which characterizes the compaction process. Then the total fraction p, the bulk porosity $\bar{\phi}$, and the integral (5.49) become functions of q. If it is possible to invert the relation $\bar{\phi} = \bar{\phi}(q)$, then the fraction p becomes $p = p(\bar{\phi})$, and equally $\sigma_0 = \sigma_0(\bar{\phi})$. Therefore, Eqs. (5.48) and (5.52) become porosity–conductivity relations which depend on the consolidation process.[6] If the condition (5.51) and the asymptotic expansion $\sigma_0(\bar{\phi}) = \bar{\phi}^{\beta}(1 + \cdots)$ and $p(\bar{\phi}) = p_c + \bar{\phi}^{\gamma}(p_1 + \cdots)$ hold, then these equations yield Archies law (5.21) with a nonuniversal cementation index $m = \beta + \gamma$. If the condition (5.51) does not hold and $\lambda(\phi)\mu(\phi) \propto \phi^{-\alpha}$, then

$$m = \beta + \gamma\left(1 + \frac{\alpha}{1-\alpha}\right) \tag{5.53}$$

which is even less universal. The validity of the expansion $p(\bar{\phi}) \propto p_c + \bar{\phi}^{\gamma}(p_1 + \cdots)$ has been tested by experiment [173, 174]. Figure 20 shows the function $p(\bar{\phi})$ obtained for sintering of glass beads. The measured data are the points, the solid curve represents a fit $p(\bar{\phi}) = 1.51\bar{\phi}^{0.45}$ through the data. This fit was chosen to indicate that the consolidation process of sintering glass beads is expected to show a percolation transition at small but finite threshold $\bar{\phi}_c$ [173, 174]. Note, however, that the data of Fig. 20 are consistent with the form $p(\bar{\phi}) \propto p_c + \bar{\phi}(p_1 + \cdots)$ corresponding to $\gamma = 1$.

5. *Dielectric Dispersion and Enhancement*

The theoretical mixing laws for the frequency dependent dielectric function discussed in Section V.B.3 can be compared with experiment. Spectral theories generally give good fits to the experimental data [287, 293] but do not allow a geometrical interpretation. Geometrical theories on the other hand contain independently observable geometric characteristics, and can be falsified by experiment.

The single parameter mean-field theories Eqs. (5.12), (5.26) and (5.28) contain only the bulk porosity as a geometrical quantity. They are generally unable to reproduce the observed dielectric dispersion and enhancement. This is illustrated in Fig. 21, which shows the experimental measurements of the real part of the frequency dependent dielectric function as solid circles [175]. The results were obtained for a brine

[6] The statement in [41] that local porosity theory predicts Archies law with a universal cementation index is incorrect.

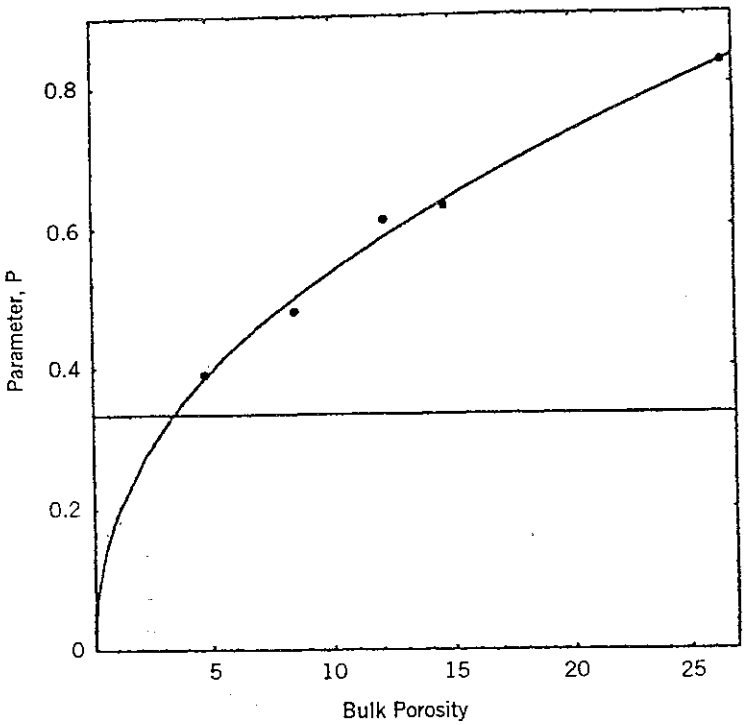

Figure 20. Total fraction of percolating local geometries p for the sintering process of 90 μm glass beads as parametrized by the bulk porosity $\bar{\phi}$ [173].

saturated sample of sintered 250-μm glass spheres. The porosity of the specimen was 10.7%, and the water conductivity was 12.4 mS m^{-1}. A cross-sectional image of the pore space has been displayed in Fig. 13. The frequency in Fig. 21 is dimensionless and measured in units of the relaxation frequency of water $\omega_W = \sigma'_W/(\varepsilon_0\varepsilon'_W)$ where σ'_W and ε'_W are the conductivity and dielectric constant of water, which are constant over the frequency range of interest.[7] With the porosity known from independent measurements the simple mean-field mixing laws can be tested without adjustable parameters. The prediction of the Clausius–Mossotti approximation (5.26) is shown as the solid line with water as the uniform background, and as the dashed line with glass as background. The prediction of the symmetrical effective medium theory [Eq. (5.27)] is shown as the dotted line. The asymmetrical (differential) effective

[7] For water with $\sigma'_W = 12.4$ mS m^{-1} the relaxation frequency is $\omega_W = 2.82$ MHz.

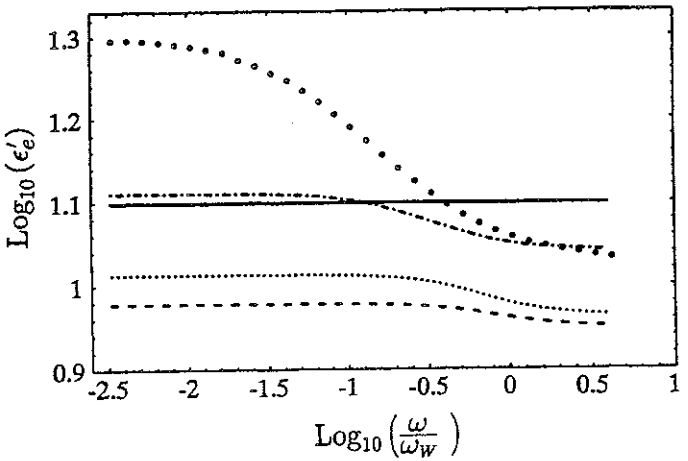

Figure 21. Comparison of simple mean-field theory predictions with the experimentally observed dielectric response of sintered glass beads as a function of frequency. The solid circles are the experimental results for a 10.7% sample of sintered 250-μm glass beads filled with water having $\sigma'_w = 12.4\ \mathrm{mS\ m^{-1}}$. The solid line is the Clausius–Mossotti prediction [Eq. (5.26)] with water background, the dashed line corresponds to the same with glass background. The dotted line is the symmetrical effective medium theory [Eq. (5.27)], the dash–dotted line is the asymmetrical effective medium theory [Eq. (5.28)] [175].

medium scheme (5.28), shown as the dash–dotted curve, appears to reproduce the high-frequency behavior correctly, but does not give the low-frequency enhancement.

To compare the experimental observations with the Sen–Scala–Cohen model [Eq. (5.34)] or with the uniform spheroid model [Eq. (5.35)] the depolarization factor L of the ellipsoids has to be treated as a free-fit parameter [175]. In the case of local porosity theory the local porosity distributions $\mu(\phi;\mathbb{K})$ have been measured independently from cross sections through the pore space using image processing techniques. The resulting distributions have been displayed in Fig. 15 for different sizes L of the cubic measurement cells.[8] The local percolation probability function $\lambda(\phi)$ on the other hand has not yet been measured directly from pore-space reconstruction. Instead, the result for $p(\bar{\phi})$ displayed as the power law fit in Fig. 20 was combined with the fact that $\lambda(\bar{\phi}) = p(\bar{\phi})$ in the limit of large measurement cells in which $\mu(\phi)$ becomes a δ distribution concentrated at $\bar{\phi}$ [see Eq. (3.32) or (3.35)]. These observa-

[8] The side length of the measurement cell and the depolarization factor have been denoted by the same symbol L. Their distinction should be clear from the context.

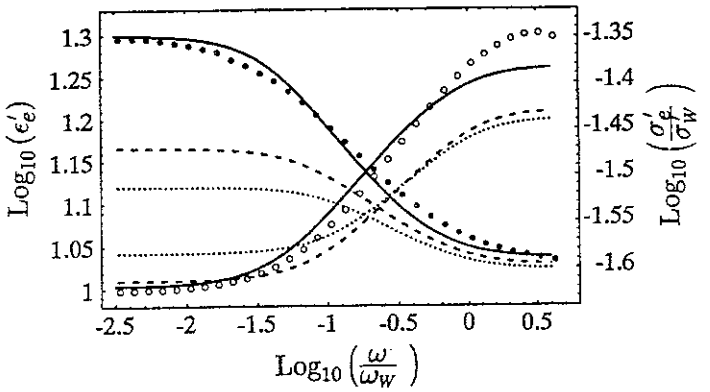

Figure 22. Log–log plot of theoretical predictions for the dielectric dispersion with experimental observations of the effect. Solid circles represent experimental measurements of the effective real dielectric constant and the effective real conductivity as a function of frequency. The dielectric function decreases from left to right, and its values are read from the labels on the left axis. The conductivity increases from left to right and is indicated on the right axis. The dotted line is obtained as a best fit to Eq. (5.34) with $L = 0.387$ for the depolarization factor. The dashed line corresponds to the uniform spheroid model [Eq. (5.34)] with $L = 0.597$ corresponding to an aspect ratio of 2.58 for the oblate spheroid. The solid lines are obtained from local porosity theory (5.36) using $\zeta = 0.2035$ [Eq. (5.28)] [175].

tions and measurements motivate the Ansatz $\lambda(\bar{\phi}) = \bar{\phi}^{\zeta}$ treating ζ as a single free-fit parameter. Fig. 22 shows fits for the frequency dependent real dielectric function $\bar{\varepsilon}'(\omega)$ and inverse formation factor $F^{-1}(\omega)$. In Fig. 22 the circles are the experimental results. All curves represent one parameter fits to the experimental data. The solid curves are obtained from local porosity theory [Eq. (5.36)] using $\zeta = 0.2035$ as the best value of the fit parameter. The local porosity distributions were those of Fig. 15 for measurement cells of side length 50 pixels. The dashed curves correspond to the uniform spheroid model [Eq. (5.35)] with a depolarization factor of 0.597 as the best value of its fit parameter. The dotted curves represent the Sen–Scala–Cohen model with a best value of 0.387 for the depolarization.

Similar experimental results for the dielectric dispersion have been observed in natural rock samples [292]. Figure 8 in [292] compares the measurements only to the uniform spheroid model. Similar to the results of [175] on sintered glass beads the uniform spheroid model did not reproduce the dielectric enhancement, and required too high aspect ratios to be realistic for the observed microstructure.

Local porosity theory has also been used to estimate the broadening of the dielectric relaxation of polymers blends [174].

C. Single-Phase Fluid Flow

1. *Permeability and Darcy's Law*

The permeability is the most important physical property of a porous medium in much the same way as the porosity is its most important geometrical property. Some authors define porous media as media with a nonvanishing permeability [2]. Permeability measures quantitatively the ability of a porous medium to conduct fluid flow. The permeability tensor $\mathbf{K}$ relates the macroscopic flow density $\bar{\mathbf{v}}$ to the applied pressure gradient ∇P or external field $\mathbf{F}$ through

$$\bar{\mathbf{v}} = \frac{\mathbf{K}}{\eta}(\mathbf{F} - \nabla P) \tag{5.54}$$

where η is the dynamic viscosity of the fluid. The parameter $\bar{\mathbf{v}}$ is the volumetric flow rate per unit area of cross section. Equation (5.54) is known as *Darcy's law*.

The permeability has dimensions of an area, and it is measured in units of Darcy (d). If the pressure is measured in physical atmospheres one has $1\text{d} = 0.9869\ \mu\text{m}^2$ while $1\text{d} = 1.0197\ \mu\text{m}^2$ if the pressure is measured in technical atmospheres. To within practical measuring accuracy one may often assume $1\text{d} = 10^{-12}\ \text{m}^2$. An important question arising from the fact that $\mathbf{K}$ is dimensionally an area concerns the interpretation of this area or length scale in terms of the underlying geometry. This fundamental question has recently found renewed interest [4, 43, 170, 172, 318–320]. Unfortunately, most answers proposed in these discussions [4, 318–320] give a dynamic rather than geometrical interpretation of this length scale. The traditional answer to this basic problem is provided by hydraulic radius theory [2, 3]. It gives a geometrical interpretation that is based on the capillary models of Section III.B.1, and it will be discussed in Section V.C.2.

The permeability does not appear in the microscopic Stokes or Navier–Stokes equations. Darcy's law and with it the permeability concept can be derived from microscopic Stokes flow equations using homogenization techniques [38, 268–271, 321], which are asymptotic expansions in the ratio of microscopic to macroscopic length scales. The derivation will be given in Section V.C.3 below.

The linear Darcy law holds for flows at low Reynolds numbers in which the driving forces are small and balanced only by the viscous forces. Various nonlinear generalizations of Darcy's law have also been derived using homogenization or volume averaging methods [1, 38, 268, 269, 271, 321–325]. If a nonlinear Darcy law governs the flow in a given

experiment this would appear in the measurement as if the permeability becomes velocity dependent. The linear Darcy law breaks down also if the flow becomes too slow. In this case interactions between the fluid and the pore walls become important. Examples occur during the slow movement of polar liquids or electrolytes in finely porous materials with high specific internal surface.

2. *Hydraulic Radius Theory*

The hydraulic radius theory or Carman–Kozeny model is based on the geometrical models of capillary tubes discussed above in Section III.B.1. In such capillary models the permeability can be obtained exactly from the solution of the Navier–Stokes Eq. (4.9) in the capillary. Consider a cylindrical capillary tube of length L and radius a directed along the x direction. The velocity field $\mathbf{v}(\mathbf{r})$ for creeping laminar flow is of the form $\mathbf{v}(\mathbf{r}) = v(r)\mathbf{e}_x$, where $\mathbf{e}_x$ denotes a unit vector along the pipe, and r measures the distance from the center of the pipe. The pressure has the form $P(\mathbf{r}) = P(x)\mathbf{e}_x$. Assuming "no-slip" boundary conditions, $v(a) = 0$, at the tube walls one obtains for $v(r)$ the familiar Hagen–Poiseuille result [326]

$$P(x) = P(0) - (P(0) - P(L))\frac{x}{L} \tag{5.55}$$

$$v(r) = \frac{P(0) - P(L)}{4\eta L}(a^2 - r^2) \tag{5.56}$$

with a parabolic velocity and linear pressure profile. The volume flow rate Q is obtained through integration as

$$Q = \int_0^a v(r)2\pi r\, dr = \frac{\pi a^4}{8\eta}\frac{P(0) - P(L)}{L} \tag{5.57}$$

Consider now the capillary tube model of Section III.B.1 with a cubic sample space $\mathbb{S}$ of side length L. The pore space $\mathbb{P}$ consists of N nonintersecting capillary tubes of radii a_i and lengths L_i distributed according to a joint probability density $\Pi(a, L)$. The pressure drop must then be calculated over the length L_i and thus the right-hand side of Eq. (5.57) is multiplied by a factor L/L_i. Because the tubes are nonintersecting, the volume flow Q_i through each of the tubes can be added to give the macroscopic volume flow rate per unit area $\bar{v} = (1/L^2)\sum_{i=1}^{N} Q_i$. Thus the permeability of the capillary tube model is simply additive, and it

reads

$$k = \frac{\pi}{8L} \sum_{i=1}^{N} \frac{a_i^4}{L_i} \tag{5.58}$$

Dimensional analysis of Eqs. (3.58), (3.59), and (5.58) shows that kS^2/ϕ^3 is dimensionless. Averaging Eq. (5.58) as well as Eqs. (3.58) and (3.59) for the porosity and specific internal surface of the capillary tube model yields the relation

$$\langle k \rangle = \frac{C}{2} \frac{\langle \phi \rangle^3}{\langle S \rangle^2} \tag{5.59}$$

where the mixed-moment ratio

$$C = L^2 \left\langle \frac{a^4}{L} \right\rangle \frac{\langle aL \rangle^2}{\langle a^2 L \rangle^3} \tag{5.60}$$

is a dimensionless number, and the angular brackets denote as usual the average with respect to $\Pi(a, L)$.

The *hydraulic radius theory* or Carman–Kozeny model is obtained from a mean-field approximation which assumes $\langle f(x) \rangle \approx f(\langle x \rangle)$. The approximation becomes exact if the distribution is sharply peaked or if $L_i = L$ and $a_i = a$ for all N. With this approximation the average permeability $\langle k \rangle$ may be rewritten in terms of the average hydraulic radius $\langle R_H \rangle$ defined in Eq. (3.66) as

$$\langle k \rangle \approx \frac{\langle \phi \rangle}{2\langle \mathcal{T} \rangle^2} \frac{\langle \phi \rangle^2}{\langle S \rangle^2} \approx \frac{\langle \phi \rangle}{2\langle \mathcal{T} \rangle^2} \left\langle \frac{\phi^2}{S^2} \right\rangle \approx \frac{\langle \phi \rangle \langle R_H \rangle^2}{2\langle \mathcal{T} \rangle^2} \approx \frac{\langle \phi \rangle \langle a \rangle^2}{8\langle \mathcal{T} \rangle^2} \tag{5.61}$$

where $\langle \mathcal{T} \rangle = \langle L \rangle / L$ is the average of the tortuosity defined above in Eq. (3.62). Equation (5.61) is one of the main results of hydraulic radius theory. The permeability is expressed as the square of an average hydraulic radius $\langle R_H \rangle$, which is related to the average "pore width" as $\langle R_H \rangle = \langle a \rangle / 2$.

It must be stressed that hydraulic radius theory is not exact even for the simple capillary tube model because in general $\langle R_H \rangle \neq \langle \phi \rangle / \langle S \rangle$ and $C \neq \langle \mathcal{T} \rangle^2$. However, interesting exact relations for the average permeability can be obtained from Eqs. (5.59) and (5.60) in various special cases without employing the mean-field approximation of hydraulic radius theory. If the tube radii and lengths are independent, then the dis-

tribution factorizes as $\Pi(a, L) = \Pi_a(a)\Pi_L(L)$. In this case the permeability may be written as

$$\langle k \rangle = \frac{1}{2} \frac{\langle 1/\mathcal{T} \rangle}{\langle \mathcal{T} \rangle} \frac{\langle a^4 \rangle \langle a \rangle^2}{\langle a^2 \rangle^3} \frac{\langle \phi \rangle^3}{\langle S \rangle^2} = \frac{\langle \phi \rangle}{8} \frac{\langle 1/\mathcal{T} \rangle}{\langle \mathcal{T} \rangle} \frac{\langle a^4 \rangle}{\langle a^2 \rangle} \tag{5.62}$$

where $\langle \mathcal{T} \rangle$ is the average of the tortuosity factor defined in Eq. (3.62). The last equality interprets $\langle k \rangle$ in terms of the microscopic effective cross section $\langle a^4 \rangle / \langle a^2 \rangle$ determined by the variance and curtosis of the distribution of tube radii. Further specialization to the cases $L_i = l$ or $a_i = a$ is readily carried out from these results.

Finally, it is of interest to consider also the capillary slit model of Section III.B.1. The model assumes again a cubic sample of side length L containing a pore space consisting of parallel slits with random widths governed by a probability density $\Pi(b)$. For flat planes without undulations the analogue of tortuosity is absent. The average permeability is obtained in this case as

$$\langle k \rangle = \frac{1}{3} \frac{\langle b^3 \rangle}{\langle b \rangle^3} \frac{\langle \phi \rangle^3}{\langle S \rangle^2} \tag{5.63}$$

which has the same form as Eq. (5.59) with a constant $C = \langle b^3 \rangle / \langle b \rangle^3$. The prefactor one-third is due to the different shape of the capillaries, which are planes rather than tubes.

3. *Derivation of Darcy's Law from Stokes Equation*

The previous section V.C.2 has shown that Darcy's law arises in the capillary models. This raises the question of whether it can be derived more generally. This section shows that Darcy's law can be obtained from Stokes equation for a slow flow. It arises to lowest order in an asymptotic expansion whose small parameter is the ratio of microscopic to macroscopic length scales.

Consider the stationary and creeping (low Reynolds number) flow of a Newtonian incompressible fluid through a porous medium whose matrix is assumed to be rigid. The microscopic flow through the pore space $\mathbb{P}$ is governed by the stationary Stokes equations for the velocity $\mathbf{v}(\mathbf{r})$ and pressure $P(\mathbf{r})$

$$\eta \, \Delta \mathbf{v}(\mathbf{r}) + \mathbf{F} - \nabla P(\mathbf{r}) = 0 \tag{5.64}$$

$$\nabla^T \cdot \mathbf{v}(\mathbf{r}) = 0 \tag{5.65}$$

inside the pore space, $\mathbb{P} \ni \mathbf{r}$, with no slip boundary condition

$$\mathbf{v}(\mathbf{r}) = \mathbf{0} \tag{5.66}$$

for $\mathbf{r} \in \partial\mathbb{P}$. The body force $\mathbf{F}$ and the dynamic viscosity η are assumed to be constant.

The derivation of Darcy's law assumes that the pore space $\mathbb{P}$ has a characteristic length scale ℓ, which is small compared to some macroscopic scale L. The microscopic scale ℓ could be the diameter of grains, the macroscale L could be the diameter of the sample $\mathbb{S}$ or some other macroscopic length such as the diameter of a measurement cell or the wavelength of a seismic wave. The small ratio $\varepsilon = l/L$ provides a small parameter for an asymptotic expansion. The expansion is constructed by assuming that all properties and fields can be written as functions of two new space variables $\mathbf{x}$, $\mathbf{y}$, which are related to the original space variable $\mathbf{r}$ as $\mathbf{x} = \mathbf{r}$ and $\mathbf{y} = \mathbf{r}/\varepsilon$. All functions $f(\mathbf{r})$ are now replaced with functions $f(\mathbf{x}, \mathbf{y})$ and the slowly varying variable $\mathbf{x}$ is allowed to vary independently of the rapidly varying variable $\mathbf{y}$. This requires to replace the gradient according to

$$\nabla f(\mathbf{r}) = \nabla f\left(\mathbf{r}_1 \frac{\mathbf{r}}{\varepsilon}\right) = \nabla_{\mathbf{x}} f(\mathbf{x}, \mathbf{y}) + \frac{1}{\varepsilon} \nabla_{\mathbf{y}} f(\mathbf{x}, \mathbf{y}) \tag{5.67}$$

and the Laplacian is replaced similarly. The velocity and pressure are now expanded in ε where the leading orders are chosen such that the solution is not reduced to the trivial zero solution and the problem remains physically meaningful. In the present case this leads to the expansions [268, 271, 280]

$$\mathbf{v}(\mathbf{r}) = \varepsilon^2 \mathbf{v}_0(\mathbf{x}, \mathbf{y}) + \varepsilon^3 \mathbf{v}_1(\mathbf{x}, \mathbf{y}) + \cdots \tag{5.68}$$

$$P(\mathbf{r}) = P_0(\mathbf{x}, \mathbf{y}) + \varepsilon P_1(\mathbf{x}, \mathbf{y}) + \cdots \tag{5.69}$$

where $\mathbf{x} = \mathbf{r}$ and $\mathbf{y} = \mathbf{r}/\varepsilon$. Inserting into Eqs. (5.64)–(5.66) yields to lowest order in ε the system of equations

$$\nabla_{\mathbf{y}} P_0(\mathbf{x}, \mathbf{y}) = 0 \quad \text{in } \mathbb{P} \tag{5.70}$$

$$\nabla_{\mathbf{y}}^T \cdot \mathbf{v}_0 = 0 \quad \text{in } \mathbb{P} \tag{5.71}$$

$$\eta \Delta_{\mathbf{y}} \mathbf{v}_0 - \nabla_{\mathbf{y}} P_1 - \nabla_{\mathbf{x}} P_0 + \mathbf{F} = 0 \quad \text{in } \mathbb{P} \tag{5.72}$$

$$\nabla_{\mathbf{x}}^T \cdot \mathbf{v}_0 + \nabla_{\mathbf{y}}^T \cdot \mathbf{v}_1 = 0 \quad \text{in } \mathbb{P} \tag{5.73}$$

$$\mathbf{v}_0 = \mathbf{0} \quad \text{on } \partial\mathbb{P} \tag{5.74}$$

in the fast variable $\mathbf{y}$. It follows from the first equation that $P_0(\mathbf{x}, \mathbf{y})$ depends only on the slow variable $\mathbf{x}$, and thus it appears as an additional external force for the determination of the dependence of $\mathbf{v}_0(\mathbf{x}, \mathbf{y})$ on $\mathbf{y}$ from the remaining equations. Because the equations are linear the solution $\mathbf{v}_0(\mathbf{x}, \mathbf{y})$ has the form

$$\mathbf{v}_0(\mathbf{x}, \mathbf{y}) = \sum_{i=1}^{3} \left(F_i - \frac{\partial P_0}{\partial x_i} \right) \mathbf{u}_i(\mathbf{x}, \mathbf{y}) \tag{5.75}$$

where the three vectors $\mathbf{u}_i(\mathbf{x}, \mathbf{y})$ (and the scalars $Q_i(\mathbf{x}, \mathbf{y})$) are the solutions of the three systems ($i = 1, 2, 3$)

$$\nabla_{\mathbf{y}}^T \cdot \mathbf{u}_i = 0 \quad \text{in } \mathbb{P} \tag{5.76}$$

$$\eta \, \Delta_{\mathbf{y}} \mathbf{u}_i - \nabla_{\mathbf{y}} Q_i - \mathbf{e}_{y_i} = 0 \quad \text{in } \mathbb{P} \tag{5.77}$$

$$\mathbf{u}_i = \mathbf{0} \quad \text{on } \partial\mathbb{P} \tag{5.78}$$

and $\mathbf{e}_{y_i}$ is a unit vector in the direction of the y_i-axis.

It is now possible to average $\mathbf{v}_0$ over the fast variable $\mathbf{y}$. The spatial average over a convex set $\mathbb{K}$ is defined as

$$\bar{\mathbf{v}}_0(\mathbf{x}; \mathbb{K}) = \frac{1}{V(\mathbb{K})} \int \mathbf{v}_0(\mathbf{x}, \mathbf{y}) \chi_{\mathbb{K}}(\mathbf{x}, \mathbf{y}) \, d^3\mathbf{y} \tag{5.79}$$

where $\mathbb{K}$ is centered at $\mathbf{x}$ and $\chi_{\mathbb{K}}(\mathbf{x}, \mathbf{y}) = \chi_{\mathbb{K}}(\mathbf{r}, \mathbf{r}/\varepsilon)$ equals 1 or 0 depending on whether $\mathbf{r} \in \mathbb{K}$ or not. The dependence on the averaging region $\mathbb{K}$ has been indicated explicitly. By using the notation of Eq. (2.20) the average over all space is obtained as the limit $\lim_{s\to\infty} \bar{\mathbf{v}}_0(\mathbf{x}; s\mathbb{K}) = \bar{\mathbf{v}}_0(\mathbf{x})$. The function P_0 need not be averaged as it depends only on the slow variable $\mathbf{x}$. If $\mathbf{v}_0$ is constant then $\overline{\mathbf{v}_0}(\mathbf{x}) = \mathbf{v}_0 \bar{\phi}(\mathbf{x})$, which is known as the law of Dupuit–Forchheimer [1]. Averaging Eq. (5.75) gives Darcy's law (5.54) in the form

$$\bar{\mathbf{v}}_0(\mathbf{x}; \mathbb{K}) = \frac{\mathbf{K}(\mathbf{x}; \mathbb{K})}{\eta} [\mathbf{F} - \nabla_{\mathbf{x}} P_0(\mathbf{x})] \tag{5.80}$$

where the components $k_{ij}(\mathbf{x}; \mathbb{K}) = (\mathbf{K}(\mathbf{x}; \mathbb{K}))_{ij}$ of the permeability tensor $\mathbf{K}$ are expressed in terms of the solutions $\mathbf{u}_j(\mathbf{x}; \mathbb{K})$ to Eqs. (5.76)–(5.78) within the region $\mathbb{K}$ as

$$(\mathbf{K}(\mathbf{x}; \mathbb{K}))_{ij} = (\overline{\mathbf{u}_j}(\mathbf{x}; \mathbb{K}))_i \tag{5.81}$$

The permeability tensor is symmetric and positive definite [268]. Its dependence on the configuration of the pore space $\mathbb{P}$ and the averaging region $\mathbb{K}$ have been made explicit because they will play an important role below. For isotropic and strictly periodic or stationary media the permeability tensor reduces to a constant independent of $\mathbf{x}$. For (quasi-) periodic microgeometries or (quasi-)stationary random media averaging Eq. (5.73) leads to the additional macroscopic relation

$$\nabla_{\mathbf{x}}^{T} \cdot \bar{\mathbf{v}}_0(\mathbf{x}; \mathbb{K}) = 0 \tag{5.82}$$

Equations (5.80) and (5.82) are the macroscopic laws governing the microscopic Stokes flow obeying Eqs. (5.64)–(5.66) to leading order in $\varepsilon = \ell/L$.

The importance of the homogenization technique illustrated here in a simple example lies in the fact that it provides a systematic method to obtain the reference problem for an effective medium treatment.

Many of the examples for transport and relaxation in porous media listed in Section IV can be homogenized using a similar technique [268]. The heterogeneous elliptic equation (4.2) is of particular interest. The linear Darcy flow derived in this section can be cast into the form of Eq. (4.2) for the pressure field. The permeability tensor may still depend on the slow variable $\mathbf{x}$, and it is therefore of interest to iterate the homogenization procedure in order to see whether Darcy's law becomes again modified on larger scales. This question is discussed next.

4. *Iterated Homogenization*

The permeability $\mathbf{K}(\mathbf{x})$ for the macroscopic Darcy flow was obtained from homogenizing the Stokes equation by averaging the fast variable $\mathbf{y}$ over a region $\mathbb{K}$. The dependence on the slow variable $\mathbf{x}$ allows for macroscopic inhomogeneities of the permeability. This raises the question whether the homogenization may be repeated to arrive at an averaged description for a much larger megascopic scale.

If Eq. (5.80) is inserted into Eq. (5.82) and $\mathbf{F} = 0$ is assumed the equation for the macroscopic pressure field becomes

$$\nabla^{T} \cdot (\mathbf{K}(\mathbf{x}) \nabla P(\mathbf{x})) = 0 \tag{5.83}$$

which is identical with Eq. (4.2). The equation must be supplemented with boundary conditions that can be obtained from the requirements of mass and momentum conservation at the boundary of the region for which Eq. (5.83) was derived. If the boundary marks a transition to a

region with different permeability the boundary conditions require continuity of pressure and normal component of the velocity.

Equation (5.83) holds at length scales L much larger than the pore scale ℓ, and much larger than the diameter of the averaging region $\mathbb{K}$. To homogenize it one must therefore consider length scales $\mathscr{L}$ much larger than ℓ such that

$$\ell \ll L \ll \mathscr{L} \tag{5.84}$$

is fulfilled. The ratio $\delta = L/\mathscr{L}$ is then a small parameter in terms of which the homogenization procedure of Section V.C.3 can be iterated. The pressure is expanded in terms of δ as

$$P(\mathbf{x}) = P_0(\mathbf{s}, \mathbf{z}) + \delta P_1(\mathbf{s}, \mathbf{z}) + \cdots \tag{5.85}$$

where now $\mathbf{s} = \mathbf{x}$ is the slow variable, and $\mathbf{z} = \mathbf{s}/\delta$ is the rapidly varying variable. Assuming that the medium is stationary, that is, $\mathbf{K}(\mathbf{z})$ does not depend on the slow variable $\mathbf{s}$, the result becomes [268, 271, 280]

$$\nabla^T \cdot (\bar{\mathbf{K}} \nabla P_0(\mathbf{s})) = 0 \tag{5.86}$$

where $P_0(\mathbf{s})$ is the first term in the expansion of the pressure that is independent of $\mathbf{z}$, and the tensor $\bar{\mathbf{K}}$ has components

$$(\bar{\mathbf{K}})_{ij} = \overline{k_{ij}(\mathbf{z}) + \sum_{l=1}^{3} k_{il}(\mathbf{z}) \frac{\partial Q_j(\mathbf{z})}{\partial z_l}} \tag{5.87}$$

given in terms of three scalar fields $Q_j (j = 1, 2, 3)$, which are obtained from solving an equation of the form

$$-\sum_{i,j} \frac{\partial}{\partial z_i} \left(k_{ij}(\mathbf{z}) \frac{\partial Q_k(\mathbf{z})}{\partial z_j} \right) = \sum_i \frac{\partial k_{ik}(\mathbf{z})}{\partial z_i} \tag{5.88}$$

analogous to Eqs. (5.76)–(5.78) in the homogenization of Stokes equation.

If the assumption of strict stationarity is relaxed the averaged permeability depends in general on the slow variable, and the homogenized equation (5.86) then has the same form as the original Eq. (5.83). This shows that the form of the macroscopic equation does not change under further averaging. This highlights the importance of the averaged permeability as a key element of every macroscopically homogeneous description. Note, however, that the averaged tensor $\bar{\mathbf{K}}$ may have a different symmetry than the original permeability. If $\mathbf{K}(\mathbf{x}) = k(\mathbf{x})\mathbf{1}$ is

isotropic (**1** denotes the unit matrix) then $\bar{\mathbf{K}}$ may become anisotropic because of the second term appearing in Eq. (5.87).

5. *Network Model*

Consider a porous medium described by Eq. (5.83) for Darcy flow with a stationary and isotropic local permeability function $\mathbf{K}(\mathbf{x}) = k(\mathbf{x})\mathbf{1}$. The expressions (5.87) and (5.88) for the effective permeability tensor $\bar{\mathbf{K}}$ are difficult to use for general random microstructures. Therefore, it remains necessary to follow the strategy outlined in Section V.A.2 and to discretize Eq. (5.83) using a finite difference scheme with lattice constant L. As before, it is assumed that $\ell \ll L \ll \mathscr{L}$, where ℓ is the pore scale and $\mathscr{L}$ is the system size. The discretization results in the linear network equations (5.5) for a regular lattice with lattice constant L.

To make further progress it is necessary to specify the local permeabilities. A microscopic network model of tubes results from choosing the expression

$$k(a, \ell, L) = \frac{\pi}{8L}\frac{a^4}{\ell} \tag{5.89}$$

for a cylindrical capillary tube of radius a and length ℓ in a region of size L. The parameters a and ℓ must obey the geometrical conditions $a \leq L/2$ and $\ell \geq L$. In the resulting network model each bond represents a winding tube with circular cross section whose diameter and length fluctuate from bond to bond. The network model is completely specified by assuming that the local geometries specified by a and ℓ are independent and identically distributed random variables with joint probability density $\Pi(a, \ell)$. Note that the probability density $\Pi(a, \ell)$ depends also on the discretization length through the constraints $a \leq L/2$ and $\ell \geq L$.

By using the effective medium approximation to the network equations the effective permeability $\bar{k}$ for this network model is the solution of the self-consistency equation

$$\int_L^\infty \int_0^{L/2} \frac{\pi a^4 - 8L\ell\bar{k}}{\pi a^4 + 16L\ell\bar{k}} \Pi(a, \ell)\, da\, d\ell = 0 \tag{5.90}$$

where the restrictions on a and ℓ are reflected in the limits of integration. In simple cases, as for binary or uniform distributions, this equation can be solved analytically, in other cases it is solved numerically. The effective medium prediction agrees well with an exact solution of the network equations [231]. The behavior of the effective permeability

depends qualitatively on the fraction p of conducting tubes defined as

$$p = 1 - \lim_{\varepsilon \to 0} \int_0^{\varepsilon} \Pi(a)\, da \tag{5.91}$$

where $\Pi(a) = \int_L^{\infty} \Pi(a, \ell)\, d\ell$. For $p > \frac{1}{3}$ the permeability is positive while for $p < \frac{1}{3}$ it vanishes. At $p = p_c = \frac{1}{3}$ the network has a percolation transition. Note that $p \neq \bar{\phi}$ is not related to the average porosity.

6. *Local Porosity Theory*

Consider, as in Section V.C.5, a porous medium described by Eq. (5.83) for Darcy flow with a stationary and isotropic local permeability function $\mathbf{K}(\mathbf{x}) = k(\mathbf{x})\mathbf{1}$. A glance at Section III shows that the one-cell local geometry distribution defined in Eq. (3.45) is particularly well adapted to the discretization of Eq. (5.83). As before, the discretization employs a cubic lattice with lattice constant L and cubic measurement cells $\mathbb{K}$ and yields a local geometry distribution $\mu(\phi, S; \mathbb{K})$. It is then natural to use the Carman equation (5.59) locally because it is often an accurate description as illustrated in Fig. 23. The straight line in Fig. 23 corresponds to Eq. (5.59). The local percolation probabilities defined in Section III.A.5.d complete the description. Each local geometry is characterized by its local porosity, specific internal surface, and a binary random variable indicating whether the geometry is percolating or not. The self-consistent effective medium equation now reads

$$\int_0^{\infty} \int_0^1 \frac{3C\phi^3 \lambda(\phi, S; \mathbb{K})\mu(\phi, S; \mathbb{K})}{C\phi^3 + 4S^2\bar{k}}\, d\phi\, dS = 1 \tag{5.92}$$

for the effective permeability $\bar{k}$. The control parameter for the underlying percolation transition was given in Eq. (3.47) as

$$p(L) = \int_0^{\infty} \int_0^1 \lambda(\phi, S; \mathbb{K})\mu(\phi, S; \mathbb{K})\, d\phi\, dS \tag{5.93}$$

and it gives the total fraction of percolating local geometries. If the quantity

$$k_0 = \left(\int_0^{\infty} \int_0^1 \frac{2S^2}{C\phi^3} \lambda(\phi, S; \mathbb{K})\mu(\phi, S; \mathbb{K})\, d\phi\, dS \right)^{-1} \tag{5.94}$$

is finite then the solution to Eq. (5.92) is given approximately as

$$\bar{k} \approx k_0(p - p_c) \tag{5.95}$$

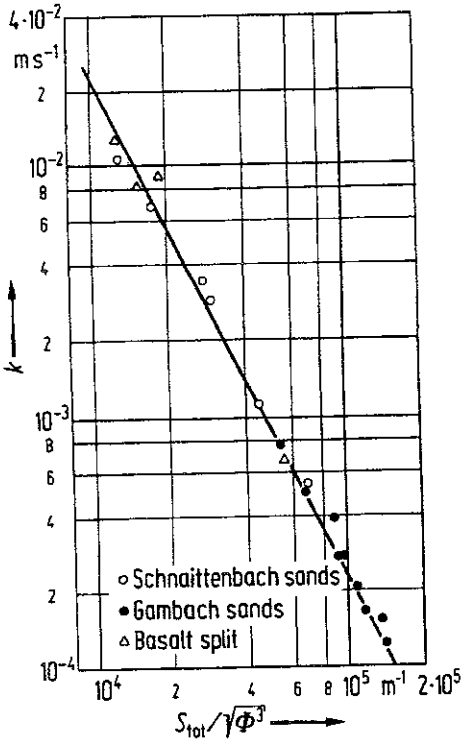

Figure 23. Log–log plot of the permeability coefficient $kg\rho/\eta$, where k is the permeability, g is the acceleration of gravity, ρ is the fluid density, and η is the fluid viscosity against the combination $S/(\phi)^{3/2}$ of porosity ϕ and specific surface S for sands and basalt split. (Reproduced with permission from J. Schopper, "Porosität und Permeabilität," in *Landolt–Börnstein: Physikalische Eigenschaften der Gesteine*, K.-H. Hellwege, Ed., Vol. V/1a, Springer, Berlin, 1982, p. 184. Copyright © Springer-Verlag, 1982.)

for $p > p_c = \frac{1}{3}$ and as $\bar{k} = 0$ for $p < p_c$. This result is analogous to Eq. (5.48) for the electrical conductivity. Note that the control parameter for the underlying percolation transition differs from the bulk porosity $p \neq \bar{\phi}$.

To study the implications of Eq. (5.92) it is necessary to supply explicit expressions for the local geometry distribution $\mu(\phi, S; L)$. Such an expression is provided by the local porosity reduction model reviewed in Section III.B.6. By writing the effective medium approximation for the number $\bar{n}$ defined in Eq. (3.87) and using Eqs. (3.86) and (3.88) it has been shown that the effective permeability may be written approximately as [170]

$$\bar{k} = \bar{\phi}^{\beta} \lambda(\bar{\phi}) \tag{5.96}$$

where the exponent β depends on the porosity reduction factor r and the type of consolidation model characterized by Eq. (3.88) as

$$\beta = (3 - 2\alpha) \frac{\ln r}{r - 1} \tag{5.97}$$

If all local geometries are percolating, that is, if $\lambda = 1$, then the effective permeability depends algebraically on the bulk porosity $\bar{\phi}$ with a *strongly nonuniversal exponent* β. This dependence will be modified if the local percolation probability $\lambda(\bar{\phi})$ is not constant. The large variability is consistent with experience from measuring permeabilities in experiment. Figure 24 demonstrates the large data scatter seen in experimental results. While in general small permeabilities correlate with small porosities the correlation is not very pronounced.

D. Permeability Length Scales

The fact that the effective permeability $\bar{k}$ has dimensions of area raises the question whether $\sqrt{\bar{k}}$ has an interpretation as a length scale. The traditional answer to this question is provided by hydraulic radius theory, which uses the approximate result of Eq. (5.61) for the capillary tube

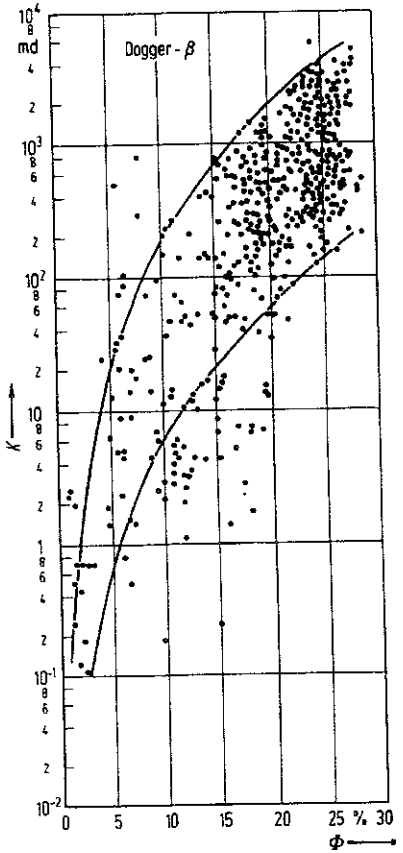

Figure 24. Logarithmic plot of permeability versus porosity for Dogger-β (Jurassic) sandstone. (Reproduced with permission from J. Schopper, "Porosität und Permeabilität," in *Landolt–Börnstein: Physikalische Eigenschaften der Gesteine*, K.-H. Hellwege, Ed., Vol. V/1a, Springer, Berlin, 1982, p. 184. Copyright © Springer-Verlag, 1982.)

model to postulate more generally the relation

$$\bar{k} \propto \frac{\bar{\phi} R_H^2}{2\mathcal{T}^2} \tag{5.98}$$

where $R_H = \phi(\mathbb{S})/S(\mathbb{S})$ is the hydraulic radius. This generalization has been modified by incorporating the formation factor to write [112, 327]

$$\bar{k} \propto \frac{\Lambda^2}{F} \tag{5.99}$$

where the length scale $\Lambda = R_H$ is still given by the hydraulic radius, and the geometrical tortuosity $\mathcal{T}^2$ was replaced by the electrical tortuosity defined as $\mathcal{T}_{el}^2 = F\bar{\phi}$. Because the length scale is still given by the hydraulic radius this theory is still faced with the objection that the hydraulic radius R_H contains contributions from the dead ends that do not contribute to the transport.

An alternative was proposed in [43, 318]. It postulates $\Lambda = l_c$, where l_c is a length scale related to the breakthrough pressure in mercury injection experiments. The length scale l_c is well defined for network models with a broad distribution of cylindrical pores. A dynamical interpretation of Λ was proposed in [319, 320, 328] as

$$\frac{2}{\Lambda} = \frac{\int |\mathbf{E}(\mathbf{r})|^2 \chi_{\partial\mathbb{P}}(\mathbf{r})\, d^2\mathbf{r}}{\int |\mathbf{E}(\mathbf{r})|^2 \chi_{\mathbb{P}}(\mathbf{r})\, d^3\mathbf{r}} \tag{5.100}$$

where $\mathbf{E}(\mathbf{r})$ is the unknown exact solution of the microscopic dielectric problem. This "electrical length" is expected to measure, somehow, the "dynamically connected pore size" [4, 319, 328]. The interpretation of Λ within local porosity theory is obtained by eliminating $(p - p_c)$ between the result [Eq. (5.48)] for the conductivity, and Eq. (5.95) for the permeability. This generally yields

$$\Lambda^2 \approx \frac{\int_0^\infty \int_0^1 \frac{\lambda(\phi, S; \mathbb{K})\mu(\phi, S; \mathbb{K})}{\sigma_{loc}(\phi, S)}\, d\phi\, dS}{\int_0^\infty \int_0^1 \frac{\lambda(\phi, S; \mathbb{K})\mu(\phi, S; \mathbb{K})}{k_{loc}(\phi, S)}\, d\phi\, dS} \tag{5.101}$$

where $\sigma_{loc}(\phi, S)$ and $k_{loc}(\phi, S)$ are the local electrical conductivity and the local permeability. Thus Λ involves macroscopic geometrical information through μ and λ and microscopic dynamical and geometrical information through the local transport coefficients. If one assumes the hydraulic radius expressions $\sigma_{loc}(\phi, S) \propto \phi$ and $k_{loc}(\phi, S) \propto \phi^3/S^2$ locally

and the expression $\mu(\phi, S; \mathbb{K}) \approx \delta(\phi - \bar{\phi})\delta(S - \bar{S})$ is valid for large measurement cells, then it follows that $\Lambda \propto \bar{\phi}/\bar{S}$ becomes the local hydraulic radius [170]. This expression is no longer proportional to the total internal surface but only to the average local internal surface. Thus the argument against hydraulic radius theories no longer apply.

VI. IMMISCIBLE DISPLACEMENT

This section discusses the transition between microscopic and macroscopic length scales for the flow of two immiscible fluids through a porous medium. Contrary to the previous sections, the macroscopic equations of motion describing the immiscible displacement process are assumed to be known from averaging the microscopic equations. The upscaling problem is addressed by comparing the dimensional analysis of the given microscopic and macroscopic equations. The original dimensional analysis dates back to [49, 329–331], but continues to attract the attention of recent authors [332–336]. This fact indicates the presence of unresolved problems, which can be seen most clearly in capillary desaturation experiments where they appear as large unexplained discrepancies in the macroscopic balance of viscous and capillary forces. Recently, these problems were traced to a tacit assumption underlying the traditional dimensional analysis [47, 48]. This finding could lead to a resolution of the discrepancies and has additional implications for laboratory measurements of relative permeabilities [337], which will be discussed in Section VI.C.3. The dimensional analysis of immiscible displacement will therefore be reviewed in this section providing a basis for quantitative estimates of the relative importance of macroscopic viscous, capillary, and gravitational forces. Such estimates were distorted in the traditional analysis. The revised analysis allows one to predict segregation front widths or gravitational relaxation times for different porous media [47, 48].

A. Experimental Observations

Consider the displacement of oil from an oil saturated porous medium through injecting water at constant velocity. After steady-state flow conditions are established a certain fraction $S_{\mathbb{O}r}$[9] of oil remains microscopically trapped inside the medium. The trapped oil can be mobilized if the viscous forces overcome the capillary retention forces [333]. Displacement experiments in a variety of porous media including micromodels show a strong correlation between the residual oil saturation $S_{\mathbb{O}r}$ and the

[9] In all of Section VI the letter S denotes saturation, and should not be confused with the usage in previous sections.

capillary number Ca of the waterflood [2, 28, 203, 332, 338–341]. The *capillary number*, defined as $\mathrm{Ca} = \mu u/\sigma$, is the dimensionless ratio of viscous/capillary forces. Here u denotes an average microscopic velocity, μ is the viscosity, and σ is the surface tension between the fluids.

The experimental curves $S_{or}(\mathrm{Ca})$ are called capillary number correlations, recovery curves, or capillary desaturation curves, and they give the residual oil saturation as a function of the capillary number of the flood. All such capillary desaturation curves exhibit a critical capillary number Ca_c below which the residual oil saturation remains constant. This critical capillary number Ca_c marks the point where the viscous forces equal the capillary forces. Figure 25 shows a schematic drawing of the capillary desaturation curves for unconsolidated sand, sandstone, and limestone (after [28, 203]). Surprisingly, all experimentally observed values for Ca_c are much smaller than 1. For unconsolidated sand Ca_c is often reported to be $\mathrm{Ca}_c \approx 10^{-4}$, while for sandstone $\mathrm{Ca}_c \approx 3 \times 10^{-6}$ and for limestone $\mathrm{Ca}_c \approx 2 \times 10^{-7}$ [28]. The exceedingly small values of Ca_c as well as their dependence on the type of porous medium strongly suggest that the microscopically defined capillary number Ca cannot be an adequate measure of the balance between macroscopic viscous and macroscopic capillary forces.

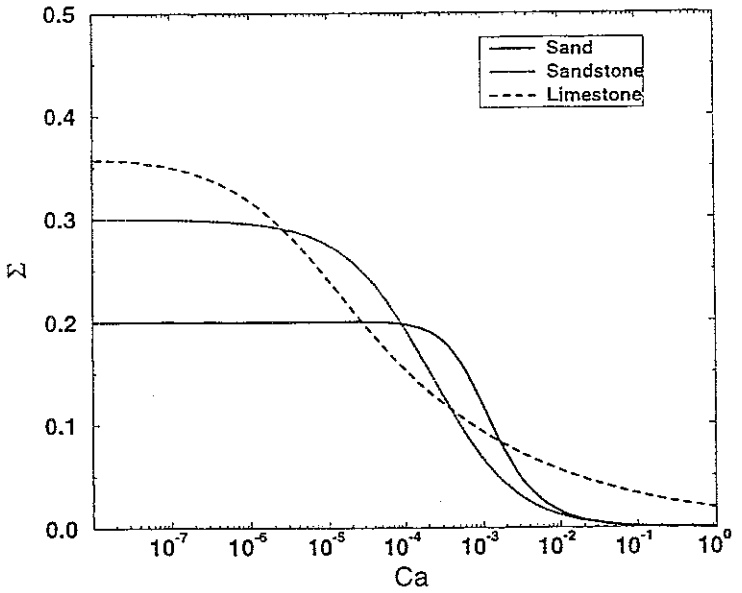

Figure 25. Schematic plot of residual oil saturation $S_{or}(\mathrm{Ca})$ as function of microscopic capillary number Ca for unconsolidated sands, sandstones, and limestones.

The subsequent sections review recent work that relates the large discrepancy between the observed force balance and the force balance estimated from Ca to an implicit assumption in the traditional dimensional analysis [49, 329–331]. First, the microscopic equations of motion and their dimensional analysis are recalled. This leads to the familiar dimensionless numbers of fluid dynamics. Next, the accepted macroscopic equations of motion are analyzed. This leads to macroscopic dimensionless number, which are then related to the traditional microscopic dimensionless groups. The results are shown to be applicable to the quantitative estimation of residual oil saturation, gravitational relaxation times, and the width of the oil–water contact.

B. Microscopic Description

1. *Microscopic Equations of Motion*

Microscopic equations of motion for two-phase flow in porous media are commonly given as Stokes (or Navier–Stokes) equations for two incompressible Newtonian fluids with no-slip and stress–balance boundary conditions at the interfaces [270, 322, 342]. In the following, the wetting fluid (water) will be denoted by a subscript $\mathbb{W}$ while the nonwetting fluid (oil) is indexed with $\mathbb{O}$. The solid rock matrix, indexed as $\mathbb{M}$, is assumed to be porous and rigid. It fills a closed subset $\mathbb{M} \subset \mathbf{R}^3$ of three-dimensional space. The pore space $\mathbb{P}$ is filled with the two fluid phases described by the two closed subsets $\mathbb{W}(t)$, $\mathbb{O}(t) \subset \mathbf{R}^3$, which are in general time dependent, and related to each other through the condition $\mathbb{P} = \mathbb{W}(t) \cup \mathbb{O}(t)$. Note that $\mathbb{P}$ is independent of time because $\mathbb{M}$ is rigid while $\mathbb{O}(t)$ and $\mathbb{W}(t)$ are not. The rigid rock surface will be denoted as $\partial\mathbb{M}$, and the mobile oil–water interface as $\partial(\mathbb{O}\mathbb{W})(t) = \mathbb{O}(t) \cap \mathbb{W}(t)$. A standard formulation of pore-scale equations of motion for two incompressible and immiscible fluids flowing through a porous medium are the Navier–Stokes equations

$$\begin{aligned} \rho_{\mathbb{W}} \frac{\partial \mathbf{v}_{\mathbb{W}}}{\partial t} + \rho_{\mathbb{W}}(\mathbf{v}_{\mathbb{W}}^T \cdot \nabla)\mathbf{v}_{\mathbb{W}} &= \mu_{\mathbb{W}} \Delta \mathbf{v}_{\mathbb{W}} + \rho_{\mathbb{W}} g \nabla z - \nabla P_{\mathbb{W}} \\ \rho_{\mathbb{O}} \frac{\partial \mathbf{v}_{\mathbb{O}}}{\partial t} + \rho_{\mathbb{O}}(\mathbf{v}_{\mathbb{O}}^T \cdot \nabla)\mathbf{v}_{\mathbb{O}} &= \mu_{\mathbb{O}} \Delta \mathbf{v}_{\mathbb{O}} + \rho_{\mathbb{O}} g \nabla z - \nabla P_{\mathbb{O}} \end{aligned} \tag{6.1}$$

and the incompressibility conditions

$$\begin{aligned} \nabla^T \cdot \mathbf{v}_{\mathbb{W}} &= 0 \\ \nabla^T \cdot \mathbf{v}_{\mathbb{O}} &= 0 \end{aligned} \tag{6.2}$$

where $\mathbf{v}_{\mathbb{W}}(\mathbf{x}, t)$, $\mathbf{v}_{\mathbb{O}}(\mathbf{x}, t)$ are the velocity fields for water and oil; $P_{\mathbb{W}}(\mathbf{x}, t)$,

$P_{\mathbb{O}}(\mathbf{x}, t)$ are the pressure fields in the two phases; $\rho_{\mathbb{W}}$, $\rho_{\mathbb{O}}$ are the densities; $\mu_{\mathbb{W}}$, $\mu_{\mathbb{O}}$ are the dynamic viscosities; and g is the gravitational constant. The vector $\mathbf{x}^T = (x, y, z)$ denotes the coordinate vector, t is the time, $\nabla^T = (\partial/\partial x, \partial/\partial y, \partial/\partial z)$ is the gradient operator, Δ is the Laplacian, and the superscript T denotes transposition. The gravitational force is directed along the z axis and it represents an external body force. Although gravity effects are often small for pore-scale processes [see Eq. (6.37)], there has recently been a growing interest in modeling gravity effects at the pore scale [42, 245, 246, 343].

The microscopic formulation is completed by specifying an initial fluid distribution $\mathbb{W}(t=0)$, $\mathbb{O}(t=0)$ and boundary conditions. The latter are usually no-slip boundary conditions at solid–fluid interfaces,

$$\begin{aligned} \mathbf{v}_{\mathbb{W}} &= 0 \quad \text{at} \quad \partial\mathbb{M} \\ \mathbf{v}_{\mathbb{O}} &= 0 \quad \text{at} \quad \partial\mathbb{M} \end{aligned} \tag{6.3}$$

as well as for the fluid–fluid interface,

$$\mathbf{v}_{\mathbb{W}} = \mathbf{v}_{\mathbb{O}} \qquad \text{at} \qquad \partial(\mathbb{OW})(t) \tag{6.4}$$

combined with stress–balance across the fluid–fluid interface,

$$\boldsymbol{\tau}_{\mathbb{W}} \cdot \mathbf{n} = \boldsymbol{\tau}_{\mathbb{O}} \cdot \mathbf{n} + 2\sigma_{\mathbb{OW}}\kappa\mathbf{n} \qquad \text{at} \qquad \partial(\mathbb{OW})(t) \tag{6.5}$$

Here $\sigma_{\mathbb{OW}}$ denotes the water–oil interfacial tension, κ is the curvature of the oil–water interface, and $\mathbf{n}$ is a unit normal to it. The stress tensor $\boldsymbol{\tau}(\mathbf{x}, t)$ for the two fluids is given in terms of $\mathbf{v}$ and P as

$$\boldsymbol{\tau} = -P\mathbf{1} + \mu\mathcal{S}\nabla\mathbf{v}^T \tag{6.6}$$

where the symmetrization operator $\mathcal{S}$ acts as

$$\mathcal{S}\mathbf{A} = \tfrac{1}{2}(\mathbf{A} + \mathbf{A}^T - \tfrac{2}{3}\operatorname{tr}\mathbf{A}\mathbf{1}) \tag{6.7}$$

on the matrix $\mathbf{A}$, and $\mathbf{1}$ is the identity matrix.

The pore-space boundary $\partial\mathbb{M}$ is given and fixed while the fluid–fluid interface $\partial(\mathbb{OW})(t)$ has to be determined self-consistently as part of the solution. For $\mathbb{W} = \emptyset$ or $\mathbb{O} = \emptyset$ the above formulation of two-phase flow at the pore scale reduces to the standard formulation of single-phase flow of water or oil at the pore scale.

2. *The Contact Line Problem*

The pore-scale equations of motion given in Section VI.B.1 contain a self-contradiction. The problem arises from the system of contact lines

defined as

$$\partial(\mathbb{MOW})(t) = \partial\mathbb{M} \cup \partial(\mathbb{OW})(t) \tag{6.8}$$

on the inner surface of the porous medium. The contact lines must in general slip across the surface of the rock in direct contradiction to the no-slip boundary condition Eq. (6.3). This self-contradiction is not specific for flow in porous media but exists also for immiscible two-phase flow in a tube or in other containers [344–346].

There exist several ways out of this classical dilemma depending on the wetting properties of the fluids. For complete and uniform wetting a microscopic precursor film of water wets the entire rock surface [344]. In that case $\mathbb{M} \cap \mathbb{O}(t) = \emptyset$ and thus

$$\partial(\mathbb{MOW})(t) = \{[\mathbb{M} \cap \mathbb{W}(t)] \cup [\mathbb{M} \cap \mathbb{O}(t)]\} \cap [\mathbb{O}(t) \cap \mathbb{W}(t)] = \emptyset \tag{6.9}$$

the problem does not appear.

For other wetting properties a phenomenological slipping model for the manner in which the slipping occurs at the contact line is needed to complete the pore-scale description of two-phase flow. The phenomenological slipping models describe the region around the contact line microscopically. The typical size of this region, called the "slipping length," is around 10^{-9} m. Therefore, the problem of contact lines is particularly acute for immiscible displacement in microporous media, and the Navier–Stokes description of Section VI.B.1 does not apply for such media.

3. *Microscopic Dimensional Analysis*

Given a microscopic model for contact line slipping the next step is to evaluate the relative importance of the different terms in the equations of motion at the pore scale. This is done by casting them into dimensionless form using the definitions

$$\mathbf{x} = \ell\hat{\mathbf{x}} \tag{6.10}$$

$$\nabla = \frac{\hat{\nabla}}{\ell} \tag{6.11}$$

$$\mathbf{v} = u\hat{\mathbf{v}} \tag{6.12}$$

$$t = \frac{\ell\hat{t}}{u} \tag{6.13}$$

$$\kappa = \frac{\hat{\kappa}}{\ell} \tag{6.14}$$

$$P = \frac{\sigma_{\mathrm{OW}}}{\ell}\hat{P} \tag{6.15}$$

where ℓ is a microscopic length, u is a microscopic velocity, and $\hat{A}$ denotes the dimensionless equivalent of the quantity A.

With these definitions the dimensionless equations of motion on the pore scale can be written as

$$\begin{aligned}
\frac{\partial \hat{\mathbf{v}}_{\mathrm{W}}}{\partial \hat{t}} + (\hat{\mathbf{v}}_{\mathrm{W}}^{T}\cdot\hat{\boldsymbol{\nabla}})\hat{\mathbf{v}}_{\mathrm{W}} &= \frac{1}{\mathrm{Re}_{\mathrm{W}}}\hat{\Delta}\hat{\mathbf{v}}_{\mathrm{W}} + \frac{1}{\mathrm{Fr}^2}\hat{\boldsymbol{\nabla}}\hat{z} - \frac{1}{\mathrm{We}_{\mathrm{W}}}\hat{\boldsymbol{\nabla}}\hat{P}_{\mathrm{W}} \\
\frac{\partial \hat{\mathbf{v}}_{\mathrm{O}}}{\partial \hat{t}} + (\hat{\mathbf{v}}_{\mathrm{O}}^{T}\cdot\hat{\boldsymbol{\nabla}})\hat{\mathbf{v}}_{\mathrm{O}} &= \frac{1}{\mathrm{Re}_{\mathrm{O}}}\hat{\Delta}\hat{\mathbf{v}}_{\mathrm{O}} + \frac{1}{\mathrm{Fr}^2}\hat{\boldsymbol{\nabla}}\hat{z} - \frac{1}{\mathrm{We}_{\mathrm{O}}}\hat{\boldsymbol{\nabla}}\hat{P}_{\mathrm{O}}
\end{aligned} \tag{6.16}$$

$$\begin{aligned}
\hat{\boldsymbol{\nabla}}^{T}\cdot\hat{\mathbf{v}}_{\mathrm{W}} &= 0 \\
\hat{\boldsymbol{\nabla}}^{T}\cdot\hat{\mathbf{v}}_{\mathrm{O}} &= 0
\end{aligned} \tag{6.17}$$

with dimensionless boundary conditions

$$\hat{\mathbf{v}}_{\mathrm{W}} = \hat{\mathbf{v}}_{\mathrm{O}} = 0 \qquad \text{at} \qquad \partial_{\mathrm{M}} \tag{6.18}$$

$$\hat{\mathbf{v}}_{\mathrm{W}} = \hat{\mathbf{v}}_{\mathrm{O}} \qquad \text{at} \qquad \partial_{\mathrm{OW}}(t) \tag{6.19}$$

$$\begin{aligned}
(\hat{P}_{\mathrm{O}} - \hat{P}_{\mathrm{W}})\mathbf{n} = &\left(\frac{\mathrm{We}_{\mathrm{W}}}{\mathrm{Re}_{\mathrm{W}}}\mathcal{S}\hat{\boldsymbol{\nabla}}\hat{\mathbf{v}}_{\mathrm{W}} - \frac{\mathrm{We}_{\mathrm{O}}}{\mathrm{Re}_{\mathrm{O}}}\mathcal{S}\hat{\boldsymbol{\nabla}}\hat{\mathbf{v}}_{\mathrm{O}}\right)\cdot\mathbf{n} \\
&+ 2\hat{\kappa}\mathbf{n} \qquad \text{at } \partial_{\mathrm{OW}}(t)
\end{aligned} \tag{6.20}$$

In these equations the microscopic dimensionless ratio

$$\mathrm{Re}_{\mathrm{W}} = \frac{\text{inertial forces}}{\text{viscous forces}} = \frac{\rho_{\mathrm{W}} u\ell}{\mu_{\mathrm{W}}} = \frac{u\ell}{\nu_{\mathrm{W}}^{*}} \tag{6.21}$$

is the Reynolds number, and

$$\nu_{\mathrm{W}}^{*} = \frac{\mu_{\mathrm{W}}}{\rho_{\mathrm{W}}} \tag{6.22}$$

is the kinematic viscosity, which may be interpreted as a specific action or a specific momentum transfer. The other fluid dynamic numbers are

defined as

$$\mathrm{Fr} = \sqrt{\frac{u^2}{g\ell}} = \sqrt{\frac{\text{inertial forces}}{\text{gravitational forces}}} \tag{6.23}$$

for the Froude number, and

$$\mathrm{We}_{\mathrm{W}} = \frac{\rho_{\mathrm{W}} u^2 \ell}{\sigma_{\mathrm{OW}}} = \frac{\text{inertial forces}}{\text{capillary forces}} \tag{6.24}$$

for the Weber number. The corresponding dimensionless ratios for the oil phase are related to those for the water phase as

$$\mathrm{Re}_{\mathrm{O}} = \mathrm{Re}_{\mathrm{W}} \frac{\rho_{\mathrm{O}}}{\rho_{\mathrm{W}}} \frac{\mu_{\mathrm{W}}}{\mu_{\mathrm{O}}} \tag{6.25}$$

$$\mathrm{We}_{\mathrm{O}} = \mathrm{We}_{\mathrm{W}} \frac{\rho_{\mathrm{O}}}{\rho_{\mathrm{W}}} \tag{6.26}$$

by viscosity and density ratios.

Table IV gives approximate values for densities, viscosities, and surface tensions under reservoir conditions [47, 48]. In the following, these values will be used to make order of magnitude estimates. Typical pore sizes in an oil reservoir are of order $\ell \approx 10^{-4}$ m and microscopic fluid velocities for reservoir floods range around $u \approx 3 \times 10^{-6}\ \mathrm{ms}^{-1}$. Combining these estimates with those of Table IV shows that the dimensionless ratios obey Re_{O}, Re_{W}, Fr^2, We_{O}, $\mathrm{We}_{\mathrm{W}} \ll 1$. Therefore, the pore-scale Eqs. (6.16) reduce to the simpler Stokes form

$$\begin{aligned} 0 &= \hat{\Delta}\hat{\mathbf{v}}_{\mathrm{W}} + \frac{1}{\mathrm{Gr}_{\mathrm{W}}} \hat{\nabla}\hat{z} - \frac{1}{\mathrm{Ca}_{\mathrm{W}}} \hat{\nabla}\hat{P}_{\mathrm{W}} \\ 0 &= \hat{\Delta}\hat{\mathbf{v}}_{\mathrm{O}} + \frac{1}{\mathrm{Gr}_{\mathrm{O}}} \hat{\nabla}\hat{z} - \frac{1}{\mathrm{Ca}_{\mathrm{O}}} \hat{\nabla}\hat{P}_{\mathrm{O}} \end{aligned} \tag{6.27}$$

TABLE IV
Order of Magnitude Estimates for Densities, Viscosities, and Surface Tension of Oil and Water under Reservoir Conditions

ρ_{O}	ρ_{W}	μ_{O}	μ_{W}	σ_{OW}
$800\ \mathrm{kg\,m^{-3}}$	$1000\ \mathrm{kg\,m^{-3}}$	$0.0018\ \mathrm{N\,m^{-2}\,s}$	$0.0009\ \mathrm{N\,m^{-2}\,s}$	$0.035\ \mathrm{N\,m^{-1}}$

where

$$\mathrm{Ca_W} = \frac{\mathrm{We_W}}{\mathrm{Re_W}} = \frac{\text{viscous forces}}{\text{capillary forces}} = \frac{\mu_W u}{\sigma_{OW}} = \frac{u}{u_W^*} \tag{6.28}$$

is the microscopic capillary number of water, and

$$\mathrm{Gr_W} = \frac{\mathrm{Fr}^2}{\mathrm{Re_W}} = \frac{\text{viscous forces}}{\text{gravity forces}} = \frac{\mu_W u}{\rho_W g \ell^2} \tag{6.29}$$

is the microscopic "gravity number" of water. The capillary number is a measure of velocity in units of

$$u_W^* = \frac{\sigma_{OW}}{\mu_W} \tag{6.30}$$

a characteristic velocity at which the coherence of the oil–water interface is destroyed by viscous forces. The capillary and gravity numbers for the oil phase can again be expressed through density and viscosity ratios as

$$\mathrm{Ca_O} = \mathrm{Ca_W} \frac{\mu_O}{\mu_W} \tag{6.31}$$

$$\mathrm{Gr_O} = \mathrm{Gr_W} \frac{\rho_W}{\rho_O} \frac{\mu_O}{\mu_W} \tag{6.32}$$

Many other dimensionless ratios may be defined. Of general interest are dimensionless space and time variables. Such ratios are formed as

$$\mathrm{Gl_W} = \frac{\mathrm{Ca_W}}{\mathrm{Gr_W}} = \frac{\mathrm{We_W}}{\mathrm{Fr}^2} = \frac{\text{gravity forces}}{\text{capillary forces}} = \frac{\rho_W g \ell^2}{\sigma_{OW}} = \frac{\ell^2}{\ell_W^{*2}} \tag{6.33}$$

which has been called the "gravillary number" [47, 48]. The gravillary number becomes the better known bond number if the density ρ_W is replaced with the density difference $\rho_W - \rho_O$. The corresponding length

$$\ell_W^* = \sqrt{\frac{\sigma_{OW}}{\rho_W g}} \tag{6.34}$$

separates capillary waves with wavelengths below ℓ_W^* from gravity waves with wavelengths above ℓ_W^*. A dimensionless time variable is formed

from the gravillary and capillary numbers as

$$\frac{\sqrt{\mathrm{Gl}_{\mathrm{w}}}}{\mathrm{Ca}_{\mathrm{w}}} = \frac{\mathrm{Re}_{\mathrm{w}}}{\mathrm{Fr}\sqrt{\mathrm{We}_{\mathrm{w}}}} = \frac{(\text{gravity f})^{3/2}}{(\text{capillary f})^{1/2} \times \text{viscous f}}$$

$$= \frac{\sqrt{\rho_{\mathrm{w}}\sigma_{\mathrm{ow}}}gt}{\mu_{\mathrm{w}}} = \frac{t}{t^*_{\mathrm{w}}} \tag{6.35}$$

where

$$t^*_{\mathrm{w}} = \frac{\ell^*_{\mathrm{w}}}{u^*_{\mathrm{w}}} = \frac{\mu_{\mathrm{w}}}{\sqrt{\sigma_{\mathrm{ow}}\rho_{\mathrm{w}}}g} \tag{6.36}$$

is a characteristic time after which the influence of gravity dominates viscous and capillary effects. The reader is cautioned not to misinterpret the value of t^*_{w} in Table V as an indication that gravity forces dominate on the pore scale.

Table V collects definitions and estimates for the dimensionless groups and the numbers ℓ^*, u^*, and ν^* characterizing the oil–water system. For these estimates the values in Table IV together with the above estimates of ℓ and u have been used. Table V shows that

$$\text{viscous forces} \ll \text{gravity forces} \ll \text{capillary forces} \tag{6.37}$$

and hence capillary forces dominate on the pore scale [2, 47, 48, 333].

From the Stokes equation (6.27) it follows immediately that for low-capillary number floods ($\mathrm{Ca} \ll 1$) the viscous term as well as the shear term in the boundary condition (6.20) become negligible. Therefore, the velocity field drops out, and the problem reduces to finding the equilibrium capillary pressure field. The equilibrium configuration of the oil–water interface then defines time-independent pathways for the flow of oil and water. Hence, for flows with microscopic capillary numbers $\mathrm{Ca} \ll 1$ an improved methodology for a quantitative description of immiscible displacement from pore-scale physics requires improved calculations of capillary pressures from the pore scale, and much research is devoted to this topic [246a, 347, 348].

C. Macroscopic Description

1. *Macroscopic Equations of Motion*

The accepted large-scale equations of motion for two-phase flow involve a generalization of Darcy's law to relative permeabilities including off-diagonal viscous coupling terms [270, 321, 322, 349–352]. The importance

TABLE V
Overview of Definitions and Estimates for Characteristic Microscopic Numbers Describing Oil and Water Flow under Reservoir Conditions

Quantity	Definition	Estimate
Re_{W}	$\frac{\rho_{\mathrm{W}} u \ell}{\mu_{\mathrm{W}}}$	3.3×10^{-4}
Ca_{W}	$\frac{\mu_{\mathrm{W}} u}{\sigma_{\mathrm{OW}}}$	7.7×10^{-8}
Gr_{W}	$\frac{\mu_{\mathrm{W}} u}{\rho_{\mathrm{W}} g \ell^2}$	2.8×10^{-5}
Gl_{W}	$\frac{\rho_{\mathrm{W}} g \ell^2}{\sigma_{\mathrm{OW}}}$	2.8×10^{-3}
ν_{W}^*	$\frac{\mu_{\mathrm{W}}}{\rho_{\mathrm{W}}}$	$9 \times 10^{-7}\ \mathrm{m^2\,s^{-1}}$
u_{W}^*	$\frac{\sigma_{\mathrm{OW}}}{\mu_{\mathrm{W}}}$	$38.9\ \mathrm{m\,s^{-1}}$
ℓ_{W}^*	$\sqrt{\frac{\sigma_{\mathrm{OW}}}{\rho_{\mathrm{W}} g}}$	1.9 cm
t_{W}^*	$\frac{\mu_{\mathrm{W}}}{\sqrt{\sigma_{\mathrm{OW}} \rho_{\mathrm{W}} g}}$	$4.9 \times 10^{-4}\ \mathrm{s}$

of viscous coupling terms has been recognized relatively late [353–357]. The equations that are generally believed to describe multiphase flow on the reservoir scale as well as on the laboratory scale may be written as [322, 350]

$$\begin{aligned} \bar{\phi}\,\frac{\partial \bar{S}_{\mathrm{W}}}{\partial \bar{t}} &= \bar{\nabla}\cdot\bar{\mathbf{v}}_{\mathrm{W}} \\ \bar{\phi}\,\frac{\partial \bar{S}_{\mathrm{O}}}{\partial \bar{t}} &= \bar{\nabla}\cdot\bar{\mathbf{v}}_{\mathrm{O}} \end{aligned} \tag{6.38}$$

$$\begin{aligned} \bar{\mathbf{v}}_{\mathrm{W}} &= -\left[\mathbf{K}_{\mathrm{WW}}^{r}\frac{\mathbf{K}}{\mu_{\mathrm{W}}}(\bar{\nabla}\bar{P}_{\mathrm{W}} - \rho_{\mathrm{W}} g\bar{\nabla}\bar{z}) + \mathbf{K}_{\mathrm{WO}}^{r}\frac{\mathbf{K}}{\mu_{\mathrm{O}}}(\bar{\nabla}\bar{P}_{\mathrm{O}} - \rho_{\mathrm{O}} g\bar{\nabla}\bar{z})\right] \\ \bar{\mathbf{v}}_{\mathrm{O}} &= -\left[\mathbf{K}_{\mathrm{OW}}^{r}\frac{\mathbf{K}}{\mu_{\mathrm{W}}}(\bar{\nabla}\bar{P}_{\mathrm{W}} - \rho_{\mathrm{W}} g\bar{\nabla}\bar{z}) + \mathbf{K}_{\mathrm{OO}}^{r}\frac{\mathbf{K}}{\mu_{\mathrm{O}}}(\bar{\nabla}\bar{P}_{\mathrm{O}} - \rho_{\mathrm{O}} g\bar{\nabla}\bar{z})\right] \end{aligned} \tag{6.39}$$

$$\bar{S}_{\mathbb{W}} + \bar{S}_{\mathbb{O}} = 1 \tag{6.40}$$

$$\bar{P}_{\mathbb{O}} - \bar{P}_{\mathbb{W}} = \bar{P}_c(\bar{S}_{\mathbb{W}}) \tag{6.41}$$

where $\bar{A}$ denotes the macroscopic volume averaged equivalent of the pore-scale quantity A. In the equations above $\mathbf{K}$ stands for the absolute (single-phase flow) permeability tensor, $\mathbf{K}^r_{\mathbb{WW}}$ is the relative permeability tensor for water, $\mathbf{K}^r_{\mathbb{OO}}$ the oil relative permeability tensor, and $\mathbf{K}^r_{\mathbb{WO}}$, $\mathbf{K}^r_{\mathbb{OW}}$ denote the possibly anisotropic coupling terms. The relative permeabilities are matrix-valued functions of saturation. The saturations are denoted as $\bar{S}_{\mathbb{W}}$, $\bar{S}_{\mathbb{O}}$, and they depend on the macroscopic space and time variables $(\bar{\mathbf{x}}, \bar{t})$. The capillary pressure curve $\bar{P}_c(\bar{S}_{\mathbb{W}})$ and the relative permeability tensors $\mathbf{K}^r_{ij}(\bar{S}_{\mathbb{W}})$, $i, j = \mathbb{W}, \mathbb{O}$ must be known either from solving the pore-scale equations of motion, or from experiment. The parameters $\mathbf{K}^r_{ij}(\bar{S}_{\mathbb{W}})$ and $\bar{P}_c(\bar{S}_{\mathbb{W}})$ are conventionally assumed to be independent of $\bar{\mathbf{v}}$ and $\bar{P}$ and this convention is followed here, although it is conceivable that this is not generally correct [354].

Eliminating $\bar{\mathbf{v}}$ and choosing $\bar{P}_{\mathbb{W}}(\bar{\mathbf{x}}, \bar{t})$ and $\bar{S}_{\mathbb{W}}(\bar{\mathbf{x}}, \bar{t})$ as the principal unknowns one arrives at the large-scale two-phase flow equations

$$\bar{\phi}\frac{\partial \bar{S}_{\mathbb{W}}}{\partial \bar{t}} = \bar{\nabla}\cdot\left\{\mathbf{K}^r_{\mathbb{WW}}(\bar{S}_{\mathbb{W}})\frac{\mathbf{K}}{\mu_{\mathbb{W}}}(\bar{\nabla}\bar{P}_{\mathbb{W}} - \rho_{\mathbb{W}} g\bar{\nabla}\bar{z}) + \mathbf{K}^r_{\mathbb{WO}}(\bar{S}_{\mathbb{W}})\frac{\mathbf{K}}{\mu_{\mathbb{O}}}[(\bar{\nabla}\bar{P}_{\mathbb{W}} - \rho_{\mathbb{W}} g\bar{\nabla}\bar{z}) + \bar{\nabla}\bar{P}_c(\bar{S}_{\mathbb{W}}) + (\rho_{\mathbb{W}} - \rho_{\mathbb{O}})g\bar{\nabla}\bar{z}]\right\} \tag{6.42}$$

$$\bar{\phi}\frac{\partial(1-\bar{S}_{\mathbb{W}})}{\partial \bar{t}} = \bar{\nabla}\cdot\left\{\mathbf{K}^r_{\mathbb{OW}}(\bar{S}_{\mathbb{W}})\frac{\mathbf{K}}{\mu_{\mathbb{W}}}(\bar{\nabla}\bar{P}_{\mathbb{W}} - \rho_{\mathbb{W}} g\bar{\nabla}\bar{z}) + \mathbf{K}^r_{\mathbb{OO}}(\bar{S}_{\mathbb{W}})\frac{\mathbf{K}}{\mu_{\mathbb{O}}}[(\bar{\nabla}\bar{P}_{\mathbb{W}} - \rho_{\mathbb{W}} g\bar{\nabla}\bar{z}) + \bar{\nabla}\bar{P}_c(\bar{S}_{\mathbb{W}}) + (\rho_{\mathbb{W}} - \rho_{\mathbb{O}})g\bar{\nabla}\bar{z}]\right\} \tag{6.43}$$

for these two unknowns. Equations (6.42) and (6.43) are coupled nonlinear partial differential equations for the large-scale pressure and saturation field of the water phase.

These equations must be complemented with large-scale boundary conditions. For core experiments these are typically given by a surface source on one side of the core, a surface sink on the opposite face, and impermeable walls on the other faces. For a reservoir the boundary

conditions depend on the drive configuration and the geological modeling of the reservoir environment, so that Dirichlet as well as von Neumann problems arise in practice [339, 351, 352].

2. *Macroscopic Dimensional Analysis*

The large-scale equations of motion can be cast in dimensionless form using the definitions

$$\bar{\mathbf{x}} = \bar{\ell}\hat{\bar{\mathbf{x}}} \tag{6.44}$$

$$\bar{\boldsymbol{\nabla}} = \frac{\hat{\bar{\boldsymbol{\nabla}}}}{\bar{\ell}} \tag{6.45}$$

$$\bar{\mathbf{v}} = \bar{u}\hat{\bar{\mathbf{v}}} \tag{6.46}$$

$$\bar{t} = \frac{\bar{\ell}\hat{\bar{t}}}{\bar{u}} \tag{6.47}$$

$$\bar{P} = \bar{P}_b\hat{\bar{P}} \tag{6.48}$$

where as before $\hat{\bar{A}}$ denotes the dimensionless equivalent of the macroscopic quantity $\bar{A}$. The length $\bar{\ell}$ is now a macroscopic length, and $\bar{u}$ a macroscopic (seepage or Darcy) velocity. The pressure $\bar{P}_b$ denotes the "breakthrough" pressure from the capillary pressure curve $\bar{P}_c(\bar{S}_{\mathrm{W}})$. It is defined as

$$\bar{P}_b = \bar{P}_c(\bar{S}_b) \tag{6.49}$$

where $\bar{S}_b$ is the breakthrough saturation defined as the solution of the equation

$$\frac{d^2\bar{P}_c(\bar{S}_{\mathrm{W}})}{d\bar{S}_{\mathrm{W}}^2} = 0 \tag{6.50}$$

Thus the dimensionless pressure is defined in terms of the inflection point $(\bar{P}_b, \bar{S}_b)$ on the capillary pressure curve, and it gives a measure of the macroscopic capillary pressure. Note that $\bar{P}_b$ is process dependent, that is, it will in general differ between imbibition and drainage. This dependence reflects the influence of microscopic wetting properties [348] and flow mechanisms on the macroscale [358].

The definition (6.48) differs from the traditional analysis [49, 329–

331]. In the traditional analysis the normalized pressure field is defined as

$$\bar{P} = \frac{\mu_{\mathrm{W}} \bar{u} \bar{\ell}}{k} \hat{\bar{P}} \tag{6.51}$$

which immediately gives rise to three problems. First, the permeability is a tensor, and thus a certain nonuniqueness results in anisotropic situations [339]. Second, Eq. (6.51) neglects the importance of microscopic wetting and saturation history dependence. The main problem, however, is that Eq. (6.51) is not based on macroscopic capillary pressures but on Darcy's law, which describes macroscopic viscous pressure effects. On the other hand, the normalization Eq. (6.48) is free from these problems and it includes macroscopic capillarity in the same was as the microscopic normalization Eq. (6.15) includes microscopic capillarity.

With the normalizations introduced above the dimensionless form of the macroscopic two-phase flow equations (6.42) and (6.43) becomes

$$\begin{aligned} \bar{\phi} \frac{\partial \bar{S}_{\mathrm{W}}}{\partial \hat{\bar{t}}} = \hat{\bar{\nabla}} \cdot \Big\{ & \mathbf{K}^r_{\mathrm{WW}}(\bar{S}_{\mathrm{W}}) (\overline{\mathbf{Ca}}_{\mathrm{W}}^{-1} \hat{\bar{\nabla}} \hat{\bar{P}}_{\mathrm{W}} - \overline{\mathbf{Gr}}_{\mathrm{W}}^{-1} \hat{\bar{\nabla}} \hat{z}) \\ & + \mathbf{K}^r_{\mathrm{WO}}(\bar{S}_{\mathrm{W}}) \frac{\mu_{\mathrm{W}}}{\mu_{\mathrm{O}}} \Big[(\overline{\mathbf{Ca}}_{\mathrm{W}}^{-1} \hat{\bar{\nabla}} \hat{\bar{P}}_{\mathrm{W}} - \overline{\mathbf{Gr}}_{\mathrm{W}}^{-1} \bar{\nabla} \hat{z}) \\ & + \overline{\mathbf{Ca}}_{\mathrm{W}}^{-1} \hat{\bar{\nabla}} \hat{\bar{P}}_c(\bar{S}_{\mathrm{W}}) + \left(1 - \frac{\rho_{\mathrm{O}}}{\rho_{\mathrm{W}}}\right) \overline{\mathbf{Gr}}_{\mathrm{W}}^{-1} \hat{\bar{\nabla}} \hat{z} \Big] \Big\} \end{aligned} \tag{6.52}$$

$$\begin{aligned} \bar{\phi} \frac{\partial (1 - \bar{S}_{\mathrm{W}})}{\partial \hat{\bar{t}}} = \hat{\bar{\nabla}} \cdot \Big\{ & \mathbf{K}^r_{\mathrm{OW}}(\bar{S}_{\mathrm{W}}) (\overline{\mathbf{Ca}}_{\mathrm{W}}^{-1} \hat{\bar{\nabla}} \hat{\bar{P}}_{\mathrm{W}} - \overline{\mathbf{Gr}}_{\mathrm{W}}^{-1} \hat{\bar{\nabla}} \hat{z}) \\ & + \mathbf{K}^r_{\mathrm{OO}}(\bar{S}_{\mathrm{W}}) \frac{\mu_{\mathrm{W}}}{\mu_{\mathrm{O}}} \Big[(\overline{\mathbf{Ca}}_{\mathrm{W}}^{-1} \hat{\bar{\nabla}} \hat{\bar{P}}_{\mathrm{W}} - \overline{\mathbf{Gr}}_{\mathrm{W}}^{-1} \bar{\nabla} \hat{z}) \\ & + \overline{\mathbf{Ca}}_{\mathrm{W}}^{-1} \hat{\bar{\nabla}} \hat{\bar{P}}_c(\bar{S}_{\mathrm{W}}) + \left(1 - \frac{\rho_{\mathrm{O}}}{\rho_{\mathrm{W}}}\right) \overline{\mathbf{Gr}}_{\mathrm{W}}^{-1} \hat{\bar{\nabla}} \hat{z} \Big] \Big\} \end{aligned} \tag{6.53}$$

In these equations the dimensionless tensor

$$\overline{\mathbf{Ca}}_{\mathrm{W}} = \frac{\mu_{\mathrm{W}} \bar{u} \bar{\ell}}{\bar{P}_b} \mathbf{K}^{-1} = \frac{\text{macroscopic viscous pressure drop}}{\text{macroscopic capillary pressure}} \tag{6.54}$$

plays the role of a macroscopic or large-scale capillary number. Similarly,

the tensor

$$\overline{\mathbf{Gr}}_{\mathrm{w}} = \frac{\mu_{\mathrm{w}} \vec{u}}{\rho_{\mathrm{w}} g} \mathbf{K}^{-1} = \frac{\text{macroscopic viscous pressure drop}}{\text{macroscopic gravitational pressure}} \tag{6.55}$$

corresponds to the macroscopic gravity number.

If the traditional normalization [Eq. (6.51)] is used instead of the normalization Eq. (6.48), and isotropy is assumed, then the same dimensionless equations are obtained with

$$\overline{\mathrm{Ca}}_{\mathrm{w}} = 1 \tag{6.56}$$

where $\overline{\mathrm{Ca}}_{\mathrm{w}}$ is the macroscopic capillary number. Thus the traditional normalization is equivalent to the assumption that the macroscopic viscous pressure drop always equals the macroscopic capillary pressure. While this assumption is not generally valid, it sometimes is a reasonable approximation as illustrated below. First, however, the consequences of the traditional assumption (6.56) for the measurement of relative permeabilities will be discussed.

3. *Measurement of Relative Permeabilities*

For simplicity only the isotropic case will be considered from now on, that is, let $\mathbf{K} = k\mathbf{1}$ where $\mathbf{1}$ is the identity matrix. The tensors $\overline{\mathbf{Ca}}_{\mathrm{w}}$ and $\overline{\mathbf{Gr}}_{\mathrm{w}}$ then become $\overline{\mathbf{Ca}}_{\mathrm{w}} = \overline{\mathrm{Ca}}_{\mathrm{w}}\mathbf{1}$ and $\overline{\mathbf{Gr}}_{\mathrm{w}} = \overline{\mathrm{Gr}}_{\mathrm{w}}\mathbf{1}$, where $\overline{\mathrm{Ca}}_{\mathrm{w}}$ and $\overline{\mathrm{Gr}}_{\mathrm{w}}$ are the macroscopic capillary and gravity numbers.

The unsteady state or displacement method of measuring relative permeabilities consists of monitoring the production history and pressure drop across the sample during a laboratory displacement process [2, 337, 359]. The relative permeability is obtained as the solution of an inverse problem. The inverse problem consists in matching the measured production history and pressure drop to the solutions of the multiphase flow equations (6.52) and (7.53) using the Buckley–Leverett approximation.

In the present formulation the Buckley–Leverett approximation comprises several independent assumptions. First, it is assumed that gravity effects are absent, which amounts to the assumption

$$\overline{\mathrm{Ca}}_{\mathrm{w}} \ll \overline{\mathrm{Gr}}_{\mathrm{w}} \tag{6.57}$$

Second, the viscous coupling terms are neglected, that is,

$$k'_{\mathrm{wo}} \frac{\mu_{\mathrm{w}}}{\mu_{\mathrm{o}}} \ll \overline{\mathrm{Ca}}_{\mathrm{w}} \qquad \text{and} \qquad k'_{\mathrm{ow}} \ll \overline{\mathrm{Ca}}_{\mathrm{w}} \tag{6.58}$$

Finally, the resulting equations

$$\bar{\phi}\frac{\partial \bar{S}_{\mathrm{W}}}{\partial \hat{\bar{t}}} = \hat{\bar{\nabla}}\cdot\left\{k^{r}_{\mathrm{WW}}(\bar{S}_{\mathrm{W}})\frac{\hat{\bar{\nabla}}\hat{\bar{P}}_{\mathrm{W}}}{\overline{\mathrm{Ca}}_{\mathrm{W}}}\right\} \tag{6.59}$$

$$\bar{\phi}\frac{\partial(1-\bar{S}_{\mathrm{W}})}{\partial \hat{\bar{t}}} = \hat{\bar{\nabla}}\cdot\left\{k^{r}_{\mathrm{OO}}(\bar{S}_{\mathrm{W}})\frac{\mu_{\mathrm{W}}}{\mu_{\mathrm{O}}}\left[\frac{\hat{\bar{\nabla}}\hat{\bar{P}}_{\mathrm{W}}}{\overline{\mathrm{Ca}}_{\mathrm{W}}} + \frac{\hat{\bar{\nabla}}\hat{\bar{P}}_{c}(\bar{S}_{\mathrm{W}})}{\overline{\mathrm{Ca}}_{\mathrm{W}}}\right]\right\} \tag{6.60}$$

are further simplified by assuming that the term involving $\hat{\bar{P}}_{c}(\bar{S}_{\mathrm{W}})$ in Eq. (6.60) may be neglected [332].

Combining Eq. (6.57) with the traditional normalization Eq. (6.56) yields the consistency condition

$$\overline{\mathrm{Gr}}_{\mathrm{W}} \gg 1 \tag{6.61}$$

for the application of Buckley–Leverett theory in the determination of relative permeabilities. It is now clear from the definition of the macroscopic gravity number [see Eq. (6.55)] that the consistent use of Buckley–Leverett theory for the unsteady-state measurement of relative permeabilities depends strongly on the flow regime. This is valid whether or not the capillary pressure term $\hat{\bar{P}}_{c}(\bar{S}_{\mathrm{W}})$ in Eq. (6.60) is neglected. In addition to these consistency problems the Buckley–Leverett theory is also plagued with stability problems [360].

4. *Pore-Scale to Large-Scale Comparison*

The comparison between the macroscopic and the microscopic dimensional analysis is carried out by relating the microscopic and macroscopic velocities and length scales. The macroscopic velocity is taken to be a Darcy velocity defined as [see discussion following Eq. (5.79)]

$$\bar{u} = \bar{\phi}u \tag{6.62}$$

where $\bar{\phi}$ is the bulk porosity and u denotes the average microscopic flow velocity introduced in the microscopic analysis [Eq. (6.12)]. The length scales ℓ and $\bar{\ell}$ are identical ($\bar{\ell} = \ell$).

Using these relations between microscopic and macroscopic length and time scales together with the assumption of isotropy yields

$$\overline{\mathrm{Ca}}_{\mathrm{W}} = \frac{\mu_{\mathrm{W}}\bar{\phi}u\ell}{k\bar{P}_{b}} = \frac{u\ell}{\overline{\nu^{*}_{\mathrm{W}}}} = \frac{\sigma_{\mathrm{OW}}\bar{\phi}\ell}{k\bar{P}_{b}}\,\mathrm{Ca}_{\mathrm{W}} \tag{6.63}$$

as the relationship between microscopic and macroscopic capillary num-

bers. Similarly, one obtains

$$\overline{\mathrm{Gr}}_{\mathrm{W}} = \frac{\mu_{\mathrm{W}}\bar{\phi}u}{\rho_{\mathrm{W}}gk} = \frac{u}{\overline{u^*_{\mathrm{W}}}} = \frac{\bar{\phi}\ell^2}{k}\,\mathrm{Gr}_{\mathrm{W}} \tag{6.64}$$

for the gravity numbers. Taking the quotient gives

$$\overline{\mathrm{Gl}}_{\mathrm{W}} = \frac{\overline{\mathrm{Ca}}_{\mathrm{W}}}{\overline{\mathrm{Gr}}_{\mathrm{W}}} = \frac{\rho_{\mathrm{W}}g\ell}{\bar{P}_b} = \frac{\ell}{\overline{\ell^*_{\mathrm{W}}}} = \frac{\sigma_{\mathrm{OW}}}{\ell\bar{P}_b}\,\mathrm{Gl}_{\mathrm{W}} \tag{6.65}$$

for the macroscopic gravillary number. Note that the ratio $\sigma_{\mathrm{OW}}/(\ell\bar{P}_b)$ is the ratio of the microscopic to the macroscopic capillary pressures. The characteristic numbers

$$\overline{\nu^*_{\mathrm{W}}} = \frac{k\bar{P}_b}{\bar{\phi}\mu_{\mathrm{W}}} \tag{6.66}$$

$$\overline{u^*_{\mathrm{W}}} = \frac{\rho_{\mathrm{W}}gk}{\mu_{\mathrm{W}}\bar{\phi}} \tag{6.67}$$

$$\overline{\ell^*_{\mathrm{W}}} = \frac{\bar{P}_b}{\rho_{\mathrm{W}}g} \tag{6.68}$$

are the macroscopic counterparts of the microscopic numbers defined in Eqs. (6.22), (6.30), and (6.34).

An interesting way of rewriting these relationships arises from interpreting the permeability as an effective microscopic cross-sectional area of flow, combined with the Leverett J function. More precisely, let

$$\Lambda = \sqrt{\frac{k}{\bar{\phi}}} \tag{6.69}$$

denote a microscopic length that is characteristic for the pore-space transport properties. Then Eqs. (6.63)–(6.65) may be rewritten as

$$\overline{\mathrm{Ca}}_{\mathrm{W}} = \frac{\bar{\ell}}{\Lambda}\frac{\mathrm{Ca}_{\mathrm{W}}}{J(\bar{S}_b)\cos\theta} \tag{6.70}$$

$$\overline{\mathrm{Gr}}_{\mathrm{W}} = \frac{\bar{\ell}^2}{\Lambda^2}\,\mathrm{Gr}_{\mathrm{W}} \tag{6.71}$$

$$\overline{\mathrm{Gl}}_{\mathrm{W}} = \frac{\Lambda}{\bar{\ell}} \frac{\mathrm{Gl}_{\mathrm{W}}}{\bar{J}(\bar{S}_b)\cos\theta} \tag{6.72}$$

where $J(\bar{S}_b) = (\bar{P}_b\sqrt{k/\bar{\phi}})/((\sigma_{\mathrm{OW}}\cos\theta)$ is the value of the Leverett–J function [2, 28] at the saturation corresponding to breakthrough, and θ is the wetting angle.

The capillary number scales as $(\bar{\ell}/\Lambda)$ while the gravity number scales as $(\bar{\ell}/\Lambda)^2$. Inserting Eqs. (6.71) and (6.72) into Eq. (6.57) implies that the Buckley–Leverett approximation (6.57) becomes invalid whenever $\bar{\ell} < \Lambda \mathrm{Gl}_{\mathrm{W}}/[J(\bar{S}_b)\cos\theta]$.

5. *Macroscopic Estimates*

This section gives order of magnitude estimates for the relative importance of capillary, viscous, and gravity effects at different scales in representative categories of porous media. These estimates illustrate the usefulness of the macroscopic dimensionless ratios for the problem of upscaling.

Three types of porous media are considered: high-permeability unconsolidated sand, intermediate permeability sandstone, and low-permeability limestone. Representative values for $\bar{\phi}$, k, and $\bar{P}_b$ are shown in Table VI.

To estimate the dimensionless numbers, the same microscopic velocity $u \approx 3 \times 10^{-6}\ \mathrm{m\,s^{-1}}$ as for the microscopic estimates will be used. The length scale ℓ, however, differs between a laboratory displacement and a reservoir process. The parameters $\ell_{\mathrm{lab}} \approx 0.1$ m and $\ell_{\mathrm{res}} \approx 100$ m are used as representative values. Combining these values with those in Tables IV and VI yields the results shown in Table VII.

The first row in Table VII can be used to check the consistency of the Buckley–Leverett approximation with the traditional normalization. The consistency condition [Eq. (6.61)] is violated for unconsolidated sand and

TABLE VI

Representative Values for Porosity, Permeability, and Breakthrough Capillary Pressure in Unconsolidated Sand, Sandstone, and Low-Permeability Limestone

Quantity	Sand	Sandstone	Limestone
$\bar{\phi}$	0.36	0.22	0.20
k	10,000 mD	400 mD	3 mD
$\bar{P}_b$	2,000 Pa	10^4 Pa	10^5 Pa

TABLE VII

Definition and Representative Values for Macroscopic Dimensionless Numbers in Different Porous Media on Laboratory ($\ell_{lab} \approx 0.1$ m) and Reservoir Scale ($\ell_{res} \approx 100$ m) under Uniform Flow Conditions ($u \approx 3 \times 10^{-6}$ m s^{-1})

Quantity	Definition	Unconsolidated Sand		Sandstone		Limestone	
		Laboratory	Reservoir	Laboratory	Reservoir	Laboratory	Reservoir
$\overline{\mathrm{Gr}}_w$	$\frac{\mu_w \bar{\phi} u}{\rho_w g k}$	0.01	0.01	0.13	0.13	18.6	18.6
$\overline{\mathrm{Ca}}_w$	$\frac{\mu_w \bar{\phi} u \ell}{k \bar{P}_b}$	0.005	4.9	0.015	15.0	0.19	187.5
$\overline{\mathrm{Gl}}_w$	$\frac{\rho_w g \ell}{\bar{P}_b}$	0.5	492	0.1	115	0.01	10
Λ	$\sqrt{\frac{k}{\phi}}$	5.2 μm	5.2 μm	1.3 μm	1.3 μm	0.1 μm	0.1 μm
$\mathrm{Ca}_w/\overline{\mathrm{Ca}}_w$	$\frac{\Lambda}{\ell} J(\bar{S}_b) \cos\theta$	1.5×10^{-4}	1.5×10^{-7}	4.8×10^{-6}	4.8×10^{-9}	2.8×10^{-7}	2.8×10^{-10}
$\frac{\mathrm{Ca}_c \overline{\mathrm{Ca}}_w}{\mathrm{Ca}_w}$	$\frac{\Lambda}{\ell} J(\bar{S}_b) \cos\theta$	0.67	–	0.63	–	0.71	–

sandstones. Such a conclusion, of course, assumes that the values given in Table VI are representative for these media.

The fifth row in Table VII gives the ratio between macroscopic and microscopic capillary numbers, which according to Eq. (6.63) is length scale dependent. The last row in Table VII compares this ratio to the typical critical capillary number Ca_c reported for laboratory desaturation curves in the different porous media. Using the $\mathrm{Ca}_c \approx 10^{-4}$ for sand, $\mathrm{Ca}_c \approx 3 \times 10^{-6}$ for sandstone, and $\mathrm{Ca}_c \approx 2 \times 10^{-7}$ for limestone [28] as before one finds that the corresponding critical macroscopic capillary number is close to 1. This indicates that the macroscopic capillary number is indeed an appropriate measure of the relative strength of viscous and capillary forces.

Consequently, one expects differences between residual oil saturation $S_{\mathrm{O}r}$ in laboratory and reservoir floods. Given a laboratory measured capillary desaturation curve $S_{\mathrm{O}r}(\mathrm{Ca}_w)$ as a function of the microscopic capillary number Ca_w the analysis predicts that the residual oil saturation in a reservoir flood can be estimated from the laboratory curve as $S_{\mathrm{O}r}(\mathrm{Ca}_c \cdot \overline{\mathrm{Ca}}_w)$ [47, 48]. For $\overline{\mathrm{Ca}}_w > 1$ the $S_{\mathrm{O}r}$ value based on macroscopic capillary numbers will in general be lower than the value $S_{\mathrm{O}r}(\mathrm{Ca}_w)$

expected from using microscopic capillary numbers. Such differences have been frequently observed, and Morrow [361] recently raised the question why field recoveries are sometimes significantly higher than those observed in the laboratory. The revised macroscopic analysis of [47, 48] suggests a possible answer to this question.

The values of the dimensionless numbers in Table VII allow an assessment of the relative importance of the different forces for a displacement. To illustrate this consider the values $\overline{\mathrm{Gr}}_w = 0.01$, $\overline{\mathrm{Ca}}_w = 0.005$, and $\overline{\mathrm{Gl}}_w = 0.5$ for unconsolidated sand on the laboratory scale. A moment's reflection shows that this implies $V \ll G \approx C$, where V stands for macroscopic viscous forces, C for macroscopic capillary forces, and G for gravity forces. The notation $A \ll B$ indicates that $A/B < 10^{-2}$, while $A < B$ means $10^{-2} < A/B < 0.5$ and $A \approx B$ stands for $0.5 < A/B < 2$. Repeating this for all cases in Table VII yields the results shown in Table VIII. Table VIII also contains the results from the microscopic dimensional analysis, as well as the results one would obtain from a traditional macroscopic dimensional analysis that assumes $\overline{\mathrm{Ca}} = 1$ [see Eq. (6.56)].

Obviously, the relative importance of the different forces may change depending on the type of medium, the characteristic fluid velocities, and the length scale. Perhaps this explains part of the general difficulty of scaling up from the laboratory to the reservoir scale for immiscible displacement.

6. *Applications*

The characteristic macroscopic velocities, length scales, and kinematic viscosities defined, respectively, in Eqs. (6.66)–(6.68) are intrinsic physical characteristics of the porous media and the fluid displacement processes. These characteristics can be useful in applications such as

TABLE VIII
Relative Importance of Viscous (V), Gravity (G), and Capillary (C) Forces in Unconsolidated Sand, Sandstone, and Limestone[a]

			Sand	Sandstone	Limestone
Pore scale			$V \ll G \ll C$		
Large scale	Traditional analysis		$V = C \ll G$	$V = C < G$	$G < V = C$
	[47]	Laboratory scale	$V \ll G \approx C$	$V < G < C$	$G < V < C$
	[48]	Field scale	$C < V \ll G$	$C < V < G$	$C < G < V$

The notation $A \ll B$ (with $A, B \in \{V, G, C\}$) indicates that $A/B < 10^{-2}$, while $A < B$ means $10^{-2} < A/B < 0.5$ and $A \approx B$ stands for $0.5 < A/B < 2$.

estimating the width of a gravitational segregation front, the energy input required to mobilize residual oil, or gravitational relaxation times.

The macroscopic gravillary number $\overline{\mathrm{Gl}}_{\mathrm{W}}$ defines an intrinsic length scale $\overline{\ell}^*_{\mathrm{W}}$ [see Eq. (6.65)]. Because $\overline{\mathrm{Gl}}_{\mathrm{W}}$ gives the ratio of the gravity to the capillary forces the length $\overline{\ell}^*_{\mathrm{W}}$ directly gives the width of a gravitational segregation front when the fluids are at rest and in gravitational equilibrium, that is when viscous forces are negligible or absent. By using the same estimates for $\bar{\phi}$, k, and $\bar{P}_b$ as those used for Table VII one obtains a characteristic front width of 20 cm for unconsolidated sand, 1 m for sandstone, and roughly 10 m for a low-permeability limestone.

Similarly, the macroscopic capillary number defines an intrinsic specific action (or energy input) ν^*_{W} via Eq. (6.63), which is the energy input required to mobilize residual oil if gravity forces may be considered negligible or absent. Representative estimates are given in Table IX.

The gravitational relaxation time is the time needed to return to gravitational equilibrium after its disturbance. This may be defined from the balance of gravitational forces versus the combined effect of viscous and capillary forces. Analogous to Eq. (6.35) for the microscopic case the dimensionless ratio becomes

$$\frac{\overline{\mathrm{Gl}}_{\mathrm{W}}}{\overline{\mathrm{Gr}}_{\mathrm{W}}} = \frac{(\text{macr gravitational pressure})^2}{(\text{macr capillary pressure}) \times (\text{macr viscous pressure drop})}$$

$$= \frac{\overline{\mathrm{Ca}}_{\mathrm{W}}}{\overline{\mathrm{Gr}}^2_{\mathrm{W}}} = \frac{\rho^2_{\mathrm{W}} g^2 k \ell}{\mu_{\mathrm{W}} \bar{\phi} \bar{P}_b u} = \frac{t}{\bar{t}^*_{\mathrm{W}}} \tag{6.73}$$

which defines the gravitational relaxation time $\overline{t}^*_{\mathrm{W}}$ as

$$\overline{t}^*_{\mathrm{W}} = \frac{\overline{\ell}^*_{\mathrm{W}}}{\overline{u}^*_{\mathrm{W}}} = \frac{\mu_{\mathrm{W}} \bar{\phi} \bar{P}_b}{\rho^2_{\mathrm{W}} g^2 k} \tag{6.74}$$

TABLE IX

Characteristic Macroscopic Energies, Velocities, Length Scales, Time Scales, and Volumetric Flow Rates for Oil–Water Flow under Reservoir Conditions in Unconsolidated Sand, Sandstone, and Low-Permeability Limestone

Quantity	Sand	Sandstone	Limestone
$\overline{\nu}^*_{\mathrm{W}}$	$6.1 \times 10^{-5}\ \mathrm{m^2\,s^{-1}}$	$2.0 \times 10^{-5}\ \mathrm{m^2\,s^{-1}}$	$1.6 \times 10^{-6}\ \mathrm{m^2\,s^{-1}}$
$\overline{u}^*_{\mathrm{W}}$	$2.99 \times 10^{-4}\ \mathrm{m\,s^{-1}}$	$2.17 \times 10^{-5}\ \mathrm{m\,s^{-1}}$	$1.61 \times 10^{-7}\ \mathrm{m\,s^{-1}}$
$\overline{\ell}^*_{\mathrm{W}}$	0.2 m	1.02 m	10.2 m
$\overline{t}^*_{\mathrm{W}}$	669 s	4.7×10^4 s	6.36×10^7 s
$\overline{Q}^*$	$1.22 \times 10^{-6}\ \mathrm{m^3\,s^{-1}}$	$2.04 \times 10^{-5}\ \mathrm{m^3\,s^{-1}}$	$1.63 \times 10^{-5}\ \mathrm{m^3\,s^{-1}}$

Estimated values are given in Table IX. They correspond to gravitational relaxation times of roughly 10 min for unconsolidated sand, 13 h for a sandstone, and 736 days for a low-permeability limestone.

Another interesting intrinsic number arises from comparing the strength of macroscopic capillary forces versus the combined effect of viscous and gravity forces

$$(\overline{\mathrm{Gl}}_{\mathrm{w}}\overline{\mathrm{Ca}}_{\mathrm{w}})^{-1} = \frac{(\text{macr capillary pressure})^2}{(\text{macr grav pressure}) \times (\text{macr viscous pressure drop})}$$

$$= \frac{\overline{\mathrm{Gr}}_{\mathrm{w}}}{\overline{\mathrm{Ca}}_{\mathrm{w}}^2} = \frac{k\bar{P}_b^2}{\bar{\phi}\mu_{\mathrm{w}}\rho_{\mathrm{w}}gu\ell^2} = \frac{\overline{Q}_{\mathrm{w}}^*}{Q} \tag{6.75}$$

where Q denotes the volumetric flow rate. Thus $\overline{Q}_{\mathrm{w}}^*$ defined as

$$\overline{Q}_{\mathrm{w}}^* = \overline{\ell}_{\mathrm{w}}^{*2}\overline{u}_{\mathrm{w}}^* = \frac{k\bar{P}_b^2}{\bar{\phi}\mu_{\mathrm{w}}\rho_{\mathrm{w}}g} \tag{6.76}$$

is an intrinsic system specific characteristic flow rate. The estimates for $\overline{v}_{\mathrm{w}}^*$, $\overline{u}_{\mathrm{w}}^*$, $\overline{\ell}_{\mathrm{w}}^*$, $\overline{t}_{\mathrm{w}}^*$, and $\overline{Q}_{\mathrm{w}}^*$ are summarized in Table IX.

In summary, the dimensional analysis of the upscaling problem for two-phase immiscible displacement suggests normalizing the macroscopic pressure field in a way that differs from the traditional normalization. This gives rise to a macroscopic capillary number $\overline{\mathrm{Ca}}$ that differs from the traditional microscopic capillary number Ca in that it depends on length scale and the breakthrough capillary pressure $\bar{P}_b$. The traditional normalization corresponds to the tacit assumption that viscous and capillary forces are of equal magnitude. With the new macroscopic capillary number $\overline{\mathrm{Ca}}$ the breakpoint Ca_c in capillary desaturation curves seems to occur at $\overline{\mathrm{Ca}} \approx 1$ for all types of porous media. Representative estimates of $\overline{\mathrm{Ca}}$ for unconsolidated sand, sandstones, and limestones suggest that the residual oil saturation after a field flood will in general differ from that after a laboratory flood performed under the same conditions. Order of magnitude estimates of gravitational relaxation times and segregation front widths for different media are consistent with experiment.

ACKNOWLEDGMENTS

The author is grateful to Thor Engøy, Karl-Sigurd Årland, and Christian Ostertag-Henning for providing him with Figs. 5, 8, and 12, and especially to Espen Haslund for allowing the use of Fig. 19 prior to publication. He thanks B. Virgin for technical assistance, Professor B. Nøst, Professor T. Jøssang, and Professor J. Feder for their hospitality in Oslo, and Professor D. H. Welte and Dr. U. Mann for their interest and support. He gratefully

acknowledges Norges Forskningsråd and Forschungszentrum Jülich for partial financial support.

REFERENCES

1. J. Schopper, Permeabilist und Porosität, in *Landolt–Börnstein: Physikalische Eigenschaften de Gesteine*, K.-H. Hellwege, Ed., Springer, Berlin, 1982, Vol. V/1a, p. 184.
2. F. Dullien, *Porous Media—Fluid Transport and Pore Structure*, San Diego, Academic, 1992.
3. A. Scheidegger, *The Physics of Flow through Porous Media*, University of Toronto Press, Toronto, 1974.
4. L. Schwartz, F. Auzerais, J. Dunsmuir, N. Martys, D. Bentz, and S. Torquato, *Physica A*, **207**, 28 (1994).
5. J. Bear and Y. Bachmat, *Introduction to Modeling of Transport Phenomena in Porous Media*, Kluwer Academic, Dordrecht, 1990.
6. G. Stell, in *The Wonderful World of Stochastics*, M. Shlesinger and G. Weiss, Eds., Elsevier, Amsterdam, 1985, p. 127.
7. G. Stell and P. Rikvold, *Chem. Eng. Commun.*, **87**, 233 (1987).
8. H. Reiss, *J. Phys. Chem.*, **96**, 4736 (1992).
9. E. Harding and D. Kendall, Eds., *Stochastic Geometry*, London, Wiley, 1974.
10. G. Matheron, *Random Sets and Integral Geometry*, New York, Wiley, 1975.
11. J. Klafter, R. Rubin, and M. Shlesinger, Eds., *Transport and Relaxation in Random Materials*, World Scientific, Singapore, 1986.
12. V. Lehmann and U. Gösele, *Appl. Phys. Lett.*, **58**, 856 (1991).
13. A. Cullis and L. Canham, *Nature (London)*, **353**, 335 (1991).
14. J. Drake, J. Klafter, R. Kopelman, and D. Awschalom, Eds., *Dynamics in Small Confining Systems*, Vol. 290, Materials Research Society, Pittsburgh, 1993.
15. M. Hoffmann, *MRS Bulletin*, **20**, 28 (1995).
16. K. Yoshida, *J. Phys. Soc. Jpn.*, **59**, 4087 (1990).
17. U. Mann, in *Geofluids: Origin, Migration and Evolution of Fluids in Sedimentary Basins*, J. Parnell, Ed., Geological Society, 1994, p. 233, Vol. 78.
18. J. Bear and M. Corapcioglu, *Advances in Transport in Porous Media*, Martinus Nijhoff, Dordrecht, 1987.
19. I. Goldsmith and P. King, in *Diagenesis of Sedimentary Sequences*, J. Marshall, Ed., Geological Society, 1987, p. 1.
20. G. Marsily, *Quantitative Hydrogeology—Groundwater Hydrology for Engineers*, Academic, San Diego, 1986.
21. Z. Kabala and A. Hunt, *Stochastic Hydrology Hydraulics*, **7**, 255 (1993).
22. D. Yale, *Geophysics*, **50**, 2480 (1985).
23. W. England, A. Mackenzie, D. Mann, and T. Quigley, *J. Geophys. Soc. (London)*, **144**, 327 (1987).
24. Y. Tang and M. Aral, *Water Resources Res.*, **28**, 1389 (1992).
25. R. Bales, S. Li, K. Maguire, M. Yahya, and C. Gerba, *Water Resources Res.*, **29**, 957 (1993).
26. Y. Jang, N. Sitar, and A. Kiureghian, *Water Resources Res.*, **30**, 2435 (1994).

27. U. Ahmed, S. Crary, and G. Coates, *J. Pet. Technol.*, 578, May 1991.
28. L. Lake, *Enhanced Oil Recovery*, Prentice Hall, Englewood Cliffs, NJ, 1989.
29. M. Honarpour, L. Koederitz, and A. Harvey, *Relative Permeability of Petroleum Reservoirs*, CRC Press, Boca Raton, FL, 1986.
30. M. Yenkie and G. Natarajan, *Separation Sci. Technol.*, **28**, 1177 (1993).
31. W. Mochan and R. Barrera, Eds., *ETOPIM 3, Proceedings of the Third International Conference on Electrical Transport and Optical Properties of Inhomogeneous Media*, Vol. Physica A 207, North-Holland, Amsterdam, 1994.
32. J. Cushman, Ed., *Dynamics of Fluids in Hierarchical Porous Media*, Academic, London, 1990.
33. P. Adler, *Porous Media*, Butterworth-Heinemann, Boston, 1992.
34. D. Stoyan and H. Stoyan, *Fractals, Random Shapes and Point Fields*, Wiley, Chichester, 1994.
35. J. Lafait and D. Tanner, Eds., *ETOPIM 2, Proceedings of the Second International Conference on Electrical Transport and Optical Properties of Inhomogeneous Media*, Vol. Physica A 157, North-Holland, Amsterdam, 1989.
36. M. Allen, G. Behie, and J. Trangenstein, *Multiphase Flow in Porous Media*, Vol. 34 of *Lecture Notes in Engineering*, Springer Verlag, Berlin, 1988.
37. D. Stoyan, W. Kendall, and J. Mecke, *Stochastic Geometry and its Applications*, Akademie-Verlag/Wiley, Berlin/Chichester, 1987.
38. E. Sanchez-Palencia and A. Zaoui, *Homogenization Techniques for Composite Media*, Vol. 272 of *Lecture Notes in Physics*, Springer-Verlag, Berlin, 1987.

38a. M. Sahimi, *Flow and Transport in Porous Media and Fractured Rock*. Weinheim: VCH Verlagsgesellschaft mbH, 1995.

39. J. Parker, *Rev. Geophys.*, **27**, 311 (1989).
40. D. Bergman and D. Stroud, in *Solid State Physics*, H. Ehrenreich and D. Turnbull, Eds., Academic, New York, 1992, p. 147.
41. M. Sahimi, *Rev. Mod. Phys.*, **65**, 1393 (1993).
42. J. Feder and T. Jøssang, in *Fractals in Petroleum Geology and Earth Processes*, C. Barton and P. L. Pointe, Eds., Plenum, New York, 1995, p. 179.
43. A. Thompson, A. Katz, and C. Krohn, *Adv. Phys.*, **36**, 625 (1987).
44. K. Meyer, P. Lorenz, B. Böhl-Kuhn, and P. Klobes, *Cryst. Res. Tech.*, **29**, 903 (1994).
45. S. Torquato, *Appl. Mech. Rev.*, **47**, S29 (1994).
46. R. Landauer, in *Electrical Transport and Optical Properties of Inhomogeneous Materials*, J. Garland and D. Tanner, Eds., American Institute of Physics, New York, 1978, p. 2.
47. R. Hilfer and P. Øren, 1993, Statoil Publ. Nr. F&U-LoU-94001.
48. R. Hilfer and P. Øren, *Transport Porous Media*, in press, 1995.
49. M. Leverett, W. Lewis, and M. True, *Trans. AIME*, **146**, 175 (1942).
50. M. Cole, J. Harvey, R. Lux, D. Eckart, and R. Tsu, *Appl. Phys. Lett.*, **60**, 2800 (1992).
51. S. Gardelis, U. Bangert, and B. Hamilton, *Thin Solid Films*, **255**, 167 (1995).
52. E. Takasuka and K. Kamei, *Appl. Phys. Lett.*, **65**, 484 (1994).
53. A. Cullis, L. Canham, G. Williams, P. Smith, and O. Dosser, *J. Appl. Phys.*, **75**, 493 (1994).

54. H. Lee, Y. Seo, D. Oh, K. Nahm, E. Suh, Y. Lee, H. Lee, Y. Hwang, K. Park, S. Chang, and E. Lee, *Appl. Phys. Lett.*, **62**, 855 (1993).
55. P. Smith, in *Phase Transitions in Soft Condensed Matter*, T. Riste and D. Sherrington, Eds., Plenum, New York, 1989, p. 353.
56. E. Weibel, in *Geometrical Probability and Biological Structures: Buffon's 200th Anniversary*, R. Miles and J. Serra, Eds., Springer, Berlin, 1978, p. 171.
57. P. Philippi, P. R. Yunes, C. Fernandes, and F. Magnani, *Transport Porous Media*, **14**, 219 (1994).
58. B. Mandelbrot, *The Fractal Geometry of Nature*, San Francisco, Freeman, 1982.
59. M. Zähle, *Math. Nachr.*, **108**, 49 (1982).
60. M. Zähle, *Math. Nachr.*, **110**, 179 (1983).
61. K. Falconer, *The Geometry of Fractal Sets*, Cambridge University Press, Cambridge, MA, 1985.
62. J. Wohlenberg, Dichte der Minerale, in *Landolt–Börnstein: Physikalische Eigenschaften de Gesteine*,K.-H. Hellwege, Ed., Vol. V/1a, Springer, Berlin, 1982, p. 66.
63. R. Hilfer, *Int. J. Mod. Phys. B*, **7**, 4371 (1993).
64. R. Hilfer, *Phys. Rev. E*, **48**, 2466 (1993).
65. R. Hilfer, in *Random Magnetism and High-Temperature Superconductivity*, W. Beyermann, N. Huang-Liu, and D. MacLaughlin, Eds., World Scientific Publishers, Singapore, 1994, p. 85.
66. R. Hilfer and L. Anton, *Phys. Rev. E, Rapid Commun.*, **51**, 848 (1995).
67. R. Hilfer, *Fractals*, **3(1)**, 211, 1995.
68. R. Hilfer, *Chaos, Solitons, Fractals*, Vol. 5, 1995, p. 1475.
69. R. Hilfer, *Physica A* 221 (1995), p. 9.
70. D. Kendall, in *Stochastic Geometry*, E. Harding and D. Kendall, Eds., Wiley, London, 1974, p. 322.
71. N. Cressie and G. Lassett, *SIAM Rev.*, **29**, 577 (1987).
72. G. Choquet, *Ann. Inst. Fourier*, V, 131 (1953).
73. W. Feller, *An Introduction to Probability Theory and Its Applications*, Vol. I, Wiley, New York, 1968.
74. W. Feller, *An Intoduction to Probability Theory and Its Applications*, Vol. II, Wiley, New York, 1971.
75. W. Rudin, *Real and Complex Analysis*, McGraw-Hill, New York, 1974.
76. Y. Bachmat and J. Bear, *Transport Porous Media*, **1**, 213 (1986).
77. R. S. Mikhail and E. Robens, *Microstructure and Thermal Analysis of Solid Surfaces*, Wiley, Chichester, UK, 1983.
78. P. Wong, J. Howard, and J. Lin, *Phys. Rev. Lett.*, **57**, 637 (1986).
79. P. Wong, *Phys. Today*, **24**, December, 1988.
80. J. Hansen and A. Skjeltorp, *Phys. Rev. B*, **38**, 2635 (1988).
81. C. Harris, in *Reservoir Characterization II*, L. Lake, H. Carroll, and T. Wesson, Eds., Academic, San Diego, 1991, p. 2.
82. C. Jacquin and P. Adler, *Transport Porous Media*, **2**, 28 (1987).
83. J. Fripiat, in *Fractal Approach to Heterogeneous Chemistry*, D. Avnir, Ed., Wiley, Chichester, UK, 1989, p. 331.

84. P. Adler, in *Fractal Approach to Heterogenous Chemistry*, D. Avnir, Ed., Wiley, Chichester, UK, 1989, p. 341.
85. O. Dinariev, *Fluid Dynamics*, **27**, 682 (1992).
86. J. Feder, *Fractals*, Plenum, New York, 1988.
87. R. Lenormand, *Physica D*, **38**, 230 (1989).
88. R. Lenormand, *Proc. R. Soc. London*, **423**, 159 (1989).
89. C. Ruffet, Y. Gueguen, and M. Darot, *Geophys.*, **56**, 758 (1991).
90. H. Davis, R. Novy, L. Scriven, and P. Toledo, *J. Phys. C*, **2**, SA457 (1990).
91. C. Barton and P. L. Pointe, Eds., *Fractals in Petroleum Geology and Earth Processes*, Plenum, New York, 1995.
92. K. Gaida, W. Rühl, and W. Zimmerle, *Erdöl Erdgas Z.*, **89**, 336 (1973).
93. S. Brunauer, P. Emmer, and E. Teller, *J. Am. Chem. Soc.*, **60**, 309 (1938).
94. R. Haul and G. Dümbgen, *Chemie-Ing.-Tech.*, **35**, 586 (1963).
95. C. Meng and Y. Wang, *J. Non-Cryst. Solids*, **122**, 41 (1990).
96. P. Debye and A. Bueche, *J. Appl. Phys.*, **20**, 518 (1949).
97. P. Debye, H. Anderson, and H. Brumberger, *J. Appl. Phys.*, **28**, 679 (1957).
98. S. Prager, *Phys. Fluids*, **4**, 1477 (1961).
99. S. Prager, *Physica*, **29**, 129 (1963).
100. H. Weissberg and S. Prager, *Phys. Fluids*, **5**, 1390 (1962).
101. H. Weissberg, *J. Appl. Phys.*, **34**, 2636 (1963).
102. W. Haller, *J. Chem. Phys.*, **42**, 686 (1965).
103. R. Reck and S. Prager, *J. Chem. Phys.*, **42**, 3027 (1965).
104. M. Doi, *J. Phys. Soc. Jpn.*, **40**, 567 (1976).
105. S. Torquato and G. Stell, *J. Chem. Phys.*, **77**, 2071 (1982).
106. S. Torquato and G. Stell, *J. Chem. Phys.*, **78**, 3262 (1983).
107. S. Torquato and G. Stell, *J. Chem. Phys.*, **79**, 1505 (1983).
108. P. Rikvold and G. Stell, *J. Chem. Phys.*, **82**, 1014 (1985).
109. P. Rikvold and G. Stell, *J. Colloid Interface Sci.*, **108**, 158 (1985).
110. G. Stell and P. Rikvold, *Int. J. Thermophys.*, **7**, 863 (1986).
111. J. Berryman, *J. Appl. Phys.*, **57**, 2374 (1985).
112. J. Berryman and S. Blair, *J. Appl. Phys.*, **60**, 1930 (1986).
113. M. Yanuka, F. Dullien, and D. Elrick, *J. Colloid Interface Sci.*, **112**, 24 (1986).
114. M. Kwiecen, I. MacDonald, and F. Dullien, *J. Microsc.*, **159**, 343 (1990).
115. F. Dullien, *Transport Porous Media*, **6**, 581 (1991).
116. S. Torquato and M. Avellaneda, *J. Chem. Phys.*, **95**, 6477 (1991).
117. C. Lin and M. Cohen, *J. Appl. Phys.*, **53**, 4152 (1982).
118. J. Thovert, J. Salles, and P. Adler, *J. Microsc.*, **170**, 65 (1993).
119. P. Spanne, J. Thovert, C. Jacquin, W. Lundquist, K. Jones, and P. Adler, *Phys. Rev. Lett.*, **73**, 2001 (1994).
120. J. Harlan, D. Picot, and P. Loll, *Anal. Biochem.*, **224**, 557 (1995).
121. K. Hosoya, K. Kimata, and N. Tanaka, *J. Liq. Chromatog.*, **16**, 3059 (1993).
122. S. Sakai, *J. Membrane Sci.*, **96**, 91 (1994).
123. S. Mochizuki and A. Zydney, *J. Membrane Sci.*, **82**, 211 (1993).
124. E. Grosgogeat, J. Fried, and R. Jenkins, *J. Membrane Sci.*, **57**, 237 (1991).

125. M. Sasthav, W. P. Raj, and M. Cheung, *J. Colloid Interface Sci.*, **152**, 376 (1992).
126. H. Kamiya, K. Isomura, and T. Jun-ichiro, *J. Am. Chem. Soc.*, **78**, 49 (1995).
127. W. W. Chen and B. Dunn, *J. Am. Ceramic Soc.*, **76**, 2086 (1993).
128. L. Garrido and J. L. Ackerman, *Ceramic Eng. Sci. Proc.*, **12**, 2042 (1992).
129. N. Naito, L. De Jonghe, and M. Rahaman, *J. Materials Sci.*, **25**, 1686 (1990).
130. R. Murdey and W. Machin, *Langmuir*, **10**, 3842 (1994).
131. S. Zeng, A. Hunt, and R. Greif, *J. Heat Transfer*, **116**, 756 (1994).
132. H. Naono, M. Hakuman, and K. Nakai, *J. Coll. Interf. Sci.*, **165**, 532 (1994).
133. B. Russell and M. LeVan, *Carbon*, **32**, 845 (1994).
134. C. Lastoskie, K. E. Gubbins, and N. Quirke, *J. Phys. Chem.*, **97**, 4786 (1993).
135. P. Gu, P. Xie, and Y. Fu, *Cement Concrete Res.*, **24**, 86 (1994).
136. L. Konecny and S. Naqvi, *Cement Concrete Res.*, **23**, 1223 (1993).
137. L. Tang and L.-O. Nilsson, *Cement Concrete Res.*, **22**, 541 (1992).
138. E. Smith, W. Powers, and P. Shea, *Soil Sci.*, **159**, 23 (1995).
139. Y. Nagarajarao, *Z. Pflanzenern. Bodenkd.*, **157**, 81 (1994).
140. H. Yamaguchi, Y. Hashizume, and H. Ikenaga, *Soils Foundations*, **32**, 1 (1992).
141. A. Netto, *Aapg Bull.*, **77**, 1101 (1993).
142. J. Howard and W. Kenyon, *Marine Petroleum Geol.*, **9**, 139 (1992).
143. F. J. Griffiths and R. C. Joshi, *Can. Geotech. J.*, **28**, 20 (1991).
144. A. Watkinson, Y. Xu, and Y. Koga, *Fuel*, **73**, 1797 (1994).
145. J. Kloubek, *J. Adhesion Sci. Technol.*, **6**, 667 (1992).
146. V. Karathanos and G. Saravacos, *J. Food Eng.*, **18**, 259 (1993).
147. W. D. Machin, *Langmuir*, **10**, 1235 (1994).
148. S. Sato, *J. Chem. Eng. Jpn.*, **21**, 534 (1988).
149. D. Milburn, B. Adkins, and B. Davis, *Appl. Catal.*, **119**, 205 (1994).
150. G. Zgrablich, S. Mendioroz, L. Daza, J. Pajares, V. Mayagoita, F. Rojas, and W. Conner, *Langmuir*, **7**, 779 (1991).
151. H. Ritter and L. Drake, *Ind. Eng. Chem. (Anal. Ed.)*, **17**, 782 (1945).
152. W. Purcell, *Am. Inst. Min. Metall. Petrol. Eng.*, **186**, 39 (1949).
153. A. Thompson, A. Katz, and R. Raschke, *Phys. Rev. Lett.*, **58**, 29 (1987).
154. A. Lane, N. Shah, and W. Conner, *J. Colloid Interface Sci.*, **137**, 315 (1991).
155. N. Wardlaw, Y. Li, and D. Forbes, *Transport Porous Media*, **2**, 597 (1987).
156. M. Ioannidis and I. Chatzis, *J. Colloid Interface Sci.*, **161**, 278 (1993).
157. M. Ioannidis, I. Chatzis, and A. Payatakes, *J. Colloid Interface Sci.*, **143**, 22 (1991).
158. C. D. Tsakiroglou and A. C. Payatakes, *J. Colloid Interface Sci.*, **146**, 479 (1991).
159. M. Spearing and P. Matthews, *Transport Porous Media*, **6**, 71 (1991).
160. C. D. Tsakiroglou and A. Payatakes, *J. Colloid Interface Sci.*, **137**, 315 (1990).
161. A. Rosenfeld and A. Kak, *Digital Picture Processing*, Academic, New York, 1982.
162. R. DeHoff, E. Aigeltinger, and K. Craig, *J. Microscopy*, **95**, 69 (1972).
163. L. Muche and D. Stoyan, *J. Appl. Probability*, **29**, 467 (1992).
164. Lu, Binglin. S. Torquato, *J. Chem. Phys.*, **98**, 6472 (1993).

165. S. Torquato and B. Lu, *Phys. Rev. E*, **47**, 2950 (1993).
166. T. B. Borak, *Radiation Res.*, **137**, 346 (1994).
167. P. Levitz and D. Tchoubar, *J. Phys. I France*, **2**, 771 (1992).
168. R. Hilfer, *Phys. Rev. B*, **44**, 60 (1991).
169. R. Hilfer, *Phys. Scr.*, **T44**, 51 (1992).
170. R. Hilfer, *Phys. Rev. B*, **45**, 7115 (1992).
171. F. Boger, J. Feder, R. Hilfer, and T. Jøssang, *Physica A*, **187**, 55 (1992).
172. R. Hilfer, *Physica A*, **194**, 406 (1993).
173. B. Hansen, E. Haslund, R. Hilfer, and B. Nøst, *Mat. Res. Soc. Proc.*, **290**, 185 (1993).
174. R. Hilfer, B. Nøst, E. Haslund, T. Kautzsch, B. Virgin, and B. Hansen, *Physica A*, **207**, 19 (1994).
175. E. Haslund, B. Hansen, R. Hilfer, and B. Nøst, *J. Appl. Phys.*, **76**, 5473 (1994).
176. J. Cardy, Ed., *Finite-Size Scaling*, North-Holland, Amsterdam, 1988.
177. V. Privman, Ed., *Finite-Size Scaling and Numerical Simulation of Statistical Systems*, World Scientific, Singapore, 1990.
178. R. Hilfer, *Z. Physik B*, **96**, 63 (1994).
179. E. O'Neill, *Introduction to Statistical Optics*, Addison-Wesley, Reading, 1963.
180. B. Lu and S. Torquato, *J. Chem. Phys.*, **93**, 3452 (1990).
181. B. Lu and S. Torquato, *J. Opt. Soc. Am. A*, **7**, 7171 (1990).
182. R. Guyer, *Phys. Rev. B*, **37**, 5713 (1988).
183. C. Ostertag-Henning, B. Virgin, Th. Rage, R. Hilfer, R. Koch, and U. Mann, 1995, to be published.
184. C. Andraud, B. Virgin, E. Haslund, R. Hilfer, A. Beghdadi, and J. Lafait, unpublished results.
185. B. Gnedenko, *The Theory of Probability*, Chelsea, New York, 1962.
186. B. Nøst, B. Hansen, and E. Haslund, *Phys. Scr.*, **T44**, 67 (1992).
187. J. Koplik, C. Lin, and M. Vermette, *J. Appl. Phys.*, **56**, 3127 (1984).
188. P. Doyen, *J. Geophys. Res.*, **93**, 7729 (1988).
188a. J. Fredrich, B. Menendez, and T. Wong, *Science*, **268**, 276 (1995).
189. C. Andraud, A. Beghdadi, and J. Lafait, *Physica A*, **207**, 208 (1994).
190. R. Hilfer, *Mod. Phys. Lett. B*, **6**, 773 (1992).
191. A. Prudnikov, Y. Brychkov, and O. Marichev, *Integrals and Series*, Gordon and Breach, New York, 1990, Vol. 3.
192. D. Ruelle, *Statistical Mechanics*, Benjamin, London, 1969.
193. P. Nutting, *London, Edinburgh Dublin Philos. Mag. Ser. 6*, **26**, 423 (1913).
194. G. Porod, *Koll. Z.*, **124**, 83 (1951).
195. G. Porod, *Koll. Z.*, **125**, 51 (1952).
196. B. Widom and J. Rowlinson, *J. Chem. Phys.*, **52**, 1670 (1970).
197. J. Ziman, *Models of Disorder*, Cambridge University Press, Cambridge, 1982.
198. J. Finney, *Proc. R. Soc.*, **319A**, 479 (1970).
199. L. Schwartz, J. Banavar, and B. Halperin, *Phys. Rev. B*, **40**, 9155 (1989).
200. S. Bryant, D. Mellor, and C. Cade, *AIChE J.*, **39**, 387 (1993).
201. L. Schwartz and J. Banavar, *Phys. Rev. B*, **39**, 11965 (1989).

202. R. Jullien, A. Pavlovich, and P. Meakin, *J. Phys. A*, **25**, 4103 (1992).
203. N. Morrow, I. Chatzis, and J. Taber, *SPE Proceedings*, Vol. 60th SPE Conference, Las Vegas, 1985.
204. S. Bryant and M. Blunt, *Phys. Rev. A*, **46**, 2004 (1992).
205. P. Sen, *Geophysics*, **49**, 586 (1984).
206. N. Martys, S. Torquato, and D. Bentz, *Phys. Rev. E*, **50**, 403 (1994).
207. I. C. Kim and S. Turquato, *J. Appl. Phys.*, **74**, 1844 (1993).
208. B. U. Felderhof, *Physica A*, **207**, 13 (1994).
209. B. U. Felderhof and P. Iske, *Phys. Rev. A*, **45**, 611 (1992).
210. R. Coleman, technical report, Department of Theoretical Statistics, University of Aarhus, Denmark, 1979.
211. S. Wicksell, *Biometrika*, **17**, 84 (1925).
212. S. Wicksell, *Biometrika*, **18**, 152 (1926).
213. D. Stauffer and A. Aharony, Taylor and Francis, London, 1992.
214. P. Sen, J. Roberts, and B. Halperin, *Phys. Rev. B*, **32**, 3306 (1985).
215. S. Feng, B. Halperin, and P. Sen, *Phys. Rev. B*, **35**, 197 (1987).
216. E. Cinlar and S. Torquato, *J. Stat. Phys.*, **78**, 827 (1995).
217. S. Miyazima, K. Maruyama, and K. Okumura, *J. Phys. Soc. Jpn.*, **9**, 2805 (1991).
218. J. A. Given, I. C. Kim, and S. Torquto, *J. Chem. Phys.*, **93**, 5128 (1990).
219. W. Elam, A. Kerstein, and J. Rehr, *Phys. Rev. Lett.*, **52**, 1516 (1984).
220. I. Fatt, *AIME Pet. Trans.*, **207**, 144 (1956).
221. I. Fatt, *AIME Pet. Trans.*, **207**, 160 (1956).
222. I. Fatt, *AIME Pet. Trans.*, **207**, 164 (1956).
223. R. Ehrlich and F. Crane, *Trans. AIME*, **246**, 221 (1969).
224. I. Chatzis and F. Dullien, *J. Can. Pet. Technol.*, 97 (January–March 1977).
225. M. Dias and A. Payatakes, *J. Fluid Mech.*, **164**, 305 (1986).
226. C. Diaz, I. Chatzis, and F. Dullien, *Transport Porous Media*, **2**, 215 (1987).
227. J. Koplik and T. Lasseter, *Chem. Eng. Commun.*, **26**, 285 (1984).
228. K. McCall, D. Johnson, and R. Guyer, *Phys. Rev. B*, **44**, 7344 (1991).
229. M. Blunt and P. King, *Phys. Rev. A*, **42**, 4780 (1990).
230. J. Bear, C. Braester, and P. Menier, *Transport Porous Media*, **2**, 301 (1987).
231. C. O'Carroll and K. Sorbie, *Phys. Rev. E*, **47**, 3467 (1993).
232. P. Øren, J. Billiotte, and W. Pinczewski, *SPE Formation Evaluation*, March, 1992, p. 70.
233. G. Matthews and M. Spearing, *Marine Petrol. Geol.*, **9**, 146 (1992).
234. U. Oxaal, *Phys. Rev. A*, **44**, 5038 (1991).
235. U. Oxaal, F. Boger, J. Feder, T. Jøssang, P. Meakin, and A. Aharony, *Phys. Rev. A*, **44**, 6564 (1991).
236. R. Lenormand, *J. Phys. C*, **2**, 79 (1990).
237. R. Lenormand, E. Touboul, and C. Zarcone, *J. Fluid Mech.*, **189**, 165 (1988).
238. M. McKellar and N. Wardlaw, *J. Can. Pet. Technol.*, **21**, 39 (1982).
239. R. Larson, L. Scriven, and H. Davis, *Chem. Eng. Sci.*, **36**, 57 (1981).
240. N. Seaton, *Chem. Eng. Sci.*, **46**, 1895 (1991).
241. M. Yanuka, *J. Colloid Interface Sci.*, **127**, 35 (1989).

242. M. Yanuka, *J. Colloid Interface Sci.*, **127**, 48 (1989).
243. M. Yanuka, *Transport Porous Media*, **7**, 265 (1992).
244. R. Chandler, J. Koplik, K. Lerman, and J. Willemsen, *J. Fluid Mech.*, **119**, 249 (1982).
245. P. Meakin, J. Feder, V. Frette, and T. Jøssang, *Phys. Rev. A*, **46**, 3357 (1992).
246. A. H. Hirsch, Lee M. Thompson, *Phys. Rev. E*, **50**, 2069 (1994).
246a. M. Blunt, M. King, and H. Scher, *Phys. Rev. A*, **46**, 7680 (1992).
247. J. Essam, *Rep. Prog. Phys.*, **43**, 835 (1980).
248. A. Aharony, in *Directions in Condensed Matter Physics*, G. Grinstein and G. Mazenko, Eds., World Scientific, Singapore, 1986, p. 1.
249. J. Quiblier, *J. Colloid Interface Sci.*, **98**, 84 (1984).
250. P. Crossley, L. Schwartz, and J. Banavar, *Appl. Phys. Lett.*, **59**, 3553 (1991).
251. R. Blumenfeld and S. Torquato, *Phys. Rev. E*, **48**, 4492 (1993).
252. J. Salles, J. Thovert, and P. Adler, *J. Contaminant Hydrology*, **13**, 3 (1993).
253. E. Guyon, L. Oger, and T. Plona, *J. Phys. D*, **20**, 1637 (1987).
254. P. Wong, J. Koplik, and J. Tomanic, *Phys. Rev. B*, **30**, 6606 (1984).
255. J. Roberts and L. Schwartz, *Phys. Rev. B*, **31**, 5990 (1985).
256. L. Schwartz and S. Kimminau, *Geophysics*, **52**, 1402 (1987).
257. H. Scher and R. Zallen, *J. Chem. Phys.*, **53**, 3759 (1970).
258. V. Shante and S. Kirkpatrick, *Adv. Phys.*, **20**, 325 (1971).
259. I. Gel'fand and G. Shilov, *Generalized Functions*, Academic, New York, 1964, Vol. I.
260. F. Leij, T. Skaggs, and M. Genuchten, *Water Resources Res.*, **27**, 2719 (1991).
261. M. Quintard and S. Whitaker, *Adv. Water Res.*, **17**, 221 (1994).
262. P. Germann, *J. Contaminant Hydrol.*, **7**, 39 (1991).
263. S. Kirkpatrick, *Rev. Mod. Phys.*, **45**, 574 (1973).
264. I. Webman, J. Jortner, and M. Cohen, *Phys. Rev. B*, **15**, 5712 (1977).
265. J. Bernasconi, *Phys. Rev. B*, **18**, 2185 (1978).
266. J. Yeomans and R. Stinchcombe, *J. Phys. C*, **11**, 4095 (1978).
267. R. Hilfer, *Renormierungsansätze in der Theorie ungeordneter Systeme*, Verlag Harri Deutsch, Frankfurt, 1986.
268. E. Sanchez-Palencia and A. Zaoui, *Non-Homogenous Media and Vibration Theory*, Vol. 127 of *Lecture Notes in Physics*, Springer Verlag, Berlin, 1980.
269. R. Burridge and J. Keller, *J. Acoust. Soc. Am.*, **70**, 1140 (1981).
270. S. Whitaker, *Transport in Porous Media*, **1**, 3 (1986).
271. H. Ene, in *Dynamics of Fluids in Hierarchical Porous Media*, J. Cushman, Ed., Academic, London, 1990, p. 223.
272. J. Keller, *J. Math. Phys.*, **5**, 548 (1964).
273. A. Dykhne, *Sov. Phys. JETP*, **32**, 63 (1971).
274. G. Milton, *Phys. Rev. B*, **38**, 11296 (1988).
275. B. Abramovich and P. Indelman, *J. Phys. A: Math. Gen.*, **28**, 693 (1995).
276. G. Matheron, *Elements pour une Theorie des Milieux Poreux*, Masson, Paris, 1967.
277. P. King, *J. Phys. A: Math. Gen.*, **20**, 3935 (1987).

278. L. Landau and E. Lifhitz, *Electrodynamics of Continuous Media*, Pergamon, Oxford, 1960.
279. B. Noetinger, *Transport Porous Media*, **15**, 99 (1994).
280. T. Levy, in *Homogenization Techniques for Composite Media*, E. Sanchez-Palencia and A. Zaoui, Eds., Springer-Verlag, Berlin, 1985, p. 63.
281. J. Hearst and P. Nelson, *Well Logging for Physical Properties*, McGraw-Hill, New York, 1985.
282. J. H. Doveton, *Log Analysis of Subsurface Geology*, Wiley, New York, 1986.
283. W. Chew and P. Sen, *J. Chem. Phys.*, **77**, 4683 (1982).
284. G. Archie, *Trans. AIME*, **146**, 54 (1942).
285. P. Sen, C. Scala, and M. Cohen, *Geophysics*, **46**, 781 (1981).
286. J. Schopper, in *Landolt–Börnstein: Physikalische Eigenschaften der Gesteine*, K.-H. Hellwege, Ed., Springer, Berlin, 1982, p. 276, Vol. V/1b.
287. I. Holwech and B. Nøst, *Phys. Rev. B*, **38**, 12845 (1989).
288. R. Maute, W. Lyle, and E. Sprunt, *J. Pet. Technol.*, 103 (January 1992).
289. D. McLachlan, M. Button, S. Adams, V. Gorringe, J. Kneen, J. Muoe, and E. Wedepohl, *Geophysics*, **52**, 194 (1987).
290. G. Keller and P. Licastro, *U.S. Geol. Surv. Bull.*, **1052**-H, 257 (1959).
291. J. Poley, J. Noteboom, and P. de Waal, *The Log Analyst*, **19**, 8 (1978).
292. W. Kenyon, *J. Appl. Phys.*, **55**, 3153 (1984).
293. D. Stroud, G. Milton, and B. De, *Phys. Rev. B*, **34**, 5145 (1986).
294. R. Knight and A. Nur, *Geophysics*, **52**, 644 (1987).
295. M. Taherian, W. Kenyon, and K. Safinya, *Geophysics*, **55**, 1530 (1990).
296. D. Stroud and D. Bergman, *Phys. Rev. B*, **25**, 2061 (1982).
297. C. Yoon and S. Lee, *Phys. Rev. B*, **42**, 4594 (1990).
298. C. Böttcher and P. Bordewijk, *Theory of Electric Polarization*, Vol. II, Elsevier Scientific Publishing, Amsterdam, 1978.
299. R. Fuchs, *Phys. Lett.*, **48A**, 353 (1974).
300. R. Fuchs, *Phys. Rev. B*, **11**, 1732 (1975).
301. D. Bergman, *Physica A*, **207**, 1 (1994).
302. P. Lysne, *Geophysics*, **48**, 775 (1983).
303. J. Korringa, *Geophysics*, **49**, 1760 (1984).
304. B. U. Felderhof and R. Jones, *Z. Physik B*, **62**, 43 (1986).
305. K. Ghosh and R. Fuchs, *Phys. Rev. B*, **38**, 5222 (1988).
306. K. Ghosh and R. Fuchs, *Phys. Rev. B*, **44**, 7730 (1991).
307. D. Bergman, *Ann. Phys.*, **138**, 78 (1982).
308. R. Fuchs and K. Ghosh, *Physica A*, **207**, 185 (1994).
309. M. Thorpe, B. Djordjevic, and J. Hetherington, *Physica A*, **207**, 65 (1994).
310. C. Böttcher, *Theory of Electric Polarization*, Vol. I, Elsevier Scientific, Amsterdam, 1973.
311. G. Milton, *Commun. Math. Phys.*, **99**, 463 (1985).
312. L. Schwartz, *Physica A*, **207**, 131 (1994).

313. P. Sheng, *Geophysics*, **56**, 1236 (1991).
314. K. Mendelson and M. Cohen, *Geophysics*, **47**, 257 (1982).
315. P. Sen, *Geophysics*, **46**, 1714 (1981).
316. P. Sheng, *Phys. Rev. B*, **41**, 4507 (1990).
317. P. Kogut and J. Straley, *J. Phys. C*, **12**, 2151 (1979).
318. A. Katz and A. Thompson, *Phys. Rev. B*, **34**, 8179 (1986).
319. D. Johnson, J. Koplik, and L. Schwartz, *Phys. Rev. Lett.*, **57**, 2564 (1986).
320. J. Banavar and D. Johnson, *Phys. Rev. B*, **35**, 7283 (1987).
321. J. Auriault, *Transport Porous Media*, **2**, 45 (1987).
322. S. Whitaker, *Transport Porous Media*, **1**, 105 (1986).
323. J. Auriault and C. Boutin, *Transport Porous Media*, **7**, 63 (1992).
324. J. Auriault and C. Boutin, *Transport Porous Media*, **10**, 153 (1993).
325. J. Auriault, O. Lebaigue, and G. Bonnet, *Transport Porous Media*, **4**, 105 (1989).
326. A. Paterson, *A First Course in Fluid Dynamics*, Cambridge University Press, Cambridge, MA, 1983.
327. J. Walsh and W. Brace, *J. Geophys. Res.*, **89**, 9425 (1984).
328. L. Schwartz, P. Sen, and D. Johnson, *Phys. Rev. B*, **40**, 2450 (1989).
329. L. Rapaport, *Trans. AIME*, **204**, 143 (1955).
330. J. Geertsma, G. Croes, and N. Schwarz, *Trans. AIME*, **207**, 118 (1956).
331. F. Perkins and R. Collins, *Petroleum Trans. AIME*, **219**, 383 (1960).
332. R. Bentsen, *J. Can. Pet. Technol.*, **25** (October–December, 1978).
333. R. Larson, H. Davis, and L. Scriven, *Chem. Eng. Sci.*, **36**, 75 (1981).
334. M. Shook, D. Li, and L. Lake, *In Situ*, **16**, 311 (1992).
335. E. Peters, N. Afzal, and R. Gharbi, *J. Petrol. Sci. Eng.*, **9**, 183 (1993).
336. D. Zhou and E. Stenby, *Transport Porous Media*, **11**, 1 (1993).
337. M. Aleman, T. Ramamohan, and J. Slattery, *Transport Porous Media*, **4**, 449 (1989).
338. N. Wardlaw and M. McKellar, *Can. J. Chem. Eng.*, **63**, 525 (1985).
339. G. Willhite, *Waterflooding*, Vol. 3 of *SPE Textbook Series*. Society of Petroleum Engineers, 1986.
340. R. Lenormand and C. Zarcone, *SPE Proceedings*, Vol. SPE Conference, Tulsa, 1986, p. 23.
341. I. Chatzis, M. Kuntamukkula, and N. Morrow, *SPE Reservoir Engineering*, August 1988, p. 902.
342. M. Aleman and J. Slattery, *Transport Porous Media*, **3**, 455 (1988).
343. V. Frette, J. Feder, T. Jøssang, and P. Meakin, *Phys. Rev. Lett.*, **68**, 3164 (1992).
344. P. deGennes, *Rev. Mod. Phys.*, **57**, 827 (1985).
345. M. Zhou and P. Sheng, *Phys. Rev. Lett.*, **64**, 882 (1990).
346. P. Sheng and M. Zhou, *Phys. Rev. A*, **45**, 5694 (1992).
347. G. Jerauld and S. Salter, *Transport Porous Media*, **5**, 103 (1990).
348. H. Princen, *Colloids Surfaces*, **65**, 221 (1992).
249. C. Marle, *Multiphase Flow in Porous Media*, Editions Technip, Institut Francais du Petrole, Paris, 1981.
350. F. Kalaydjian, *Transport Porous Media*, **2**, 537 (1987).

351. J. Trangenstein, in *Multiphase Flow in Porous Media*, M. Allen, G. Behie, and J. Trangenstein, Eds., Springer-Verlag, Berlin, 1988, p. 87.
352. M. Allen, in *Muliphase Flow in Porous Media*, M. Allen, G. Behie, and J. Trangenstein, Eds., Springer-Verlag, Berlin, 1988, p. 1.
353. F. Kalaydijan, *Transport Porous Media*, **5**, 215 (1990).
354. B. Bourbiaux and F. Kalaydjian, *SPE Reservoir Engineering*, August 1990, p. 361.
355. T. Mannseth, *Transport Porous Media*, **6**, 469 (1991).
356. W. Rose, *Transport Porous Media*, **3**, 163 (1988).
357. R. Ehrlich, *Transport Porous Media*, **11**, 201 (1993).
358. N. Morrow, *J. Petrol. Technol.*, 1476 (December, 1990).
359. J. Heaviside, in *Interfacial Phenomena in Petroleum Recovery*, N. Morrow, Ed., Vol. 36 of *Surfactant Science Series*, Marcel-Dekker, New York, 1991, p. 377.
360. H. Langtangen, A. Tveito, and R. Winther, *Transport Porous Media*, **9**, 165 (1992).
361. N. Morrow, in *Interfacial Phenomena in Petroleum Recovery*, N. Morrow, Ed., Vol. 36 of *Surfactant Science Series*, Marcel-Dekker, New York, 1991, p. 1.
362. E. Hasłund, *Geophysics*, in press, 1996.